Thèse de doctorat

Pour obtenir le grade de Docteur de

l'UNIVERSITE POLYTECHNIQUE HAUTS-DE-FRANCE et

l'INSA HAUTS-DE-FRANCE

Spécialité: **Automatique**

Présentée et soutenue par Viet Thuan NGUYEN

Le 21/01/2021, à Valenciennes

Ecole doctorale :
Sciences Pour l'Ingénieur (ED SPI 072)

Equipe de recherche, Laboratoire :
Département Automatique, Laboratoire d'Automatique, de Mécanique et d'Informatique industrielles et Humaines (LAMIH - UMR CNRS 8201)

Commande partagée basée modèle pour fauteuil roulant à assistance électrique avec Joystick à retour d'effort

JURY

Président du jury
- BOURHIS, Guy. Professeur. LCOMS, Université de Lorraine

Rapporteurs
- BABEL, Marie. Maître de Conférence/HDR. IRISA/INRIA, INSA Rennes.
- ADOUANE, Lounis. Professeur. Heudiasyc, Université de Technologie de Compiègne

Examinateurs
- CARLSON, Tom. Associate Professor. Aspire CREATe. University College London
- KLINGER, Evelyne. HDR. Equipe HACS. Université de Bordeaux

Directeur de thèse
- POPIEUL, Jean-Christophe. Professeur. LAMIH, Université Polytechnique Hauts-de-France.

Co-directeur de thèse
- PUDLO, Philippe. Professeur. LAMIH, Université Polytechnique Hauts-de-France.

Encadrant
- SENTOUH, Chouki. Maître de Conférence/HDR. LAMIH, Université Polytechnique Hauts-de-France.

Membres invités
- BENSMAIL, Djamel. Professeur. Hôpital Raymond-Poincaré - AP-HP

A MODEL-BASED SHARED CONTROL APPROACH FOR ASSISTANCE SYSTEM ON POWER WHEELCHAIR VIA HAPTIC FORCE FEEDBACK JOYSTICK

Viet Thuan NGUYEN

Laboratory of Industrial and Human Automation control, Mechanical engineering and Computer Science (LAMIH - UMR CNRS 8201)

Polytechnic University of Hauts-de-France

January 2021

Dedicated to my parents
Kính tặng Ba Mẹ

ABSTRACT

This thesis focuses on the design, implementation, and evaluation of a customizable assistance system for power wheelchair users. The system is based on a shared control approach interacting with the user via a force feedback joystick.

The proposed assistance system targets three main objectives: i) Predict the user's intention using the movements of the joystick; ii) Reduce the user's effort to manipulate the joystick during the navigation task; iii) Assist the user to avoid the obstacle while resolving the conflict between the user's decision and the intention of the system. At the operational level, this system estimates user intention using linear observers with unknown inputs. The Tagaki-Sugeno model-based fuzzy control and linear matrix inequalities are used to design the shared controller which provides the assistance torques to the joystick to reduce user efforts. At the tactical level, we have proposed conflict-risk management functions to predict potential collisions, to find alternative trajectories to avoid these collisions and to communicate them to the user via the haptic joystick. The experimental results based on a virtual reality-based simulator validate the proposed assistance system. Manual torques for manipulating the joystick have been reduced and the level of assistance can be adjusted via the model settings. The haptic torques assist the user to avoid the obstacles while retaining his authority, that is, his ability to overrule the system suggestions.

To validate the proposed shared control approach, we have developed a comprehensive dynamic wheelchair model that is integrated into an experimental virtual reality platform in our laboratory. The goal of this model is to reproduce the real movements of wheelchair in the virtual reality environment and therefore to increase the sense of movements for the wheelchair user on the simulator platform. This model considers the interaction of tire-road contact, the effects of the free front casters and the yaw resistance torques at low speeds. The experimental results confirmed the ability of the proposed model to reproduce the dynamic behavior of the wheelchair where the model responses are consistent with the real recorded data.

To characterize the hand-joystick interaction which aims to personalizing the assistance system according to the user impairments, this thesis proposes a biomechanical model which inherited a five-bar robot arm mechanism to mimic the motions of the joystick and the user's hand. This mechanism is operated by four Hill's muscle models which allow to reflect the characteristic of user hand muscle properties. The simulation results showed the different evolutions of hand muscles activation level depending on the hand muscles biomechanical parameters.

Keywords: Model-based control, shared control, haptic, joystick force feedback, human-machine interaction

RESUME

Cette thèse se concentre sur la conception, la mise en œuvre et l'évaluation d'un système d'assistance personnalisable pour les utilisateurs d'un fauteuil roulant électrique. Le système est basé sur une approche de commande partagée interagissant avec l'usager via un joystick à retour de force.

Le système d'assistance proposé cible trois objectifs principaux : i) Prédire l'intention de l'utilisateur à l'aide des mouvements du joystick ; ii) Réduire l'effort de l'utilisateur pour manipuler le joystick pendant la tâche de navigation ; iii) Aider l'utilisateur à éviter l'obstacle tout en résolvant le conflit entre la décision de l'utilisateur et l'intention du système. Au niveau opérationnel, ce système estime l'intention de l'utilisateur en utilisant les observateurs linéaires à entrées inconnues. La commande floue de type Tagaki-Sugeno et les inégalités matricielles linéaires sont utilisées pour concevoir le contrôleur partagé qui fournit les couples d'assistance au joystick afin de réduire les efforts de l'utilisateur. Au niveau tactique, nous avons proposé des fonctions de gestion des risques-conflits permettant de prévoir les collisions potentielles, de rechercher les trajectoires alternatives permettant d'éviter ces collisions et de les communiquer à l'utilisateur via le joystick haptique. Les résultats expérimentaux basés sur un simulateur à base de réalité virtuelle valident le système d'assistance proposé. Les couples manuels pour manipuler le joystick ont été réduits et le niveau d'assistance peut être ajusté via les paramètres du modèle. Les couples haptiques ont guidé l'utilisateur pour éviter les obstacles tout en conservant son autorité, c'est-à-dire sa possibilité d'annuler les suggestions du système.

Pour valider l'approche de contrôle partagé proposée, nous avons développé un modèle dynamique complet de fauteuil roulant qui est intégré dans une plateforme expérimentale de réalité virtuelle dans notre laboratoire. Le but de ce modèle est de reproduire les mouvements réels du fauteuil roulant dans l'environnement de réalité virtuelle et donc d'augmenter le sens des mouvements pour l'utilisateur du fauteuil roulant sur la plateforme du simulateur. Ce modèle prend en compte l'interaction de contact pneu-route, les effets des roulettes avant libres et les couples de résistance au lacet à basse vitesse. Les résultats expérimentaux ont permis de valider le modèle proposé, les réponses du modèle étant cohérentes avec les données réelles enregistrées.

Pour caractériser l'interaction main-joystick qui vise à personnaliser le système d'assistance en fonction des déficiences de l'utilisateur, cette thèse propose un modèle biomécanique qui s'inspire d'un mécanisme de bras robotisé à cinq segments pour imiter les mouvements du joystick et de la main de l'utilisateur. Ce mécanisme est opéré par quatre modèles musculaires de Hill qui permettent de refléter la caractéristique des propriétés musculaires de la main de l'utilisateur. Les résultats de la simulation ont montré les différentes évolutions du niveau d'activation des muscles de la main en fonction des paramètres biomécaniques des muscles de la main.

Mots clés: commande basée modèle, commande partagé, haptique, retour de force, interaction homme-machine

REMERCIEMENTS

Table of Contents

List of Tables

List of Figures

Chapter 1

General introduction

1.1   Context of the thesis

The work in this thesis (except for chapter 3) is supported by the ELSAT2020 (Eco-mobilité, Logistique, Sécurité & Adaptabilité des Transports à l'horizon 2020) research program funded by the European Regional Development Fund, the State, and the Hauts-de-France Region.

A part of this thesis, *chapter 3: Dynamical model of wheelchair*, is supported in part by the QBA (Quantification Biomécanique de la locomotion pour l'Accessibilité aux utilisateurs de fauteuil roulant manuel) project through the Carnot ART under Grant of the National Research Agency, in part by the ELSAT2020 research program funded by the European Regional Development Fund, the State, and the Hauts-de-France Region.

This work is also sponsored by the Regional Delegation for Research and Technology, the Ministry of Higher Education and Research, and the French National Center for Scientific Research.

1.2   Problem statement

According to World Health Organization estimations, the number of persons with disabilities was growing around the world, from about 10% world's population in the 1970s to 15% (more than a billion people) in 2010 [1]. A survey conducted by the Census Bureau in the United States in 2010 showed that mobility impairments were the largest group with 7.3% of the US

population within the disability [1]. Similar results also were obtained in the survey at four African countries which so that walking is the most common type of difficulties, especially for the population with serve impairments [2].

The people with mobility limitations have to deal with many difficulties in their daily life when the aids from other people are unavailable. The current global Covid-19 pandemic which limits the contact human-human is a typical example of the difficult situations that the disabled people have to face up to. The electric power wheelchair (EPW) was invented to help these populations in order to overcome some of these difficulties. The benefits of EPW are obvious such as increased mobility, increased independence, increased freedom, able to be more social, and able to contribute to family and society [3]. However, the challenges are still there. There exist many causes of motor impairments such as neurological trauma, cerebral palsy, multiple sclerosis ... and the clinical and functional consequences can be variable. [4][5]. As a result, every individual has their own needs and specific requirements for their EPW. Also to help the wheelchair users, depending on the capacity of disabled person, some kinds of interface wheelchair-user were proposed to adapt to their needs.. A comprehensive clinical survey on power wheelchair control interfaces [5] showed that 81% of patient participants used a joystick interface. Only 19% power wheelchair users reported the other types of control interface such as head/chin control, Sip and Puff, etc. Recently, several modern interfaces have been proposed such as Brain-Computer Interface [6], eye tracking [7], etc . However each of them possess their limitations [8]. According to [8], the classic joystick has shown its advantage in comparison to the gaze tracking interface when implementing the doorway passing task. Users with a joystick interface finished this task with a lower number of collisions and a higher rate of success than the users using gaze interface.

Despite the benefits of EPW which help the user to overcome these first difficulties in their daily life, users also face up to other challenges that come along with EPW. The survey reported in [3] showed that 21% of more than 200 participants experienced various kinds of accidents such as collision with car, wall or doors, tips, and falls. 33% of this population got damage to their EPW while 11% were hospitalized due to the body injuries. Inherit the achievement in path planning and obstacle avoidance from robotics fields, some researchers

applied these methods to develop the assistance system for EPW to eliminate the unexpected collisions. These EPW are equipped with the obstacle detection sensors (LIDAR, Infra-red, or camera) and some additional algorithms to avoid the obstacles without human intervention in navigation tasks. However, the authors in [4] stated that "providing simple collision avoidance or navigational assistance would not be sufficient to allow unmonitored use of the power wheelchair, due to safety risks". This may come from the fact that unlike the specific mobile robots which normally operate in a specific environment, the EPWs work in various complex environments, from indoor to outdoor spaces. Equipping EPW with many sensors also increases the final price which finally becomes unaffordable to major EPW customers. Besides, EPW users, despite their impairments, always want to be active in EPW control instead of being driven by autonomous systems [9] [10]. The shared control technique appears to solve the above problems.

Shared control, ideally, is a form of cooperation between humans (wheelchair user) and machine (wheelchair controller) where each of them has full capacity to control a wheelchair independently. "Only human controls wheelchair" is manual mode while "only controller controls wheelchair" is the autonomous mode. When working together (shared control mode), it is expected that humans will be assisted by machine to achieve a common task (ex: obstacle avoidance while maintaining the comfort of the user). To share the control authority efficiently, the human and machine should understand each other [10] . It means that the human factors should be considered in the wheelchair controller design. On the other side, the human perceives the machine through the so-called interaction interface. This interface can be a joystick, EEG in Brain-Machine Interface (BMI) or a screen, etc. where the human can feel intuitively the intentions and the actions of the wheelchair controller. With the advantage of contacting directly with the human hand, the joystick interface is a good candidate for haptic shared control for EPW.

Although widely used in the community [9], the joystick-interface still has some disadvantages which prevent the people with serve motor impairments benefit the advantages of EPW. These disadvantages come from both user and wheelchair. Firstly, as mentioned before, each wheelchair user has his difficulties according to the type of disability he suffers. Therefore

the wheelchair users manipulate the joystick in different ways. Not only that, for each user, but their capacity in control joystick changes over time, and therefore their needs also change correspondingly [4]. The conventional joystick can adapt to the changes in user needs in a simple way. Most wheelchair manufacturers allow us to change the configurations of the joystick according to some specific environment. For example, an adjustment can be set to increase the output power of electric motors corresponding to the outdoor environment. Some common adjustable parameters are forward/turn speed, forward/turn acceleration, etc. [4]. In general, when the users needs to change the configuration of the joystick to adapt to their needs, they have to do it through appointments with the healthcare professionals. This procedure, in general, can take weeks and make the users have difficulties in managing an inappropriate joystick. Dealing with these problems, a motivation question is "*How to design an assistance system for power wheelchair users which is customizable to their needs, assures their autonomy while providing the appropriate assistance as needed?*"

Another problem that limits the development of the assistance system for wheelchair is the limitations of the evaluation experiments. Ideally, these real-world experiments have to be conducted with the participation of the disabled people. However, due to the constraints in safety conditions, long time implementation, and repeatability of the real-world test, many researchers validate the proposed approaches by recruiting the able-bodied peoples to realize the tests [11],[6], [12] . This leads to unanswered questions about the effectiveness of those methods when applied to people with disabilities. The so-called virtual-reality simulator may be a solution that allows the disabled people to participate safely in the validation experiments before the real-world ones are conducted. This simulator, which has repeatable, customizable scenarios and eliminates safety problems, can be used also as a tool for testing and evaluating assistive technology for the wheelchair.

The experimental platform, called LAMIH "PSCHITT PMR" platform (French acronym for Collaborative Simulation Platform, Hybrid, Intermodal in Land Transport for Person with Reduced Mobility), has been developed at our laboratory for these purposes. This platform allows performing three-dimensional movements because it is mounted on GoughStewart parallel robot and therefore increases significantly the feeling of movements of the user. This platform

allows not only experiments with electric wheelchair but also manual wheelchair thanks to two motor-driven rollers where the wheelchair's wheels are attached to. The visualization part is responded by a specific software SCANeR. To provide a realistic movement experience to the target users, *it is necessary to develop a new dynamical model of the wheelchair which will be used to mimic the real motions of wheelchair for this platform*.

1.3   Objectives of the thesis

The main objectives of this thesis are:

- Develop a haptic shared control-based assistance system for EPW with the joystick interface using the model-based control approach. This assistance system should ensure the user activeness in control of the wheelchair, reduce their workload, guide them to avoid the obstacles, and take into account the difficulties related to driving the wheelchair (fatigue, weakness, etc.).

- Develop a hand-joystick interaction model that includes the muscular biomechanical parameters which can be used for controller synthesis purposes. The main purpose of this model is to personalize the interaction model according to each specific user.

- Develop a dynamical model of wheelchair applied to the virtual-reality wheelchair simulator platform. This model should take into account the wheelchair-environment interaction such as tire-road contact, slope/inclined ground, etc. to mimic the real motions of the wheelchair.

1.4   Thesis contributions

The main contribution of this thesis is to develop an assistance system for power wheelchair which takes into account the motor difficulties of human. Throughout the development of this assistance system, we used Linear Matrix Inequality techniques and optimal Fuzzy logic controller that are the novel approaches for designing the assistance for the power wheelchair. They provide a systematic way to synthesize controller for the highly nonlinear human-machine system.

Another contribution is building a hand-joystick interaction model based on a robot arm

with a four bars closed-chain mechanism. This is a control-oriented way to represent the interaction between hand and joystick. Using this equivalent model can simplify the complex biomechanical one and maintain the bio-properties of hand muscles through 4 equivalent muscles. By integrating the parameters of the muscles model, this model can be personalized to adapt to every individual.

Building a dynamic model of EPW applied to develop the wheelchair simulator platform "PSCHITT PMR" is also another contribution. This model tries to cover some interaction between wheelchair and the environment through the tire-ground forces using Pacejka tire models. The effect of free front caster wheels on the dynamics of the wheelchair is considered to make the behavior of the proposed model converge to the real EPW.

- LIST OF PUBLICATIONS:

1. **V. T. Nguyen**, C. Sentouh, P. Pudlo and J. Popieul, "**Joystick Haptic Force Feedback for Powered Wheelchair - A Model-based Shared Control Approach**", accepted in 2020 IEEE International Conference on Systems, Man and Cybernetics (SMC), 2020.

2. **V. T. Nguyen**, C. Sentouh, P. Pudlo and J. Popieul, "**A Biomechanical Model of Hand-Joystick Interaction of Powered Wheelchair User**", accepted in 2020 IEEE International Conference on Systems, Man and Cybernetics (SMC), 2020.

3. **V. T. Nguyen**, T. Bentaleb, C. Sentouh, P. Pudlo and J. Popieul, "**On a Complete Dynamical Model of Manual Wheelchair for Virtual Reality Simulation Platform**", 2019 IEEE International Conference on Systems, Man and Cybernetics (SMC), Bari, Italy, 2019, pp. 2417-2422, doi: 10.1109/SMC.2019.8913960.

4. T. Bentaleb, **V. T. Nguyen**, C. Sentouh, G. Conreur, T. Poulain and P. Pudlo, "**A Real-Time Multi-Objective Predictive Control Strategy for Wheelchair Ergometer Platform**", 2019 IEEE International Conference on Systems, Man and Cybernetics (SMC), Bari, Italy, 2019, pp. 2397-2404, doi: 10.1109/SMC.2019.8914220.

5. **V. T. Nguyen**, C. Sentouh, P. Pudlo and J. Popieul, "**Path Following Controller for Electric Power Wheelchair Using Model Predictive Control and Transverse Feedback Linearization**", 2018 IEEE International Conference on Systems, Man, and Cybernetics (SMC), Miyazaki, Japan, 2018, pp. 4319-4325, doi: 10.1109/ SMC.2018.00730.

1.5 Structure of the thesis

The work of this thesis consists of seven chapters. The first one is reserved for the introduction and the rest part is organized as follows:

   - Chapter 2 is the literature review part to summary the recent developments in the field of assistive technology for EPW around the world. Starting by the general intelligent wheelchair, this chapter will then focus on the shared control approach which allows maintaining the activeness of the wheelchair's driver during the navigation task. The diversity of the user-wheelchair interfaces such as BMI interface, haptic touchpad, joystick force feedback, etc. are also involved in. The advantages and disadvantages of each application will be addressed to identify an unexplored area for this research.

   - Chapter 3 presents the dynamic model of EPW for the PSCHITT PMR wheelchair simulator. Adapted from the vehicle model, this model considers the wheelchair as a car with two rear driven wheels and two front freewheels. The rotation of front wheels is taken into account because they influence the dynamics of wheelchairs. The experimental results will present the effectiveness of this model.

   - Chapter 4 presents the biomechanical model of hand-joystick interaction. Firstly the idea of using a 4-bar robot arm mechanism to represent the ways humans hold joystick is explained. Then, the whole forearm muscles participating in the joystick controller will be replaced equivalently by 4 muscles which are built based on the well known Hill's model. The simulation results are compared with published experiments data to show the perspective of this model.

   - Chapter 5 focuses on developing an assistance system for power wheelchair in the so-called normal driving mode (without risk of collision). The first step is to develop an augmented human - wheelchair dynamical model which then is represented in the Tagaki-Sugeno model to deal with the nonlinearity inside. After that, the haptic shared controller is synthesized by using LMI-based linear quadratic optimization to find the optimal assistance torques applied to the joystick to assist the human. The simulation results show that the proposed approach can reduce the user effort when the human hand torques are reduced significantly with the assistance from the system.

   - Chapter 6 designs the assistance system in the obstacle avoidance mode and the con-

flict management functions. At this step, the assistance systems are ready to be tested in the wheelchair simulator. A joystick force feedback designed at the LAMIH based on a commercial joystick is mounted to a self-developped virtual reality simulator for the wheelchair. The experimental results show that the proposed assistance system can reduce user hand torque in manipulating the joystick, guide them to avoid the obstacles, and follow the user decision in case of conflict.

- Chapter 7 gives an overall discussion and conclusion about the work. The open questions and perspectives will be also presented.

Chapter 2

Literature review

2.1 Introduction

Commercialized firstly from 1950s power wheelchair now plays an important role in the daily life of the people with limited mobility. There are many research works, both in the industry as well as in academics, to increase the safety and comfort to the users of this means. The wheelchair now can be equipped with many sensors/actuators to assist or even replace the users to realize many different tasks. These wheelchairs are generally called "intelligent wheelchair". From the primitive simple idea of putting a chair on a mobile robot, the modern power wheelchair now in general is integrated with different interfaces and sensors to increase the situation awareness of users and assist them to avoid the potential accident. Some commercial wheelchairs are presented with some basic collision prevention functions and user interfaces such as the joystick, touch screen ... However, due to the diversity in the kinds and the levels of the user's impairments such as motor defects, perceptual or cognitive impairments, the smart assistance on wheelchair should adapt to its specific users. This feature is still a big challenge for the researchers.

This chapter will firstly review the recent development of the intelligent wheelchair. Then the "shared control", a kind of cooperation between the wheelchair user and the assistant system, will be presented through the recent researches.

2.2 Intelligent wheelchair

The conventional wheelchair, in general, comprises the main components such as motorized wheels, power regulators, joystick, or maybe other input devices (touch screen, chin joystick, ...), and an ergonomics frame adapted to the users. The user controls the wheelchair by manipulating their joystick (or other input devices) which sends the commands to the controller block. The controller, in the most simple case, will amplify the received commands to the applied voltages on the appropriate electric motors to move the wheelchair. While the control loop seems easy, it indeed requires many efforts from the user, especially the people with severe motor deficiency. The user needs not only the good motor skills but also a good spatial awareness to well operate the wheelchair and avoid accidents such as wall/object collision, falling off at the curb,... As mentioned above, there are a lot of wheelchair users who face many difficulties in maneuvering the wheelchair due to their limited capacities. There are much research works focus on assisting these users. We summarize here some recent development in the assistive technology integrated into the wheelchair.
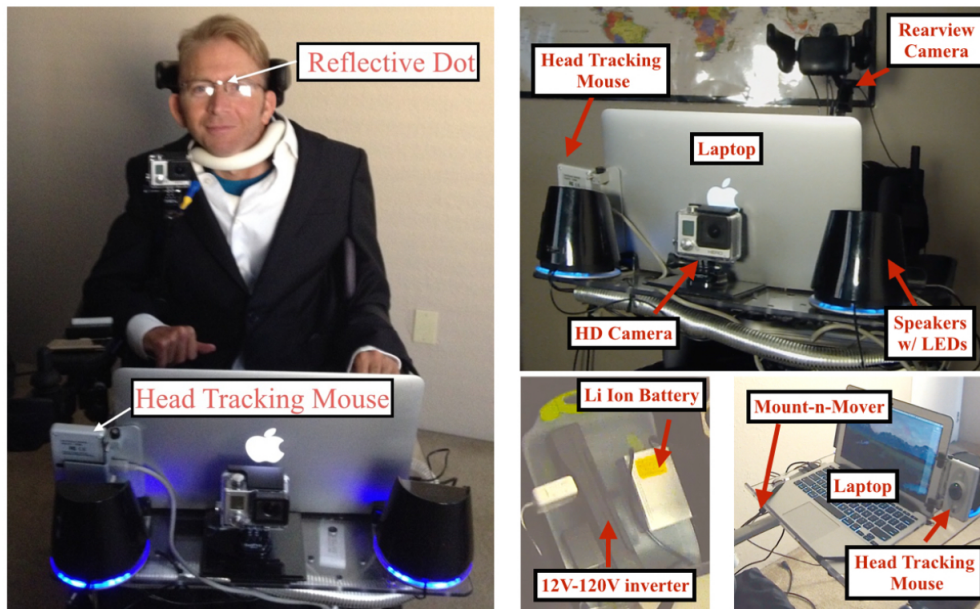
Figure 2.1: iChair developed at Univeristy of Nevada [13]

The researchers at the University of Nevada presented an intelligent wheelchair designed for people with severe disabilities [13]. Figure 2.1 shows the configuration of this wheelchair with a head tracking module, cameras, and the speaker. It has also a laser range sensor to detect the

near object. The user operates the wheelchair by using the Head Tracking Mouse which helps him/her interact with a Human-Computer Interface. In this system, the assistance is a kind of "all-or-nothing" meaning that without assistance, the user cannot accomplish his/her tasks. The user will select the function mode on the screen by moving his/her head and then, the iChair will realize his/her command. Therefore, the iChair performs mostly in the autonomous mode which uses the camera and image library for detecting the near object/obstacle to accomplish the navigation tasks. This wheelchair is designed for the user with severe impairments and therefore the Human-Machine interaction is the "one-way" where the user gives the command and the system plays the roles of an intelligent actuator.

Another approach to design the user-machine interface is the wearable-chairable input device for wheelchair users with mobility impairments that affect their hands, arms, neck, and head [14]. The users that experience difficulties due to their limited capacity to control the transitional interface, or for whom the fixed wheelchair frame is not convenient, may benefit this proposed Gest-Rest device. This devices uses a grid of pressure-sensitive sensors mounted on the armrest as in Figure 2.2 so that the user can manipulate the wheelchair with different hand poses. This device supports multiple interactions on a small surface, and allows the user to perform their familiar gestures. Users can also operate this interface by their fingers, hands, or arms and therefore it is flexible depending on the motor impairments of each user. However, the users also experience the errors in gesture recognition, which make this system become less reliable [14].

The research in [15] proposed an autonomous wheelchair for the table docking tasks to reduce the workload of users. This research exploited the algorithms in image processing to detect the available/possible safe docking place. As a result, this system does not work directly with the user but communicates the safe docking position as the destination to the navigation assistance system. A similar approach was used in [16], [17] where the image processing technique was exploited to provide the task suggestions to the user as in Figure 2.3. The user can switch between the manual and autonomous mode by manipulating the joystick. The autonomous mode was designed to reduce the user effort in two tasks: narrow door passage and corridor following. While the first task represents difficult manoeuvrers, the second one re-

11

Figure 2.2: Gest-rest pad developed at UMBC and University of Colorado Boulder, USA [14]

quires the trajectory stabilization capacity. Once the desired destination is confirmed (using joystick too) the wheelchair will plan and realize the task. The effectiveness of the proposed assistance system was evaluated through the experiments conducted with healthy participants. The evaluation indicators were travel time, user's comfort, reaction time, and attention. The experimental results show that the assistance mode can reduce user efforts and attention, increase user comfort by replacing the human in difficult tasks. However, the travel time increases significantly (two times more) while the user's attention and efforts increase when using the joystick and screen interface to communicate with the system. Overall results suggest that the user-system interface plays an important role in improving the driving experience of the user. An unfriendly interface can make efforts to improve the user experience become meaningless due to the increase of cognitive prerequisites.

To enhance the user comfort during the autonomous navigation task, the acceleration and jerk of the wheelchair were considered in the synthesis of the path following controller of the wheelchair [18]. By constructing a relation among wheelchair speed, yaw rate, and path curvature, a Lyapunov-based kinematic control law was developed taking into account the limitation of acceleration and jerk of wheelchair. While the experiments (Figure 2.4) validated this approach, the authors noted that the effect depended also on the dynamic of the wheelchair which was not considered in controller design. To overcome this concern, a path following controller

Figure 2.3: Intelligent wheelchair and the interaction srceen where the user selects their desired task developed at University of Lorraine, France [17]

for power wheelchair based on model predictive control (MPC) and transverse feedback linearisation (TFL) was presented in [19]. TFL allows to archive path invariance properties, which is useful for path following tasks, while the MPC controller takes into account the constraints in solving optimal control problems, which maintains the comfort and safety for users. The simulations are conducted in both the circular path and arbitrary path in a typical office environment. Results show the perspective of the proposed approach when the desired path is followed exactly and the constraints are well respected. However, validation experiments have not been performed. Instead of using the acceleration and jerk as the indicators for user comfort, a "Human-Comfort Factor Map" was proposed in [20] (Fig. 2.5). This approach takes into account the space around the wheelchair, wheelchair's speed, and yaw rate to design the human comfort model of an indoor straight corridor. This model was integrated into the global path planning using A^* algorithm to plan the comfort trajectory for the wheelchair. The comfort parameters (distance, speed, and yaw rate) were identified before the evaluation experiments were conducted. The experimental results show that most of the participants prefer the comfort-path than the shortest-path in the traditional path planning function.

The above researches represent a research direction where the advances in robotics were applied to power wheelchair to improve comfort and safety for the users. This approach aims to replace the human by the autonomous functions and therefore the human is generally passive
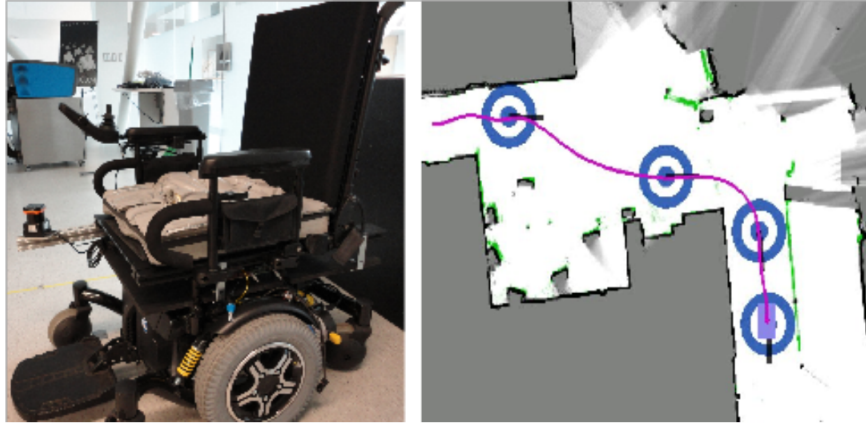
Figure 2.4: Left: Wheelchair robot developed [18]. Right: Robot trajectory in a office environment, intermediate targets are marked as concentric circles [18].

once the auto-mode is activated. This is appropriated for a group of users who experience severe impairments. However, for another group of users who have better wheelchair control skills, the authors in [21] found that the autonomous functions may irritate because the assistance was too safe for them. They also noted that the auto-system which only focused on avoiding collision may resist the user from doing some simple actions, such as take a book on the cupboard.
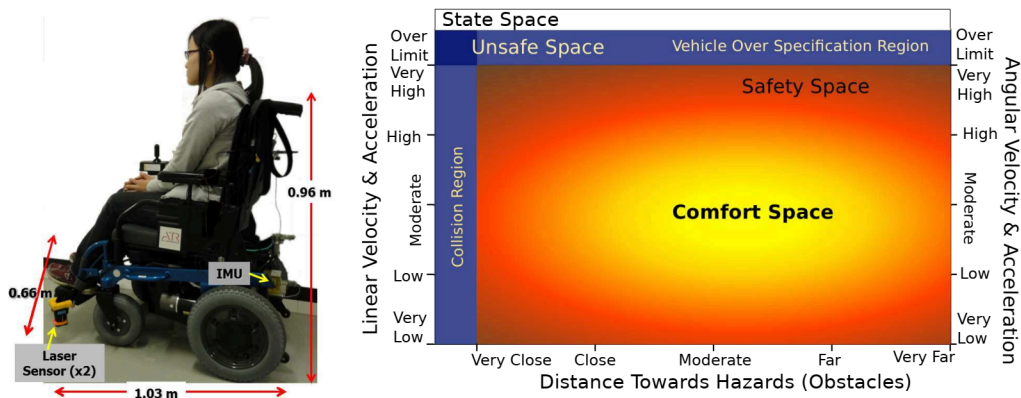
Figure 2.5: Power wheelchair configuration and the Human-Comfort Factor Map [20]

A comprehensive survey in [22] presented an overall picture of the wheelchair user's needs and desires. By studying ten participants who were over 50 years old, had mild-to-moderate cognitive impairment, and were able to operate a joystick, the finding in this research is remarkable. Firstly, all participants "preferred to drive themselves rather than to be driven". To be more detailed, they "preferred semi-autonomous mode of control over fully autonomous modes of control, regardless their cognitive status". In both high-level decision making and low-level driving behaviors, the user wants to be active "to go my own way". In a new environ-

14

ment, they want a chance to try it out before using the autonomous control. It means that the assistance system should help the users to realize what the user wants instead of doing what it wants. Secondly, the participants also noted their difficulties in situation awareness or lacking information about the surrounding environment, especially when they cannot see/know obstacles around them. As a result, they "wanted richer feedback on the location of the obstacle and the correct steering direction". The conflict concerns were noticed when the user wanted to go "(his) own way", and the assistance system let him get closer to the obstacles if necessary. Besides that, instead of helping to gain the driving capacity, in some cases, the autonomous mode may decrease the driving capacity of wheelchair users. For the semi-autonomous mode, the users preferred maintaining the wheelchair speed and getting steering assistance to avoid the obstacles without being stopped. Because stopping the wheelchair increases the jerk and the travel time, the users want to "ensure safety without compromising speed". Also, steering correction can help to gain the user's capacity of driving independently. The final design recommendations suggest that the assistance system should have customizability and adaptiveness to fit the user's "functional abilities and preferences". In other words, each user has different capacities/limitations and thus the assistance should be personalized for her/him. Another suggestion is that the human-machine interaction interface plays an important role in improving user control and awareness. Various feedback interfaces can be employed to increase the user's situation awareness. However, "communication interfaces must be carefully designed" to reduce the user workloads as the user's sensory channels are highly loaded during the driving task. As the steering correction was preferred than the autonomous mode, they suggest that the assistance on both speed and direction may provide the user "a higher level of perceived control of wheelchair". These findings confirm the central roles of the user in designing the assistive system for the power wheelchair where "the most important design aim should ... maximise and augment the pilot's skills, not to replace them" [9]. Therefore, leaving the autonomous mode with its above drawbacks, there was a research direction that tries to take into account the human factors in the performance of the assistance system. To overcome the drawbacks of autonomous mode, there are some requirements for these assistance systems:

- The design of the assistance system should take into account the levels of impairments of

users. The system should also be customizable and adaptable depending on the user's capacities as well as their preferences, for a short time or long time.

- The system should understand (by predicting, estimating, ...) the user desired motions of his/her wheelchair.

- The system should assist/support the users to realize their desired displacement to reduce their workload/efforts without replacing them completely. This point means in fact that the user and wheelchair "work together" to achieve the common goals.

- The system can inform/communicate the user the potential collision/accident, the near obstacles to enhance the user situation awareness through the appropriate interfaces.

- The system should provide the appropriate assistance to help/guide the user to avoid the obstacles or prevent potential accidents. This assistance should be given through an appropriate interface in the manner such that the user can understand/sense/feel the suggestions/intentions of the system.

- The system should have conflict management functions that will resolve the conflict between the user's actions/decisions and the suggestions from the system. These functions have to assure the final decision maker role of the user.

These above requirements are not something new but were mentioned under different forms in many works on the assistance system for power wheelchair [22], [23]. The term "work together" is often expressed under different terms such as "shared control", "cooperate control", "collaborative control", "bilateral communication", in which the "shared control" term is used the most. The next section will focus on this term and its application on the wheelchair.

2.3 Shared control - Assistance technology for EPW

The term "shared control" is used widely in engineering domains where exists the human-machine interaction. This interaction can be direct e.g joystick, car steering wheels, or indirect e.g. teleoperator robot. Depending on the specific applications, there are many different concepts on the implementation of "shared control". The differences among these concepts can be identified using six "basic" questions: Who? What? Why? Where? When? and How?. The two

first questions determine the objects, the agents participating in the shared-control framework. In most cases, there is the participation of one person and one system who will work together to reach a common goal. The "why" for this cooperation are generally to exploit and to combine the advantage of the human and system to archive common goals while satisfying the safety, comfort, and performance constraints. The three last questions will define the user-system interfaces, the interaction protocols, the necessary sensors/actuators, the algorithms which will be used to design the system. The answers vary from specific applications to the others.

One typical application of shared control is on the advanced driver support systems (ADAS) in the automotive domain. To support the driver on the longitudinal direction, the haptic force feedback gas pedal for the adaptive cruise control proposed in [24] had demonstrated to be an effective way to improve driving performance and reduce risk of collision [25]. By providing an appropriate pedal pushback force, this system aimed to warn the driver of the closing gap to the lead vehicle, to slow the vehicle a little so that the driver has more time to react. On the lateral direction, the user-system interface is the steering wheel which allows two types of shared control: input-mixing shared control and haptic shared control [25]. The input-mixing approach focuses on negotiating the desired steering angles of the system and driver [26], [27]. While this method may work well where the system is reliable and the user does not want to be involved in control the car, its main drawback is that the driver cannot overrule the system [28]. In contrast, the haptic shared control provides the assistance torque to the steering wheel which allows the driver to understand intuitively the intention of the system, reduces driver workload while still allows the driver to overrule the system if needed [29], [30].

Several research works try to propose a shared control architecture for a power wheelchair. As mentioned above, these research provided different approaches in designing the user-machine interface to define how the user's and system's actions are jointed together. The research group from KU Leuven [31] presented two schemes of shared control as shown in Fig. 2.6. It can be seen that in the traditional scheme, the connection between user and wheelchair is one-way interaction where the user's commands are blended by the system before arriving at the actuators. A similar approach as shown in Fig. 2.7 can be found in [32], [7], [33]. These configurations have two main drawbacks. Firstly, the user is disconnected from the actuators and therefore

17
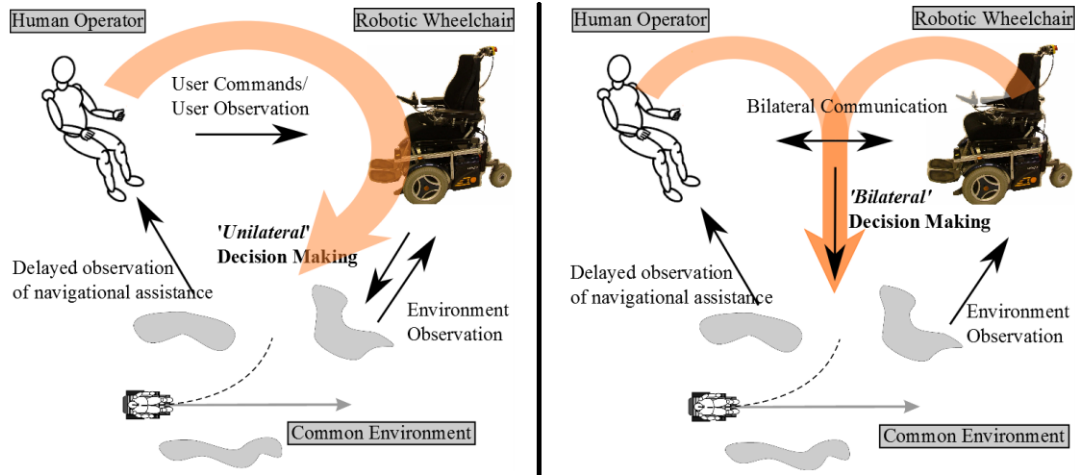
Figure 2.6: Two schemes of shared control proposed in [31]. Left: Traditional scheme. Right: Bilateral scheme

they cannot overrule the actions of the assistance system. Secondly, the human has to wait for the movements of the wheelchair to understand the decisions of the system. While being assisted by the system, the user lost their initiative in decision making. Another scheme, called "bilateral" shared control, blend the actions of both user and system into the final decision at the haptic joystick interface. This approach allows the user to overrule the system if necessary and sense intuitively the actions of the system. The authors proposed the two assistance modes, collision avoidance, and obstacle avoidance. While the collision avoidance mode tried to stop the wheelchair in front of an obstruction, the obstacle avoidance one bent the wheelchair motions toward a free-collision alternative path. The alternative path was the circular curve delivered from the kinematic properties and the dimensions of the wheelchair. The experiment results showed the interest of this approach. However, the effectiveness in reducing user workloads and conflict management was not mentioned.

A haptic guidance-based shared control was presented in [34], [35] using a force feedback joystick. The obstacles, both static and dynamic, are detected using the ultrasonic sensors mounted around the experimented wheelchair. To provide the assistance haptic feedback to the user, the authors firstly mapped the joystick's velocities plan to the build map from the sensors to create the allowed area and the forbidden area on the joystick velocities plan as shown in Fig. 2.8. Once the map was built, the optimal solution was calculated so that it is nearest the user command while maximizing the linear velocity possible as shown in Fig. 2.9. The number
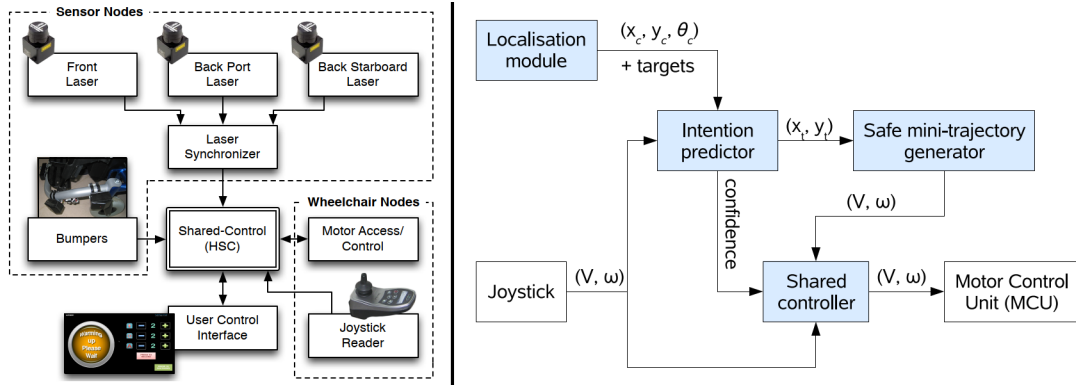
Figure 2.7: Proposed shared control architectures which are similar to the unilateral schemes [32], [7], [33]

.

of collisions reduced considerably in the validation experiments with 4 participants showed the effectiveness of the proposed assistance system. The participants also reported that the haptic force warned them while they were getting too close to the obstacle. This approach was also extended in [11] to assist the wheelchair user in avoiding the negative obstacle, occurring when the ground drops off, to prevent a falling or tipping hazard for the wheelchair. However, besides the reported concerns of joystick dimensions, the conflict between the user and the system was not mentioned.
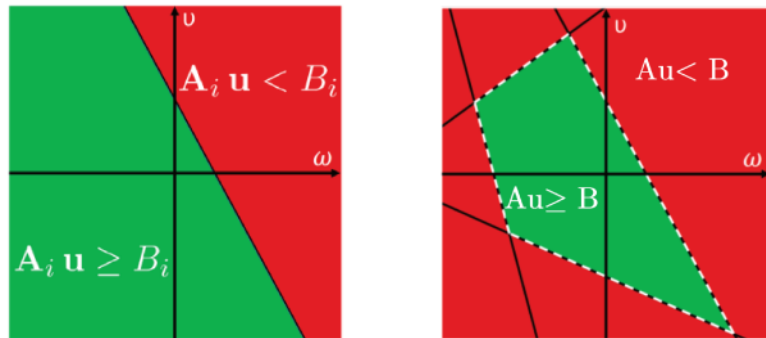
Figure 2.8: The build allowed and forbidden area of linear and angular velocity map on the joystick plan. A, B are the matrices build from the kinematic of wheelchair and the surrounding map. Left: Build map with one sensor. Right: Build map with several sensors. [34]

The researchers in [36] presented another method to provide the haptic force to the joystick. Instead of pushing the wheelchair away from the obstacles, the haptic force guides the user to the free collision path designed by the Vector Field Histogram method. The experiments on a virtual simulator were carried out with a group of children who suffer from cerebral palsy and muscular dystrophy. While most of the research using the number of collisions as a perfor-
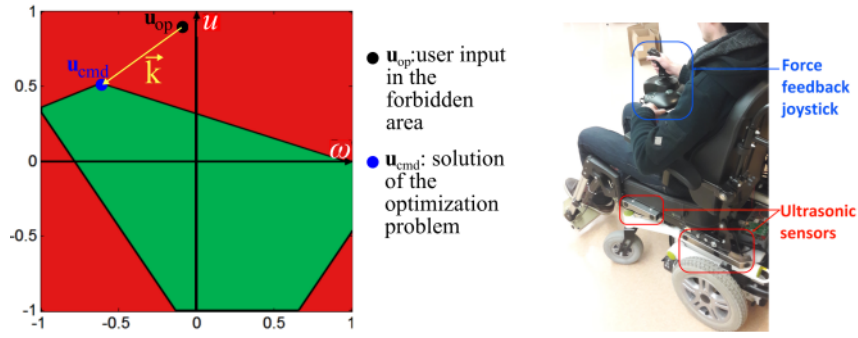
Figure 2.9: The optimal solution on the joystick velocities map and the experimental wheelchair [35]

mance indicator, this research uses the joystick movements and trajectory analysis as the driving performance indicators. The results showed that the haptic force reduced the travel time, the amplitude and angle variation of the joystick. It means that the users had smoother trajectories and therefore increase their comfort. However, while some users were being guided by the joystick, some others reported their inconvenience ("feeling to fight against the wheelchair"). The reason may be that the designed assistance system lacked an efficient procedure to manage the conflict between users and the system.

Figure 2.10: Experiment wheelchair with joystick force feedback modified from the Microsoft Sidewinder Force Feedback 2 [36]

To augment the user motor's performance, the traditional force feedback joystick was combined with a wearable skin-sketch device in [12]. This device consists of actuators, a timing belt, and several transmission mechanisms as in Fig. 2.11. It provides the haptic force by

stretching the user's skin thanks to the timing belt. Using this device, the user receives the angular velocity suggestion from the assistance system. The experiments were conducted with a virtual reality simulator. The results showed that combined sensory feedback improves the quality of driving, provides more distinct effects on the improvement of the user's performance. The authors suggested that "skin is a good receptor; therefore, cutaneous stimulations have the great feasibilities to serve as an efficient augmented sensory feedback."
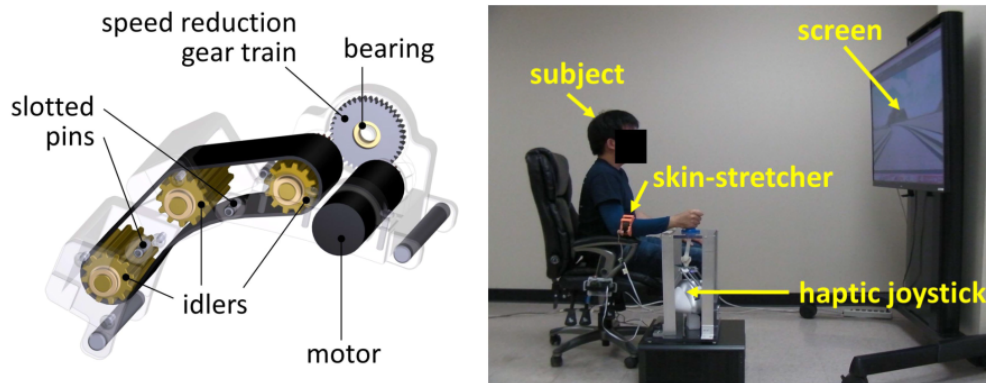
Figure 2.11: The skin-stretch device used for skin haptic feedback and the experiment setup with virtual-reality simulator [12]

Argue that the joystick force feedback does not allow the users to overrule the guidance of the assistance system, the authors in [11] used a wearable vibrotactile armband device as the unique haptic feedback interface for wheelchair users. The advantages of this device are flexible, inexpensive and compatible with different patient conditions and wheelchair configurations. Different from the above skin-stretch device, this device using four vibrating motors as shown in Fig. 2.12. The real-world experiments were conducted with fifteen able-bodied participants in two cases: with one vibrotactile armband; and with two vibrotactile armbands. The haptic vibrators can be configured to provide the information about the nearest obstacles or the suggested path to follow. The experiment results confirmed the effectiveness of this approach where the number of collisions reduces significantly and the participants provided positive feedback on the usability and comfort of this device. However, the guidance for obstacle avoidance function was not successful because the participants found uncomfortable with the sustained vibration. Also, even the user can overrule the suggestion from the system, how the system reacts in the case of conflict was not detailed.

Another human-wheelchair interface that attracted much interest is the brain-machine in-
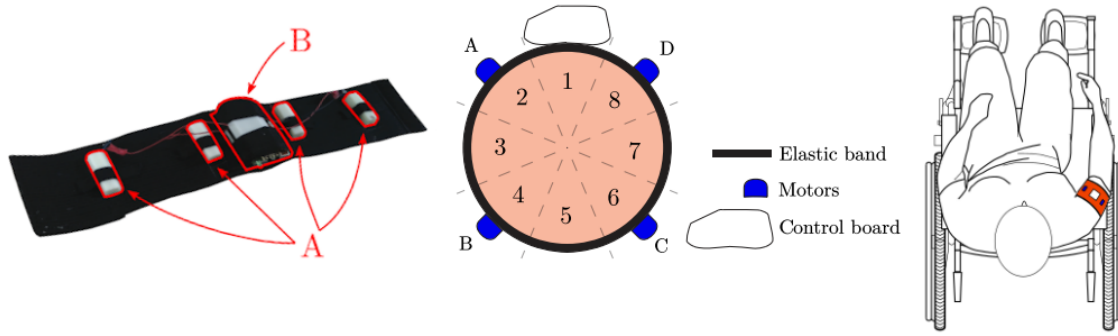
Figure 2.12: Left: The vibrotatile device with 4 vibrating motors (A) and control board (B); Center: Eight directions provided by joint action of four motors; Right: Wheelchair user with armband on the right upper arm. [11]

terface (BMI). The most important advantage of BMI is that it does not require the peripheral nervous system to mechanically interact with the world but only use the brain signals directly. Therefore, this interface is suitable for the user who is unable to operate a conventional interface due to their severe motor-disabilities. This method uses an array of electrodes placed on the scalp which allow monitoring in real-time the electrical activities of the brain (Fig. 2.13). This process is called electroencephalography (EEG). Recognizing patterns allows the researchers to determinate the desired user's actions linked to the specific brain signal patterns. These patterns will be synchronized with the surrounding environment to detect the user's intentions which will be realized by the low-level motor controllers.
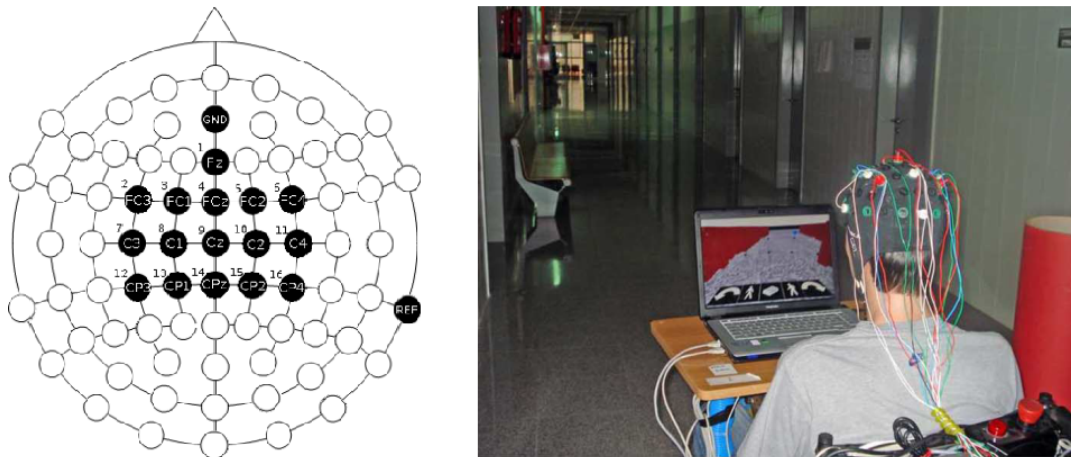
Figure 2.13: Brain-Machine Interface. Left: Electrode array for the acquisition EEG data [6]. Right: An example of head scalp for collecting the EEG data to control a wheelchair [37].

A navigation assistance system for power wheelchair using BMI was presented in [37]. Fig. 2.14 shows the architecture of the proposed approach where the human-machine interac-

tion was through BMI and laptop screen. To drive the wheelchair, the user had to rely on an augmented reality representing the surrounding environment on the laptop screen in front of him/her and the command icons which allow them to choose the desired motions. By focusing on the stimulus point or command icons (Fig. 2.14) the user can choose his/her desired destination or the actions. The Brain-Computer system will detect the decisions using the brain's EEG signals and pattern recognition function. The user's decision is then transferred to the navigation system to realize wheelchair motions thanks to the TCP/IP protocol. It can be seen that the BCI in this case aimed to replace the tradition joystick where the users can express continuously their intentions. The sharing action was presented where the system tried to detect these intentions and helped to realize them. The visual feedback is used to provide the options to users and also to confirm the user selections. The experimental results showed that the BCI can help the users realize their navigation task where the learnability and the confidence of the user during the test were high. However, the main drawback of this approach was the low information transfer rate and the workload of the user. Focusing continuously on-screen during navigation tasks may increase user workload. The waiting time for input from the user which accounts for at least 60% of travel time needs to be reduced.
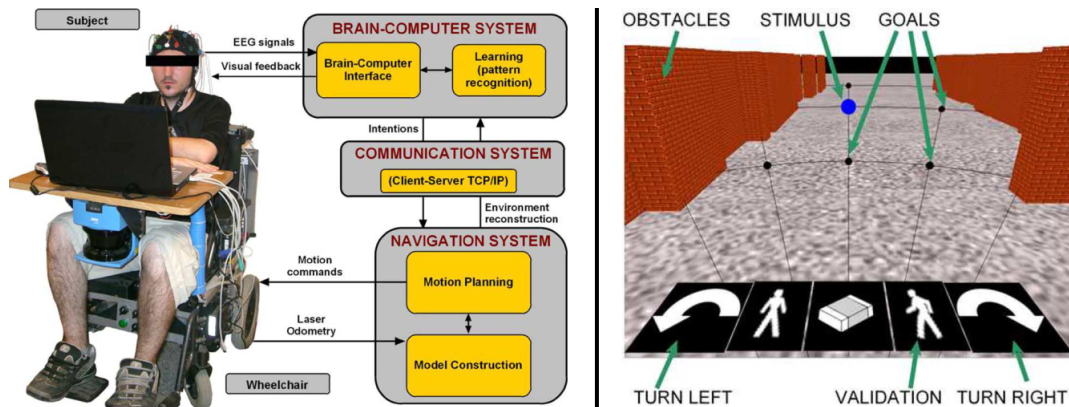
Figure 2.14: Shared control architecture of the Assistance system using BMI in [37].

The researchers in [6] proposed shared control solutions (Fig. 2.15) to overcomes these drawbacks. Instead of requiring a continuous control of the wheelchair by the user using BMI, this mission was transferred to an automatic navigation controller which made the wheelchair continues to travel forward and automatically avoid obstacles without user intervention. The user was placed as a supervisor who only intervenes when necessary by issue a high-level turn

left or turn right command through a BMI. With this architecture, the authors expected to reduce the user's cognitive workload and travel time. While the user issue his command using BMI, he/she receives the system's feedback about the surrounding environment and his/her decisions thanks to a small screen in front of them (Fig. 2.15). The camera and sonar sensors were used for the automatic navigation task. Experimental results showed that the travel and stationary time was reduced significantly compared to that of [37].
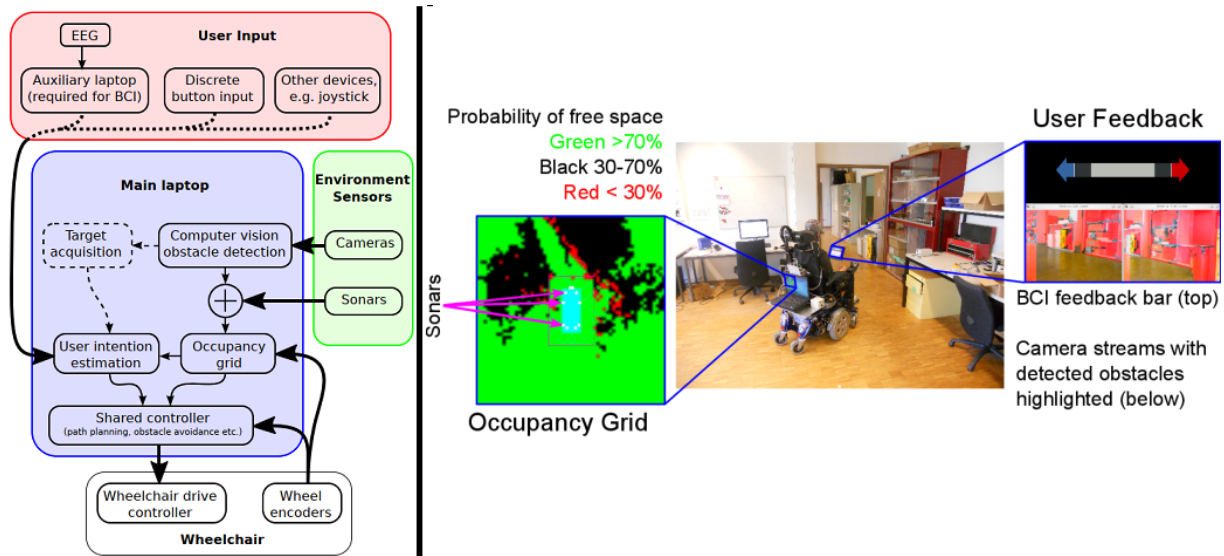
Figure 2.15: Architecture of the Shared control Assistance system using BMI (left) and user-machine interface (right) in [6]. In case of no user command, the wheelchair continues to move forward thanks to the shared controller.

While the above researches design the assistance system based on an explicit model linked to the environment which is discovered by the sensors (laser, sonar, camera,..), the researchers in [38] proposed a method to learn shared control policies from demonstrations offered by a human assistant (Fig. 2.16). The idea is that the assistance through haptic force feedback joystick will be trained to mimic the assistance force provided by a human remote assistance. Firstly, they created a map among the user's inputs, environment information, and appropriate assistance commands by training a Gaussian process regression model to continuously regulate the level of assistance. Then experiments were conducted with both remote human and the trained assistance programs. One important finding is that the efforts of the user in manipulating the joystick were reduced with the presence of haptic feedback. Different from other researches where the haptic force is provided only when approaching the obstacles, this finding may sug-

gest an assistance system that provides haptic forces continuously, not only limited in obstacle avoidance goal, to reduce the user efforts.

Figure 2.16: Experiment set up in [38] where the remote assistant who is provided with a visualization and real-time camera capture.

While the above research showed that the assistance system can learn how to assist from human assistant, a robotic wheelchair trainer was proposed in [39] to help the children with a severe movement disability learn the wheelchair driving skills. Basically, this robotic wheelchair is an autonomous robot that operates by a camera to detect the predefined path pasted on the floor (Fig. 2.17). The haptic force was delivered base on the estimation values of position, velocity errors, and joystick's stiffness and damping coefficients. There were 22 non-disabled children and 01 child with a severe motor impairment due to cerebral palsy involved in the experiments. The results showed that this approach can help to improve the steering skill, the travel speed of both the non-disabled children as well as the child with motor impairment.

The above review on shared control, especially applied to designing the assistance system for power wheelchair reveals a fact that there are different conception around so-called "shared control". The differences come from the protocol of each research which defines where, when, and how the control actions are shared between the human and automatic system. Aim to provide a common topology of shared control for multi-domain applications and inspired by the hierarchical control, a hierarchical framework for shared control between human and machine (automatic/assistance system) was proposed in [25] (Fig. 2.18). Vertically, this architecture consists of 4 task levels: strategy, tactile, operation, and execution. At each level, the human and robot have their capacities to realize the task at this level. The task at each level requires a

Figure 2.17: Robotic wheelchair guided the children to learn driving skills using force feedback joystick [39].

different type of capacities, e.g. the tasks at the strategy level require knowledge-based capacity while that at the operational level demands the skill-based capacities. Horizontally, the tasks at each level are shared between the human and machine (or user and assistance system in case of a power wheelchair) through the so-called Multi-modal interaction interface. This can be the joystick on a wheelchair, steering wheel in a car, or haptic screen for another application, ... The contents to be shared at these interfaces depend on which level the shared task belongs to. At the strategic and tactical levels, the knowledge-based contents are more relevant to increase the situation awareness for both agents, human, and assistance systems. On the other hand, the skill and rule-based contents are often shared at the operational and executive levels to realize together a specific task. Between two tasks, there is a goal sharing function that will allocate the goals for the tasks at the next sub-level depending on the decisions at this higher-level. It should be noted that the robot/assistance system, which has full capacities as in Fig. 2.18, is an ideal robot which does not exist now. At this moment, each robot/assistance system is designed for a specific task, possesses some specific capacities/interfaces, and works on some task levels among 4 levels in Fig. 2.18.
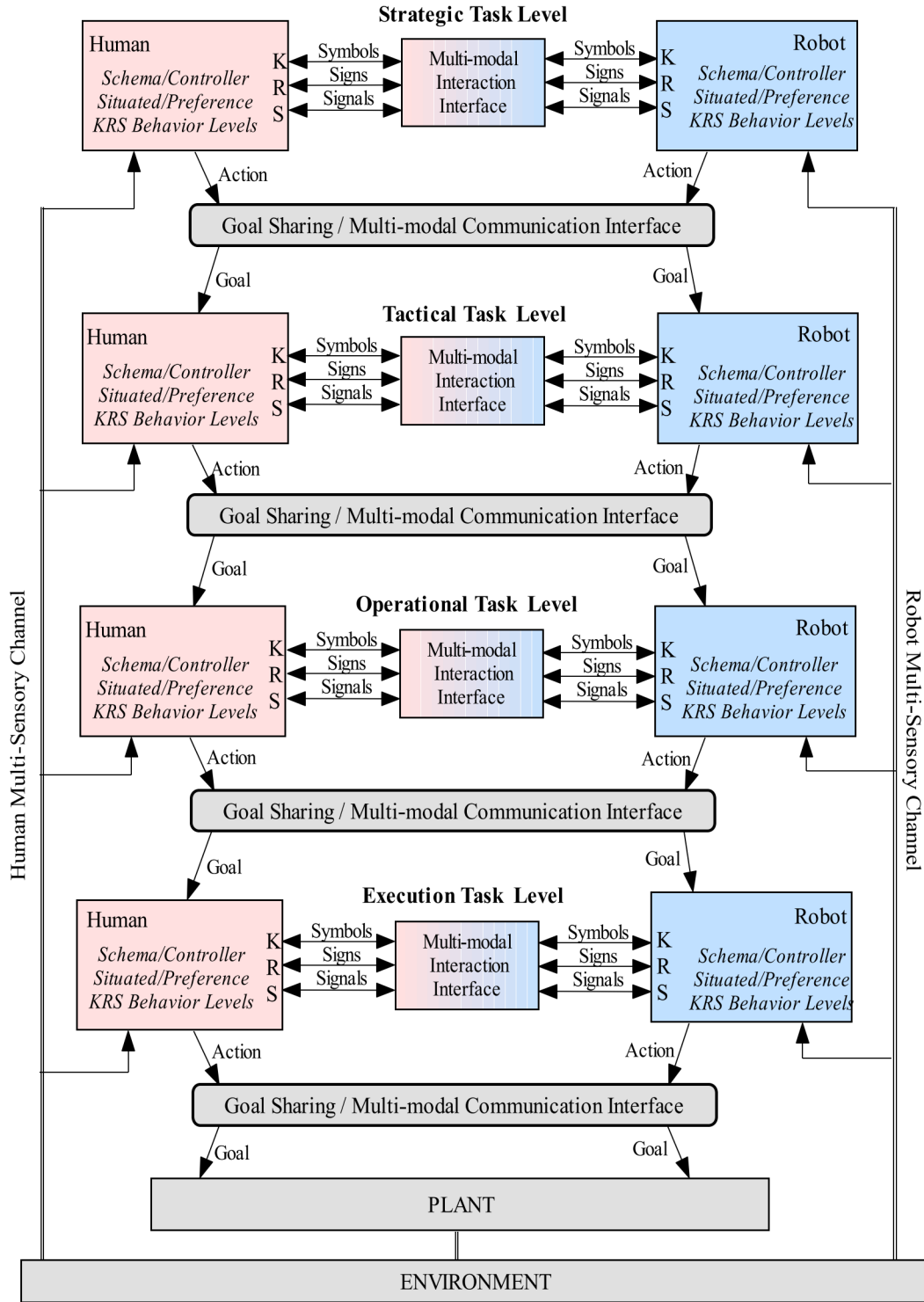
Figure 2.18: Hierarchical framework for shared control between human and machine [25]. At each task level, the human or robot receives its goal from the higher level and gets the environment data. It then exchanges selective information with its collaborator and provides the appropriate action which will be merged with that of its collaborator before acting on the plant or the lower level.

2.4 Discussion and conclusion

This chapter has presented an overview of the recent development of an intelligent wheelchair with emphasizing on the shared control method applied to the design assistance system for a power wheelchair.

In general, the power wheelchair works in an unstructured environment, with a user who has limited capacities, and user's needs/preferences vary depending on their mental and physical health status. Therefore designing a general assistance system that can adapt to every different user seems to be an impossible task now. Each research on assistance system now focuses on a specific group of users who have similar capacities in driving the power wheelchair. With the advance in robotics and sensor fields, the proposed assistance systems have shown their advantages such as reducing workload, improving driving skills, maintain comfort during navigation tasks. Combining the strong points of both user and system, the shared control method allows maintaining the activeness of the user during navigation tasks while always assists as needed the user. Although there is much advance in shared-control design for the wheelchair, the researches only focus on some aspects of the navigation task. While some research focus on the wheelchair performances (number of collisions, travel time ..), the other concern with the user's comfort (joystick movements, jerk, ...). Also, the conflict between users and the system does not receive much attention in designing the assistance system.

In this thesis, we aim to develop a shared control-based assistance system for electric power wheelchair users which satisfies the requirements as mentioned at the end of section 2.2 through a haptic force feedback joystick. To that end, chapters 5 and 6 will detail the design steps and the validation results.

From the above review on development of assistance system for power wheelchair, it can be seen that there are several research using the virtual reality simulator to validate their proposed systems [12] [36] [34]. This approach helps to reduce the time, cost and satisfy the safety constraints of the validation experiments [40]. In the next chapter, we review the existent virtual reality wheelchair simulator solutions and then develop a dynamic model of a wheelchair used for wheelchair simulator platform at our laboratory, which is necessary for developing the validation experiments.

Chapter 3

Dynamical model of wheelchair

Contents

This chapter presents the development of a dynamical model of wheelchair specified for a wheelchair simulator platform. We present here the context and motivations for this work. Then we start with the kinematic and dynamic models inherited from the vehicle ones. With focus on the performance of wheelchair at the low-speed region, this model comprises the tire-road contact forces and the influence of the front free caster wheels. Validation experiments simulating several typical daily manoeuvrers of the manual wheelchair were conducted. Compared to previous research, the new model presented in this chapter overcomes the problem

of overestimating the yaw rate. The content of this chapter has been presented at the IEEE International Conference on Systems, Man and Cybernetics (SMC), Bari, Italy in 2019.

3.1 Introduction

As mentioned in section 1.2, the virtual reality (VR) wheelchair simulator is a promising tool for testing and validating the concepts, strategies, and algorithm of the new assistance systems before conducting the real-world tests. Allowing to conduct the human-in-the-loop simulation without risk of collision and safety problems, it thus reduces the required time in design and performance evaluation of complex systems [41], [42, 43]. In the rehabilitation context, VR technology is a very effective tool for cognitive assessment and recovery [44]. It enables therapist to record patients' responses in real-time (e.g. emotion, motion control, perception), which is impossible with traditional tools. As with rapid prototyping, safety, customizable, repeatable scenarios are the advantages of VR simulator allowing to adapt to user conditions and facilitate the rehabilitation.

Figure 3.1: Virtual-reality System: PSCHITT-PMR (LAMIH) dynamic interactive platform for wheelchair simulations. It can be used with the manual, powered or hybrid wheelchairs (Hybrid wheelchair is basically a motorized version of manual wheelchair which can operate in both manual and powered mode or even assisted-manual mode).

The experimental platform called LAMIH "PSCHITT PMR" platform (French acronym for Collaborative Simulation Platform, Hybrid, Intermodal in Land Transport for Person with Reduced Mobility), has been developed for the design, validation and evaluation purposes. This platform allows to study the mobility of not only a power wheelchair but also a manual and hybrid wheelchair in a simulated environment (see Fig. 3.1). Thanks to the GoughStewart parallel robot, this platform allows performing three-dimensional movements in order to reproduce the real senses of motions for the participants. Six large screens in front of participants display the virtual environment of designed scenarios. The immersive aspect is ensured by the SCANeR Studio software environment (AVSimulation). To mimic the sense of hand-propulsion in case of manual wheelchairs, the two wheels are put on two rollers which are motorized by two electric motors. The mission of these motors is to reproduce the real-world resistance to the wheels based on the provided conditions about the simulated environment such as slope/inclined angles, tire-road interaction properties,...

Fig. 3.2 shows the structure of PSCHITT-PMR simulator platform. The software parts are built on the Matlab/Simulink environment connecting to the hardware parts through the application programming interfaces (API). The software parts consist of a dynamical model of wheelchair and a haptic controller. The participant acts on the joystick or hand rim to provide motor/hand torques to the wheels. Based on these measured torques and the predefined virtual environment conditions (tire road contact, slope/incline, etc.) the dynamic model of wheelchair block calculates the appropriate wheels' rotation speed profiles which are expected to be coherent with the real-world motions. These speeds are sent, on the one hand, to the SCANeR Studio software which reproduces these motions on the virtual-reality screens. On the other hand, these speed profiles are the references for the speed control system (haptic controller) which regulates the wheel's speeds to provide the real feeling of resistance torques to the user (in the case of manual wheelchair).

The development of the haptic controller for this simulator had been presented at the IEEE International Conference on Systems, Man and Cybernetics (SMC), Bari, Italy in 2019 [45]. The rest of this chapter will focus on the development of a dynamical model of wheelchair which can be applied to manual, power and hybrid wheelchair with an appropriate modification
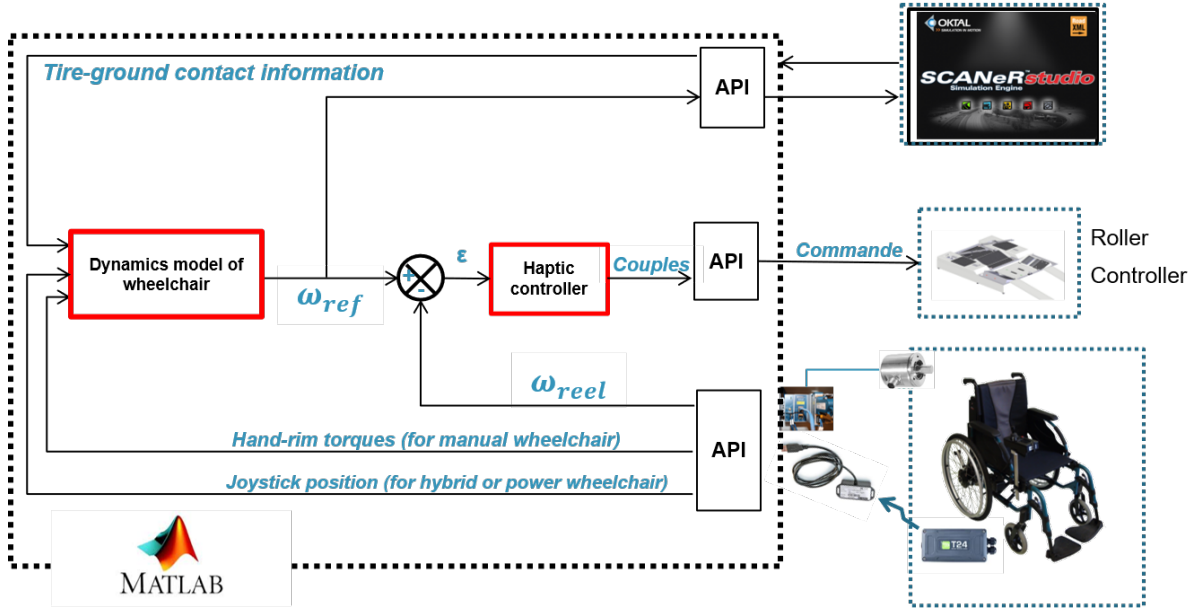
Figure 3.2: The general platform schema of PSCHITT-PMR simulator at LAMIH

to provide a more realistic propulsion and movement experience to the target users in the virtual scenes. This model can be also used as a virtual wheelchair to validate the automatic control algorithms (navigation, obstacle avoidance ...) for wheelchair, for example, as in [19].
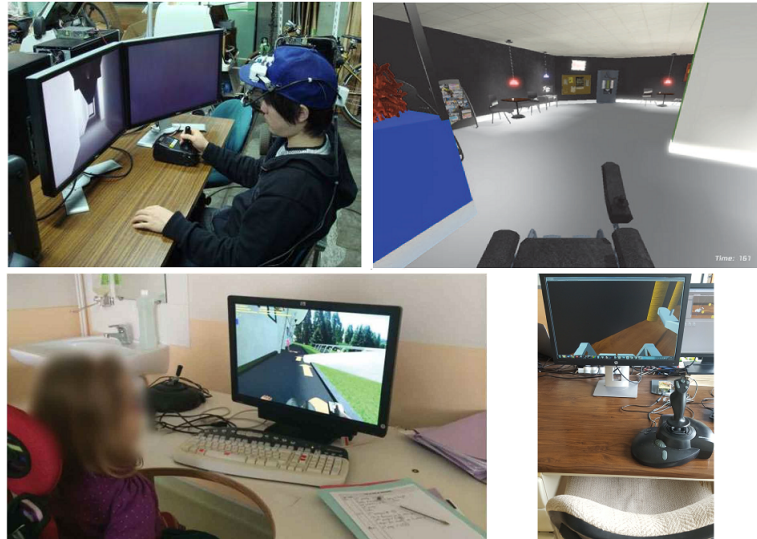
Figure 3.3: Several virtual reality experiment configurations with a single screen [12] [36] [46] [47] [48]

Many power wheelchair simulators have been developed with different configurations. Most of simulators come with a single screen [12] [36] [46] [47] [48] [49] (Fig. 3.3). To increase the sense of presence of user in the virtual environment and the realism in users' inter-

actions, the wheelchair simulators in [45], [48], [50] are equipped with multiple screens around the participants, Stewart platform and the rollers (Fig. 3.4). While these researches evaluated different aspect of user's driving such as joystick movements, wheelchair trajectories, sense of presence, user's workload, the dynamical model of wheelchair which links the joystick commands to the motions of the virtual wheelchair were not well addressed.
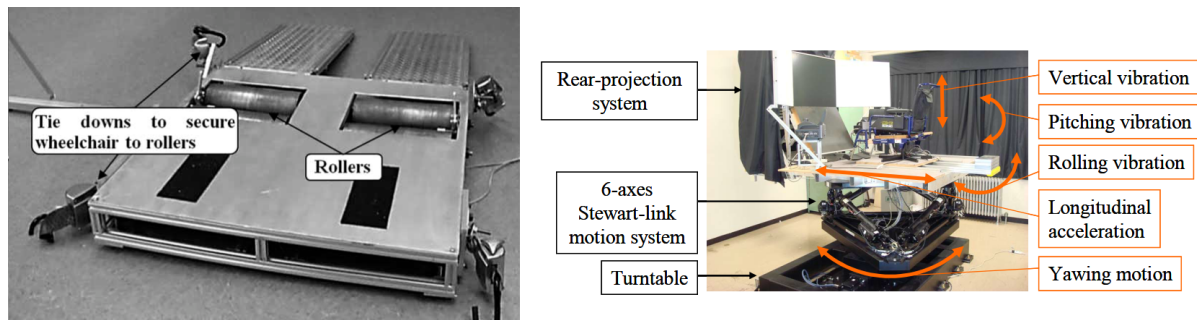
Figure 3.4: Wheelchair simulator with multiple screens, roller and Stewart platform [48], [50]

To develop a longitudinal stability system for power wheelchair, a dynamical model which takes into account the dynamic of front caster wheels and mass distribution was developed in [51]. However, the tire-ground interaction was not considered. The kinematic model of front free caster wheels was developed in [52] in order to design a driving assistance system for wheelchair. While the result shows that the first-order transfer function is enough to model the caster wheel behaviour, its application to the wheelchair simulator was still unrevealed. While the manual and power wheelchairs are different from the power sources and ergonomic configurations, the motion laws and tire forces creation principles are the same. Therefore, we review here also the development of dynamical model of manual wheelchair. A comprehensive model of manual wheelchair was developed in [53] for wheelchair simulation platform in the Challenging Environment Assessment Laboratory (CEAL) at Toronto Rehabilitation Institute. This model integrated the tire-ground contact forces using the Pacejka Tire Model for the longitudinal, lateral forces and alignment moments. The validation experiments showed that while the simulations of wheels velocities at high speed were coherent with the real ones, the overestimate problem of yaw rate of the wheelchair was still a challenge due to the complexity of tire-road contact at the low-speed region. The mechanical properties of wheelchair tires were evaluated through directly measuring the tire forces in [54]. The longitudinal, lateral forces and

alignment moments were investigated using the Magic Formula tire model. In [55] a dynamic model of manual wheelchair on the straight and curvilinear paths was given. An identification process to estimate the inertia and friction parameters of the manual wheelchair were presented also. Although the estimation of wheels speeds was reasonable, the authors also concluded the moment of inertia of the yaw motion was underestimated. The influence of the front wheels on the turning resistance of the wheelchair was exploited in [56]. The research results showed the linear dependence of the turning resistance on the geometry parameters and the ground surface. However, a dynamical model of the wheelchair was not given. In [57] an open-loop observer was developed to estimate the caster wheel's orientation. Based on a simple kinematic model of the wheelchair, this observer neglected the influence of the tire-road contact and therefore, the model of the front wheels became quite sensible and started turning earlier than reality. The rolling resistance acting on manual wheelchair was investigated in [58] where the coast-down test was used. Some configurations of manual wheelchair were considered such as tire types, ground surfaces, and load distribution.

The rest of this chapter reports the results of the performed research activity and is organized as follows: The general dynamical model of wheelchair based on a vehicle model [59] will be presented in Section 3.2. Section 3.3 shows the system of forces and moments acting on the wheelchair. Section 3.4 shows the experimental set-up and the experiment results. Finally, some remarks on the model of power wheelchair based on the proposed dynamical model and some conclusions are withdrawn in the last sections.

3.2 Dynamical model of wheelchair

3.2.1 Configuration of systems

Fig. 3.5 presents the right-hand coordinate frames used to describe the motions of the wheelchair. The configuration of the wheelchair dynamics model consists of two rear drive wheels, body (human and wheelchair body) and two front caster wheels. The wheelchair center of gravity of is placed at a distance d from the rear wheel axis. The global frame $GXYZ$ is fixed with the

earth while the body frame $Oxyz$ is located at the wheelchair center of gravity. The Ox axis is along the direction of wheelchair and the Oz axis points out of the screen. The center of gravity of the user-wheelchair system is located at distance l_d front the rear axle and w_d from the centerline of the wheelchair. The motion equations in the next section are derived within the body frame while the position and direction of wheelchair are expressed in the global one. In this research, the motion of the free front caster wheels are considered as an important factor contributing to the motions of wheelchair and therefore each front wheel is attached to a coordinate frames $O_{c_i} x_{c_i} y_{c_i} z_{c_i}$ as in Fig. 3.6.
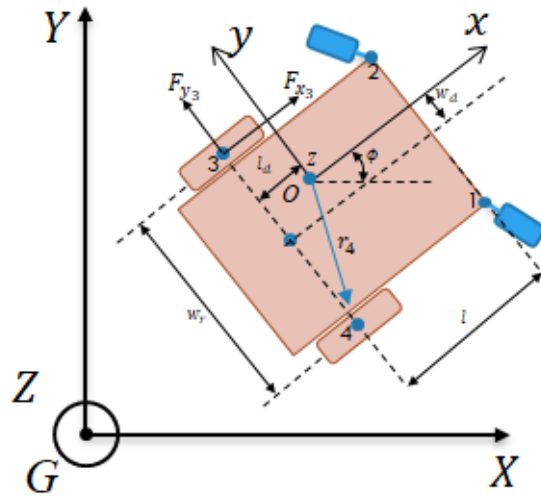
Figure 3.5: Coordinate systems and configuration of wheelchair
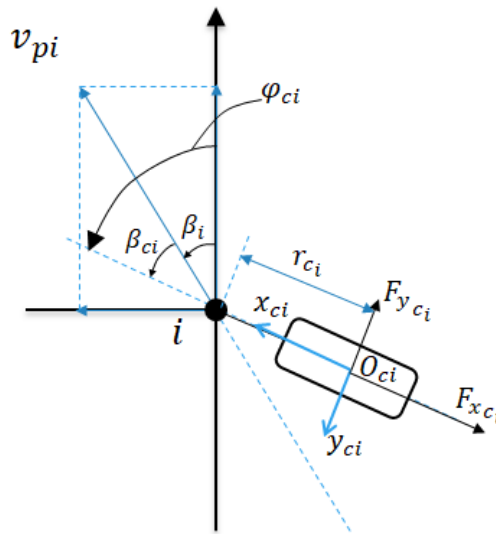
Figure 3.6: Coordinate systems and configuration of the front caster wheels

35

Given the wheelchair velocity $v = [v_x \; v_y \; v_z]^T$ at the center of gravity, the velocity of the pivot points where the wheels are attached to the body of wheelchair are

$$v_{p_i} = v + r_i \times \omega, \quad i \in \{1...4\} \tag{3.1}$$

where ω is the angular velocity of the wheelchair and v_{p_i}, r_i are the velocity and position of the mounted points, respectively. The side-slip angles of the two rear wheels are

$$\beta_i = \arctan \frac{v_{y_i}}{v_{x_i}}, \quad i \in \{3,4\} \tag{3.2}$$

The front free caster wheels can rotate about the vertical axis at their mounted points. In order to derive the tire-road contact forces at the front wheels, their velocities in the body frame should be projected to their own frames by the rotation matrix about $z-$axis (3.3). The velocities of these wheels in the their own frames are

$$R_z(\cdot) = \begin{bmatrix} cos(\cdot) & -sin(\cdot) & 0 \\ sin(\cdot) & cos(\cdot) & 0 \\ 0 & 0 & 1 \end{bmatrix} \tag{3.3}$$

$$v_{c_i} = R_z(\varphi_{c_i}) \left[v_{p_i} + r_{c_i} \times \omega_{c_i} \right], \quad i \in \{1...2\} \tag{3.4}$$

where φ_{c_i} is the angle between the direction of the front wheels and the direction of the wheelchairs. r_{c_i} are the position vectors and ω_{c_i} are the angular velocity vectors of the rotation about vertical axis at their pivots.

3.2.2 Motion equations of systems

In this research, we consider the planar motions of the manual wheelchair including the longitudinal, lateral and rotational motions. The kinematic equations of the wheelchair model is

36

given by

$$\dot{v}_x = a_x + \omega v_y \tag{3.5}$$

$$\dot{v}_y = a_y - \omega v_x \tag{3.6}$$

where a_x, a_y are the longitudinal and lateral accelerations, respectively, which are described by

$$a_i = \frac{1}{M}\sum F_i = \frac{1}{M}\left(F_{tr_i} + F_{gr_i}\right) \quad i \in \{x, y\} \tag{3.7}$$

$$\dot{\omega} = \frac{1}{J_z}\sum T = \frac{1}{J_z}\left(T_{act} + T_{res} + T_{fr}\right) \tag{3.8}$$

where F_{tr_i} and F_{gr_i} are the traction forces and gravity forces, respectively. M and J_z are the total mass human-wheelchair and the inertial moment about $z-$axis, respectively. T_{res} is the resistance on the yaw motion of the wheelchair and T_{fr} the effect of the direction of the front wheels. These torques will be detailed in the next section. T_{act} denotes for the whole of rotation torques from wheelchair user and the tire-ground contacts

$$T_{act} = \sum^{i=3,4} r_i \times F_i + \sum^{i=1,2} (r_i + r_{c_i}) \times F_i \tag{3.9}$$

where $F_i = [F_{x_i}\ F_{y_i}\ F_{z_i}]^T$.

The rotations of the wheels are under the actions of hand-rim torques from the user T_h, the traction torques from the tire-road contact T_{tr}, the rolling resistance torque T_{rr} and the the viscosity resistance T_{vi}

$$\dot{\omega}_i = \frac{1}{J_{w_i}}\sum T_i = \frac{1}{J_{w_i}}\left(T_{h_i} + T_{tr_i} + T_{rr_i} + T_{v_i}\right), \ i \in \{1...4\} \tag{3.10}$$

where J_w denotes for the inertial moment of the wheels. It should be noted that the hand-rim torques of the front wheels are null, obviously. The front wheels of the manual wheelchairs are generally made by the undeformed material and thus the rolling resistance acting on these wheels can be neglected. The viscosity resistance can be described by a simple model $T_{v_i} =$

$-\eta \omega_i$ where η is the viscosity coefficient. The traction torque T_{tr} can be found by $T_{tr_i} = R_i \times F_{tr_i}, i \in \{1...4\}$ where $R_i = [0\ 0\ -r_i]^T$ denotes for the radius vectors of the wheels and F_{tr_i} is the traction force vector.

The rotation of the front wheel about its pivot is caused by the lateral force F_{y_i} appearing when the wheel direction are deviated from the direction of the mounted point's velocity. This motion is described by

$$\dot{\omega}_{c_i} = \frac{1}{J_{c_i}} \sum T_{c_i} = \frac{1}{J_{c_i}} \left(T_{y_i} + T_{vc_i} \right), \quad i \in \{1,2\} \tag{3.11}$$

where $T_{y_i} = R_{c_i} \times F_{y_i}$ and $T_{vc_i} = -\eta_c \omega_{c_i}$ is the viscosity resistance. $R_{c_i} = [r_{c_i}cos(\varphi)\ r_{c_i}sin(\varphi)\ 0]^T$ is the position vectors of front wheels and r_{c_i} is the radius of rotation motion about the pivots. η_c is the viscosity coefficient of the rotation about the mounted points of the front free castor wheels.

3.3 Force system

All external forces acting on the wheelchair come from the interaction between the tire and the ground. These forces comprise the longitudinal traction/braking forces, lateral forces, rolling resistance and resistance on the rotation of the wheelchair.

3.3.1 Longitudinal and lateral tire forces

Among many tire model that exist in the literature, we adopted the Pacejka Tire Model (Magic Formula) (3.12) for the longitudinal tire force in this paper. This model determinates the normalized adhesion coefficient $\mu_i = F_{x_i}/F_{z_i}$ from the slip ratio λ_i of the wheels and comprises four parameters B,C,D,E that have to be identified from the experiments.

$$\lambda_i = \frac{r_i \omega_i - v_{x_i}}{max\left(v_{x_i}, r_i \omega_i\right)} \qquad i \in \{1...4\}$$

$$\mu_i = Dsin\left(C\arctan\left(B\lambda_i - E\left(B\lambda_i - \arctan B\lambda_i\right)\right)\right) \tag{3.12}$$

For the rear wheels, the lateral tire forces F_{y_i} depend on the side slip angles of the tires and vertical loads on them. Based on the research [60], we use here a simple linear model (3.14) for the lateral forces with assumption that these forces are saturated when the side slip angles excess β_{lim}.

$$F_{y_i} = \begin{cases} -C_{\beta_i}\beta_i F_{z_i} & \beta_i < \beta_{lim} \\ -C_{\beta_i}\beta_{lim}F_{z_i} & \beta_i \geq \beta_{lim} \end{cases} \quad i \in \{3,4\} \quad (3.13)$$

where C_{β_i} is the cornering stiffness. For the front free castor wheel, the lateral forces are created by the deviation of wheel's direction from the pivot movement direction. This deviation angle β_{c_i} can be deduced as illustrated in Fig. 3.6 and a simple model of lateral forces is given by

$$\beta_{c_i} = \varphi_{c_i} - \beta_i \quad (3.14)$$

$$F_{y_i} = \begin{cases} -C_{\beta_{c_i}}\beta_{c_i}F_{z_i} & \beta_{c_i} < \beta_{c_{lim}} \\ -C_{\beta_{c_i}}\beta_{c_{l}im}F_{z_i} & \beta_{c_i} \geq \beta_{c_{lim}} \end{cases} \quad i \in \{1,2\} \quad (3.15)$$

3.3.2 Modeling of the rotational torques of the wheelchair

In this section, we consider the resistance torques acting on the rotation of the wheels and the yaw motion of wheelchair. Although all these resistances appear at the contact patch between tire and ground, it is complicated to integrate them in a unique tire-ground contact model. Thus these resistances will be considered separately from the tire force model.

3.3.2.1 Rolling resistance on the rotation of the wheels

Rolling resistance represents the dissipated energy during the rolling motion of the wheels due to the hysteresis phenomenon of tire material when the tire is deformed. In general, this force is considered as a constant during the movement of the wheelchair. We consider here a rolling resistance model (3.16) with a modification at low speed to deal with numerical simulation

problem at zero speed.

$$F_{rr_i} = \mu_{rr_i} \left(1 - e^{-2\omega_i}\right) F_{z_i} \tag{3.16}$$

3.3.2.2 Resistance on the yaw motion of the wheelchair

The moment that is against the yaw motion of the wheelchair T_{res} is generally considered as the alignment moment at tire-road contact. According to the Pacejka Tire Model, this moment depends on the side slip angles of the tire. However, the movement of a wheelchair is more complicated than that of a vehicle, for example, turning 180° on place or turning with a stationary wheel. Therefore, we propose here a model of resistance torque (3.17) which depends on the rotation speed and is independent of the side-slip angle of the wheels.

$$T_{res}(\omega) = k\left(1 - e^{-b\omega}\right)\left(\frac{1}{2} + \frac{1}{2}\tanh(c\omega - d)\right)(h - (h - 1)\tanh(c\omega - d)) \tag{3.17}$$

where k, b, c, d, h are the model parameters needed to be identified. The main part of this model is the simple expression $k\left(1 - e^{-b\omega}\right)$ while the part $0.5 + 0.5\tanh(c\omega - d)$ adjusts the curve at the zero-speed region to deal with the chattering problem in numerical simulation. The expression $h - (h - 1)\tanh(c\omega - d))$ inserts high starting torque at the low speed. This expression comes from the fact that the starting torque is always much greater than that of high speed.

3.3.2.3 Effect of the direction of the front wheels

In general, the directions of the front wheels align the movement direction of the corresponding pivots. However, when staring, the deviation angles β_{c_i} can be large enough to create a considerable influence on the rotation of wheelchair. This phenomenon mostly comes from the rotation resistance at the contact wheel-ground of the front wheels. In this model, we propose a model (3.18) to reflect this phenomenon where a supplementary rotation resistance appears when the deviation angles β_{c_i} excess a threshold and the rotation torque T_{act} is opposite to the direction of the front wheels.

$$\bar{\beta}_c = \frac{1}{2}\left(\beta_{c_1} + \beta_{c_2}\right) \tag{3.18}$$

$$\bar{\varphi}_c = \frac{1}{2}\left(\varphi_{c_1} + \varphi_{c_2}\right) \tag{3.19}$$

$$T_{fr} = \begin{cases} -K_{fr}\bar{\beta}_c & \bar{\beta}_c < \bar{\beta}_{c_{lim}} \ and \ \bar{\varphi}_c T_{act} < 0 \\ 0 & otherwise \end{cases} \tag{3.20}$$

3.4 Experimental validation of the model

3.4.1 Experimental set-up

Fig. 3.7 shows the wheelchair used in the experiment. Two encoders are attached to the rear wheels to measure the rotation speeds of the wheels. For measuring the human hand torques, two torque transducers are installed between the hand-rim and the rear wheels. The obtained signals from these sensors are sent to the data acquisition center through the wifi connection. An inertial measurement unit is fixed under the chair to measure the yaw rate of wheelchair and the recorded data are transferred to the computer through the cables. The experiment scenarios are shown in Fig. 3.8 which comprise several common tasks that the users often use in their daily living. Test 1, test 3, test 5 and test 7 are the tests where the user pushes the wheelchair with a single push. Test 2 represents for turning slightly and passing a doorway. In test 4 the driver turning 90^0 with a stationary wheel while turning 180^0 in place in test 6. Table 3.1 summaries the parameters of wheelchair and the models which was identified by trial and error method from the experimental results in the next section.

3.4.2 Experiment results

Fig. 3.9 shows the evolution of the left and right-hand torques of the driver during the tests while Fig. 3.10 presents the evolution of the deviation angles of the front free caster wheels φ_{c_1} and φ_{c_2}. It can be seen that the rotation of the front wheels about the pivot axis are reasonable. The deviation angles increase when the wheelchair makes a turn and decrease to about zero

Table 3.1: Parameters of the wheelchair and the proposed models

Parameter	Value	Unit	Parameter	Value	Unit
m	100	kg	B	2	
J_z	7	$kg \cdot m^2$	C	2	
J_{c_i}	0.05	$kg \cdot m^2$	D	0.2	
$J_{w_{1,2}}$	0.008	$kg \cdot m^2$	E	0.8	
$J_{w_{3,4}}$	0.27	$kg \cdot m^2$	$C_{\beta_{3,4}}$	1.72	rad^{-1}
η_c	0.65	$kg \cdot m^2 \cdot s^{-1}$	$C_{\beta_{c1,2}}$	6	rad^{-1}
η	0.05	$kg \cdot m^2 \cdot s^{-1}$	β_{lim}	0.15	rad
w_r	0.575	m	$\beta_{c_{lim}}$	0.25	rad
l	0.5	m	$\bar{\beta}_{lim}$	0.1	rad
l_d	0.08	m	k	10	
$r_{c_{1,2}}$	0.05	m	b	8	
μ_{rr}	0.01		c	8.5	
K_{fr}	12	$Nm \cdot rad^{-1}$	d	9.5	
			h	9	
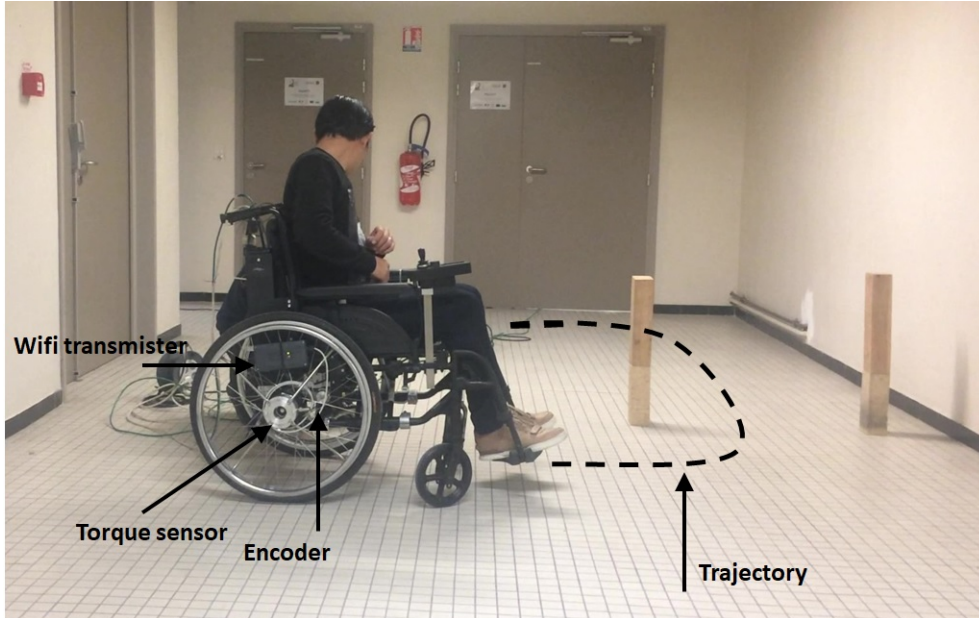
Figure 3.7: Experiment setup for the manual wheelchair.
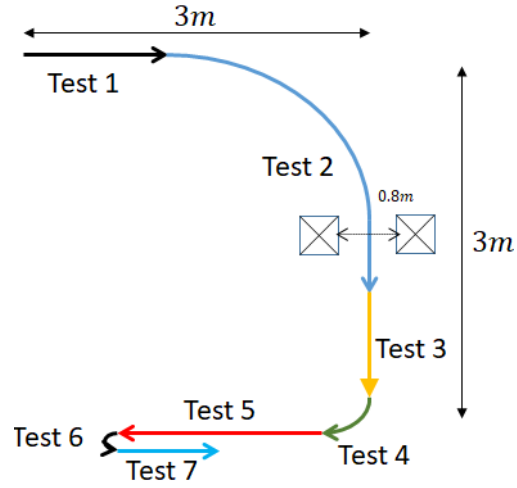
Figure 3.8: The trajectory and the tests used in the experiments
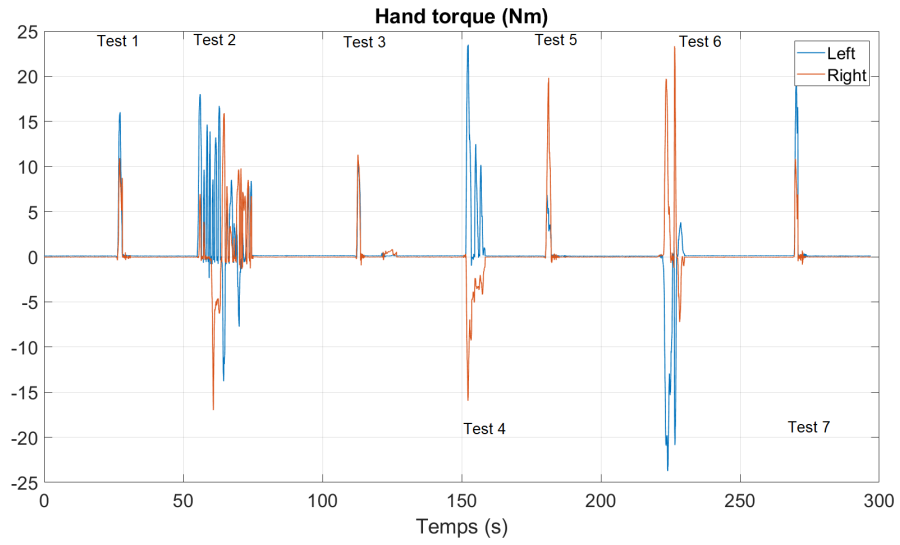
Figure 3.9: The left and right hand torques of driver in the tests.
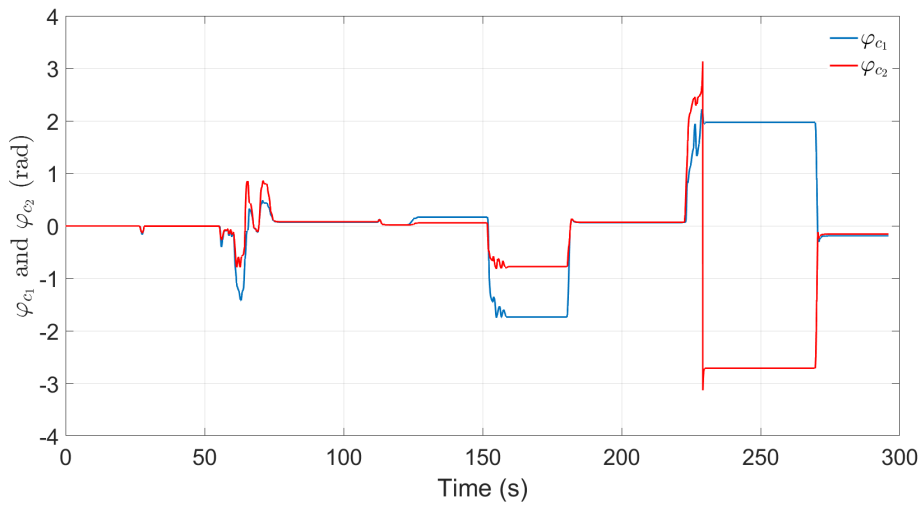
Figure 3.10: The left and right rotation angles of the front free wheels in the tests.

43

when the wheelchair goes straight.

Fig. 3.11 compares the experimental and simulation results in the case where the wheelchair goes straight with a single push in test 1, test 3, test 5 and test 7. It can be seen that the experiment results are different from each other and the simulation results show the coherent with the experiment results. The input hand torques are also different from test to test due to the influence of the deviation angles of the front wheels. In test 1 and test 3, the input hand torques of the right and left hand are only slightly different from each other because the deviation angles of front wheels are small. However, in test 5 and test 7 the deviation of the front wheels lead to a significant difference between the right and left torques and the errors of wheel speed simulation.
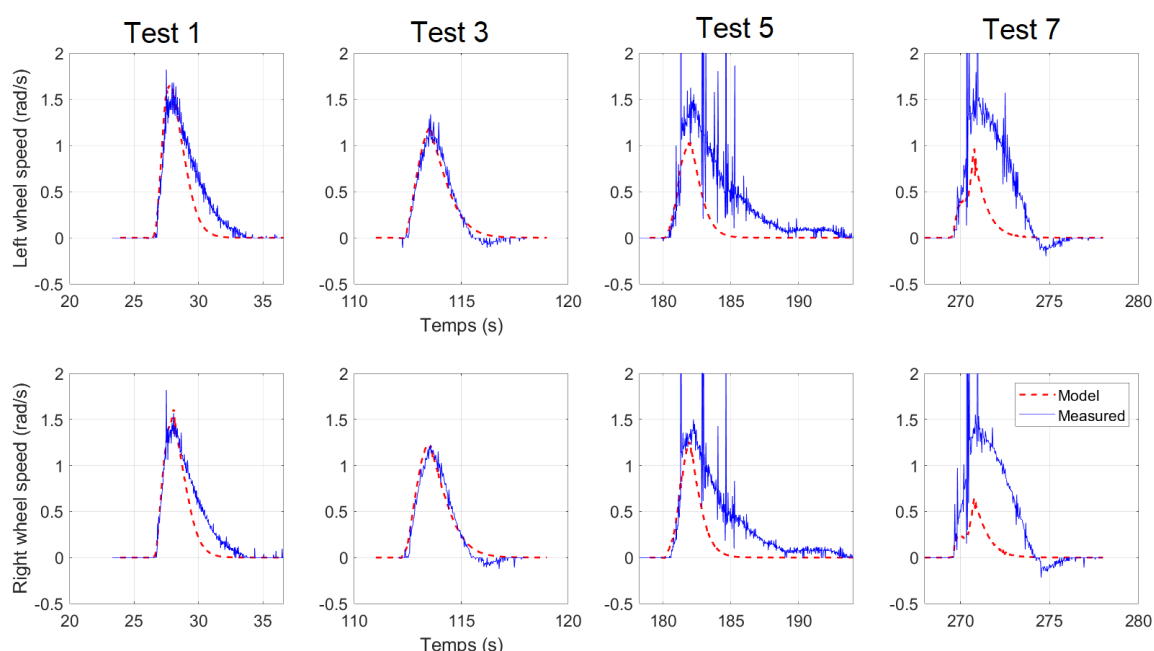
Figure 3.11: The simulated (red line) and measured (blue line) speed of the left and right wheel speed of the go-straight tests.

Fig. 3.12 shows the results of step 2 where the driver is required to turn slightly and then to pass the doorway. It can be seen that the simulation results are quite good when they are near the experiment ones. By considering the effect of the direction of the front wheels, the response of the yaw rate is more accurate than that in the case without the model of the front wheel's direction. The errors in the response of wheel speeds may come from the small incline of testing ground which was not included in the model. Fig. 3.13 shows clearly the effect of

front wheels direction on the wheelchair dynamics. In real performance, the user has to create a considerable rotation torque to make the wheelchair goes straight when the front wheels are not aligned with the motion direction of the wheelchair. This phenomenon is integrated into the model of the effect of the front wheel direction in section 3.3.2.3.
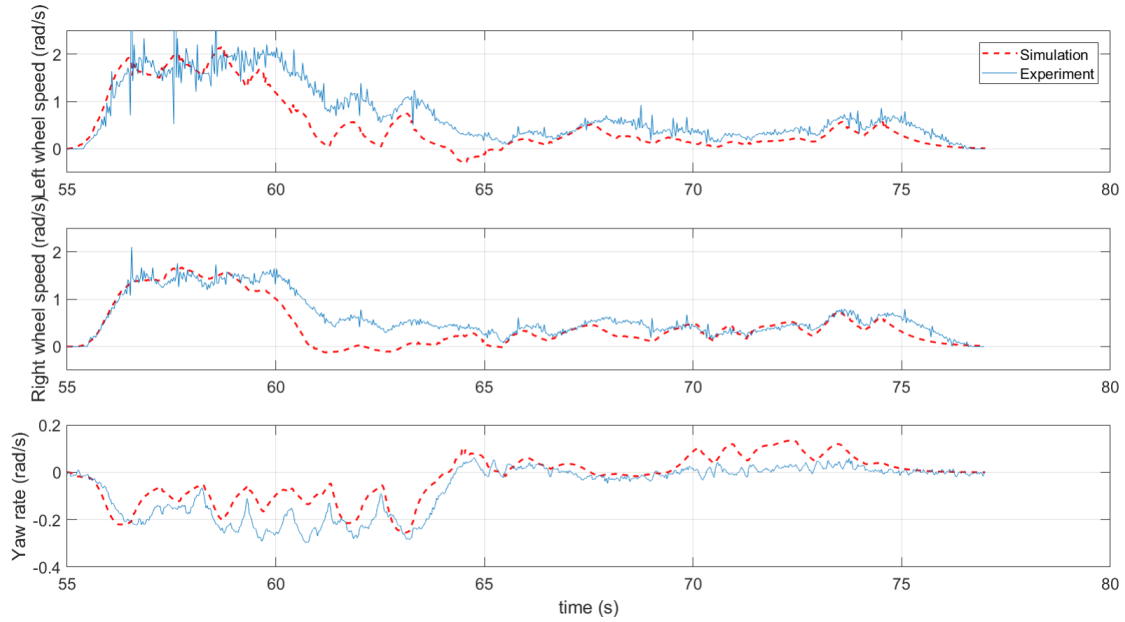
Figure 3.12: Comparison the simulated (red line) and measured (blue line) wheel speeds and yaw rate in the test 2

Fig. 3.14 shows the simulation and experimental results in step 4 where the wheelchair turns 90^0 with the stationary right wheel. It can be seen that, in general, the simulation results of yaw rate, left and right wheel speeds are consistent with the real ones, especially in amplitude. The simulation speed of the right wheel fluctuates about $\pm 0.1 (rad/s)$ and it is very near to the real one. The simulated left wheel speed and yaw rate have the same amplitude with the experiment results although they increased faster, about $0.25sec$. This can be explained by the lack of the starting torque in the model of rolling resistance. In addition, the user controls the speed and the torque at the same time and therefore this leads to the challenge in modeling the dynamics of the wheelchair.

Fig. 3.15 shows the results at step 6 where the wheelchair rotates 180^0 in place. The model responds consistently relative to real measurements.. In the first phase (from 223 to $226s$), the right wheel speed and yaw rate are similar to the real ones. The simulation speed of the left wheel increased faster than the real one in the first phase of the simulation, but was consistent

45
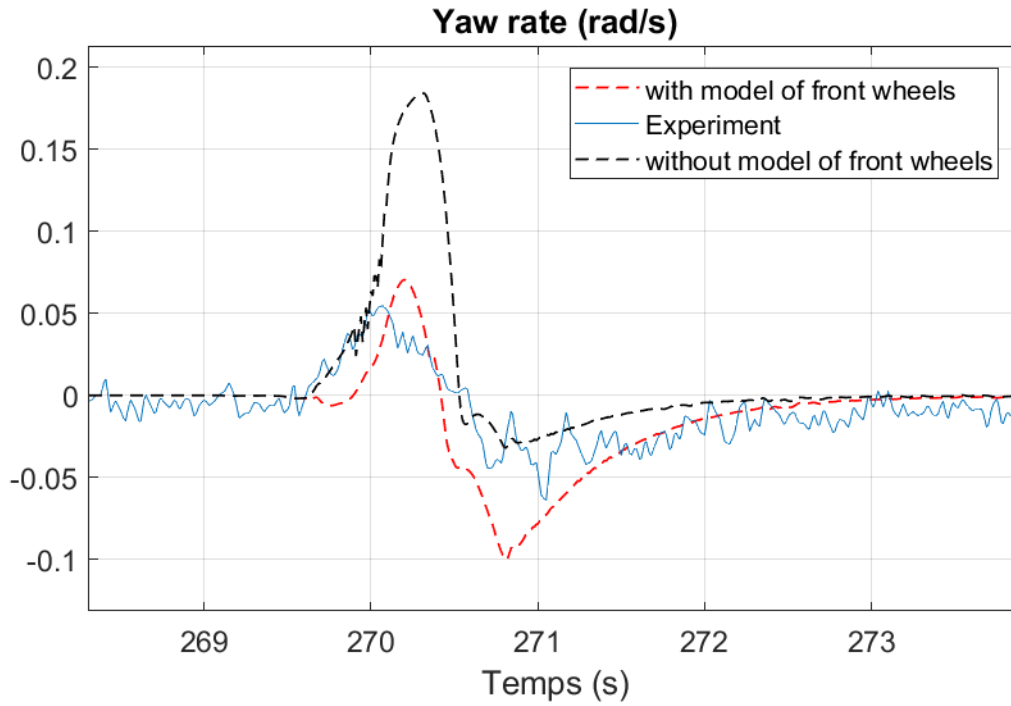
Figure 3.13: Yaw rate responses in the test 7 show the effect of the direction of the front wheels to wheelchair dynamics.
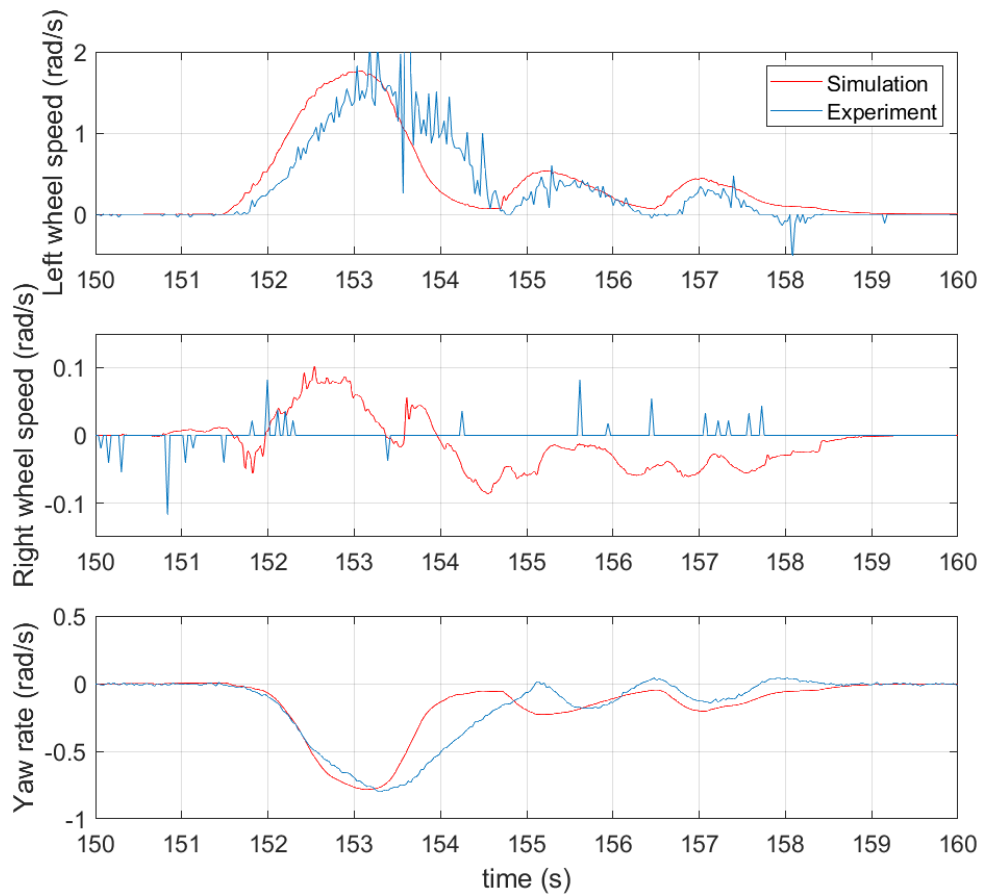
Figure 3.14: Simulation and experiment results in the test 4

46

with real data during the second phase (from 226 to 230s). In contrast, the amplitude of right wheel speed and yaw rate do not correspond exactly to reality in the second phase. These errors may arise from the tire-road contact model and the model of starting torque.
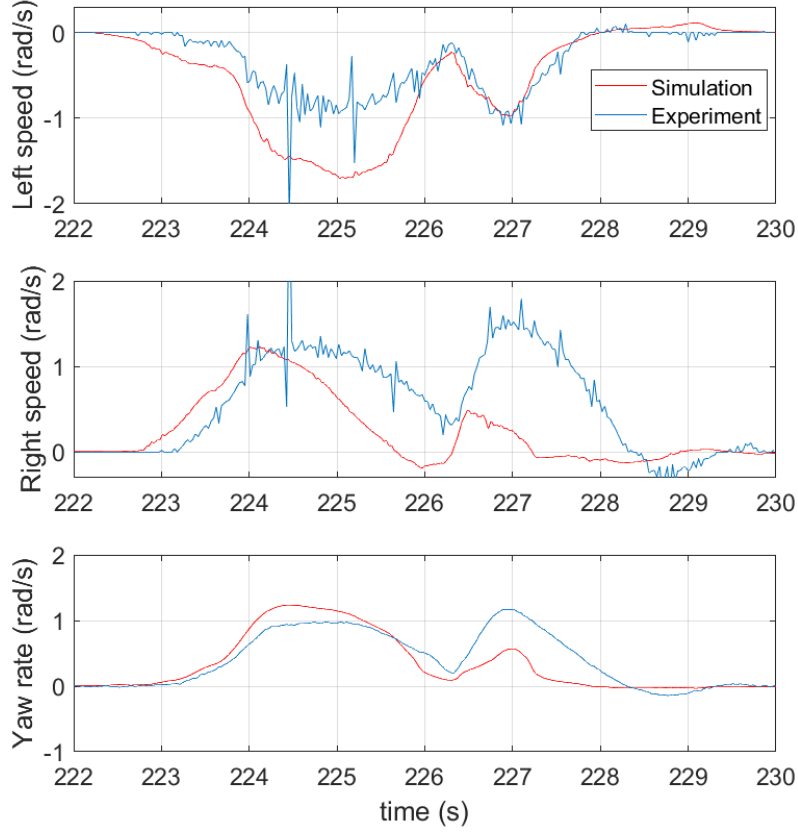
Figure 3.15: Simulation and experiment results in the test turning 180^0 on place

3.5   Toward a dynamical model of power wheelchair

In order to adapt the proposed model to a power wheelchair, it should be noted that the dynamical equations are always the same but the model parameters have to be re-identified. The tire-ground contact, mass, inertia, dimension parameters should be updated to the new wheelchair. Other important components are the electric motors which provide the traction/braking forces, instead of human muscles. Because the dynamic of electric motors are generally much faster than that of the other remain mechanical elements on the wheelchair, it is often neglected in the dynamic model of wheelchair and is replaced by a map between joystick positions and the linear/rotational speeds of wheelchair. However, this assumption is valid only if the wheelchair

moves on a horizontal surface. On a slope or incline surface, this assumption is not sufficient to reflect effects of gravity force on the motions of wheelchair. Therefore consider the dynamic of electric motors and build a map from joystick positions to the applied voltages to motors are necessary to complete the dynamical model of power wheelchair.

3.6   Conclusion

This chapter presents a comprehensive model of manual wheelchair integrated into the simulator platform with a focus on the dynamical phenomenons happening at low speed. This model takes into account the tire-ground contact forces and the influence of the front wheel direction. The evaluation experiment is conducted with a manual wheelchair during some typical manoeuvrers. The experiment results show that the simulation responses are coherent with the real ones and hence confirm the effectiveness of the proposed model. Under the influence of the deviation angle of front wheels, the yaw rate responses are generally consistent with the real measurements and the yaw rate overestimate problem is corrected. By inserting the dynamic model of electric motors, the proposed model can be used to build the dynamic model of a power wheelchair.

Chapter 4

A Biomechanical Model of Hand-Joystick Interaction of Powered Wheelchair User

Contents

In the previous chapter, we presented a dynamical model of wheelchair for virtual reality which concerns the validation/evaluation aspect of the designed assistance system for power wheelchair. This chapter will deal with another aspect of assistance system which tries to answers the questions "How can we personalize the assistance system according to the user im-

pairment conditions?". We propose here a power wheelchair user model focusing on a biome-chanical model of the hand-joystick interaction. Taking into account the biomechanical aspect of the hand muscles, this model is expected to be able to personalize the assistance according to the specific disability of each wheelchair user. The content of this chapter has been accepted at the IEEE International Conference on Systems, Man and Cybernetics (SMC) in 2020.

4.1 Introduction

In general, the powered wheelchair user modeling can be seen as the user intention estimation task which aims to determine the desired motion or the path that the user would follow. In that context, the model of user plays the tactical role which gives the reference path to the low-level tracking controllers. In [61] [62], an implicit estimation of the user's intention based on the Bayesian plan recognition framework is used to estimate long term goals, while the sub-optimal short term goals are predicted to avoid the uncertainty in [63]. An implicit user model is presented in [21] which can vary the parameters of the model to adapt to a specific user based on learning data. The improved Directed Potential Field is employed in [64] for trajectory planning to improve wheelchair's steering control. In [64], the Artificial Potential Field method is used to define the desired path and the influence of risks is specified by two parameters which are the time to risk and the distance to risk. Different from the above studies, the authors in [65] focus on the operational level of the hierarchy by proposing a behavioral model based on the generalized force. Border, static obstacle and user vision are taken into account for force generation. Although the hand-joystick interaction is required for manipulating the powered wheelchair, to the best of authors knowledge, there is no research currently integrating this relationship into the user model.

Otherwise, from the point of view of biomechanical engineering, the motions of the hand are well documented with a considerable number of muscles are taken into account. In [66] an anatomical data-set of 48 hand and wrist muscles is completed by evaluating the optimal fiber length, physiological cross-sectional area, tendon length, mass, inertia, and pennation angle of each muscle. A complete musculoskeletal model is also provided. This model, however, is im-

practical in clinical control application [67]. For simplification purposes, a lumped-parameter model was proposed where only four equivalent muscles represent dozens of hand muscles in the complete model. Experimental results demonstrated that this simplified model can predict relatively accurately the performance of the complete one [67].

The difficulties on operating the wheelchair joystick attracted many researches over the years. A clinical survey [5] on 200 clinicians found that 81% of their patients use joystick interface and 40% of observed patients experienced the difficulties in steering and manoeuvring tasks. In addition, many patients cannot control the wheelchair due to insufficient motor skills and strength. The tremor symptom of the patients with Parkinson's and patients with multiple sclerosis make difficult to operate the conventional joystick [68]. In [69], the patterns of forearm muscles activation of the children with cerebral palsy were collected during piloting the powered wheelchair. The results imply that the muscles activation patterns can represent the joystick control during piloting the powered wheelchair.

To deal with the need for personalizing the driving assistance system, the features of joystick manipulating which change over the time were focused in [4] for regulating the driver assistance system. The concerned features were the joystick position mapping, the smoothness and frequency of tremors, and the velocity of wheelchair. Toward a human-like assistance, another approach for personalizing assistance system is to exploit the machine learning technique to mimic the behaviours of human [70] [38].

Although recognizing the difficulties of the users in operating powered wheelchair through the joystick as well as the variety in the user's motor deficiencies, there are no studies considering the specific biomechanical aspects of each user. Thus, the objective of this study is to develop a powered wheelchair user model based on the interaction between the human hand and joystick. By integrating the biomechanical parameters of hand muscles, this model makes it possible to personalize the assistance system with respect to the user's level of physical impairment.

The rest of this chapter is organized as follow. Section II presents the general model of hand-joystick interaction with a focus on the inverse kinematic problem, forces system and a solution to multi-body dynamical equations system by using Newton-Euler approach. Section

III introduces the lumped model of hand muscles which drive the motions of hand-joystick interaction mechanism. Path following controller and low-level muscle controller will be shown in section IV. Simulation and experimental results will be discussed in section V while the conclusion will be drawn in the last section.

4.2   General model description

From the point of view of model-based control approach, the control steps of a wheelchair user can be illustrated in Fig. 4.1. Firstly, the user collects information about the surrounding environment. Combining collected information and his knowledge/experience (is this a known area? the traffic sign ...), an "optimal path" is approximately planned in his head. Then a path-following controller computes the required velocity of the wheelchair to follow the planned path. This velocity is now relatively mapped to the reference position of joystick based on the experience of the user. A lower-level controller will then activate the hand muscles to manipulate the joystick to follow its reference position. The wheelchair's controller drives electric motors leading to move the wheelchair, from the real values of joystick rotation angles. New position and velocity of the wheelchair are now updated by the user and this closed loop is repeated.

As can be seen in Fig. 4.1, the proposed user model simulates the above control process which includes hand muscles model, hand-joystick interaction model, path following controller and a low-level controller. It should be noted that this model only focused on the operational control level while the path planning step belongs to the tactical level and will not be shown in this thesis.

4.3   Multibody Dynamics Model of Interaction Hand-Joystick

The shaded part in Fig. 4.2 presents one of the ways in which users hold and manipulate the joystick using the wrist, thumb and pointer finger. Although users can manipulate joystick in many different ways in reality, the motions of the joystick are always the same: rotation
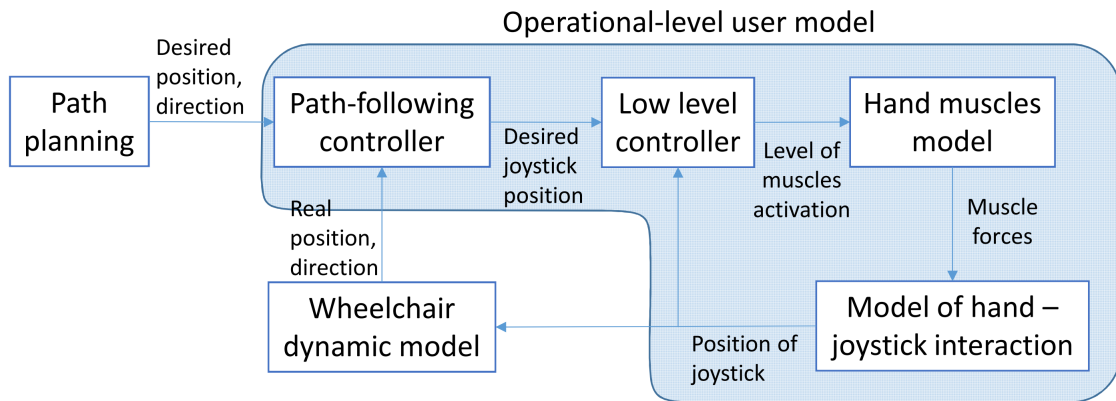
Figure 4.1: Structure of user model at operational control level
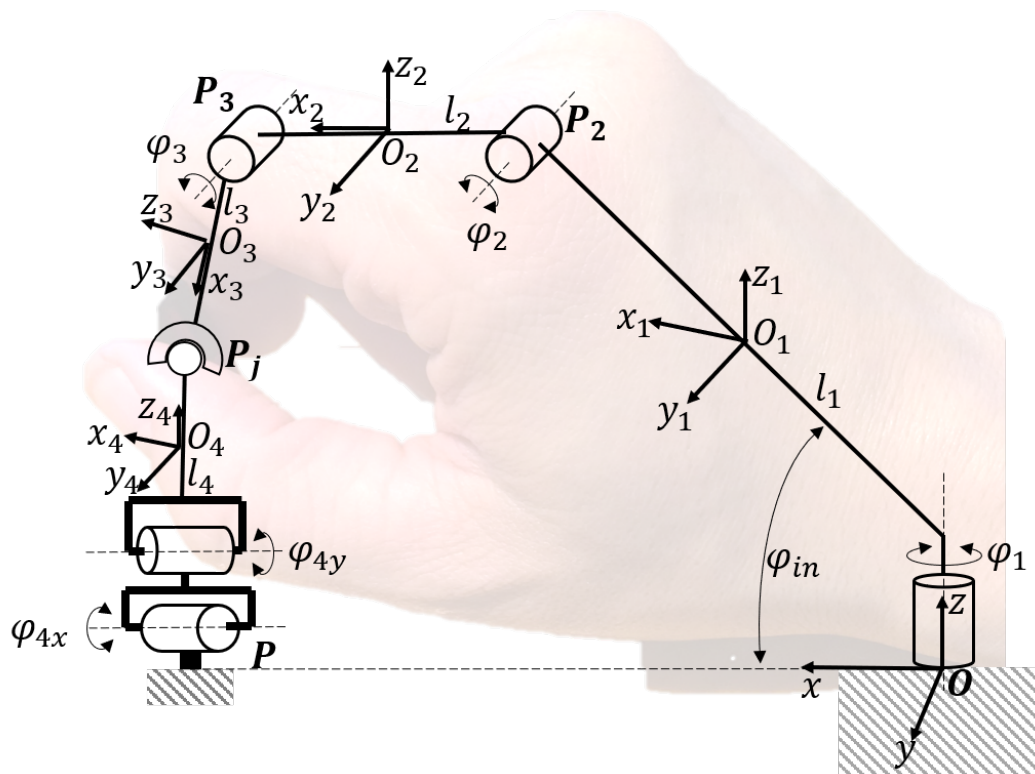
Figure 4.2: Hand - joystick interaction model under form of a robot arm

about x-axis and y-axis. In general, the joystick cannot rotate about itself. Inspired from this hand position, we propose a robot-arm model as in Fig. 4.2 which is considered as an equivalent model of interaction hand-joystick. This model is a five-bars closed-chain spatial mechanism with 2 degrees of freedom. The first link represents the palm of hand which is inclined at a fixed angle φ_{in} and is assumed can rotate only about z-axis through a revolute joint O. While in reality, the palm has many motions such as flexion, extension, radial/ulnar deviation, pronation/supination, this assumption presents a simplified model of palm motions at wrist joint for joystick manipulating purpose. The second and the third links are inspired from pointer fingers with only two "phalanges" (instead of three phalanges of real fingers) and they are linked to the first link and linked together by two revolute joints P_2, P_3 as shown in Fig. 4.2. These motions are equivalent to the flexion and extension motions of the fingers. The last link models the joystick handle and is attached to ground at a fixed point P through a universal joint and to the third link by a spherical joint P_j. l_1, l_2, l_3, l_4 are the lengths of robot links. The aim of this configuration is that the position of joystick P_j, which is equivalent to the angles φ_{4x} and φ_{4y}, can be controlled through the regulation of the angles φ_1, φ_2 and φ_3 which are similar to the fingers and palm rotational motions about the wrist of hand. The x-axis of the global frame is on the line between the wrist and joystick. Each link (bar) has its own coordinate system attached to its center of gravity and its x-axis is along the length of the bar as can be seen in Fig. 4.2 except for the first and fourth links. y_2 and y_3 axes are parallel to the rotation axis of revolute joints P_2. This setting allows us to describe the motions of each link independently. The joints will be considered as the constraints to motions of links and will be described in the next sections.

4.3.1 Inverse geometric problem

It is well known that the rotation matrix is used for the transformation of coordinates. In this research, the rotation matrix are given as

$$R_x(\varphi) = \begin{bmatrix} 1 & 0 & 0 \\ 0 & cos(\varphi) & -sin(\varphi) \\ 0 & sin(\varphi) & cos(\varphi) \end{bmatrix} \tag{4.1}$$

$$R_y(\varphi) = \begin{bmatrix} cos(\varphi) & 0 & sin(\varphi) \\ 0 & 1 & 0 \\ -sin(\varphi) & 0 & cos(\varphi) \end{bmatrix} \tag{4.2}$$

$$R_z(\varphi) = \begin{bmatrix} cos(\varphi) & -sin(\varphi) & 0 \\ sin(\varphi) & cos(\varphi) & 0 \\ 0 & 0 & 1 \end{bmatrix} \tag{4.3}$$

As we discussed earlier, it is required to determinate the "palm angle" φ_1 and "finger angles" φ_2 and φ_3 to manipulate the joystick with respect to a given position of joystick $(\varphi_{4x}, \varphi_{4y})$. The position of P_j in the global frame is calculated with

$$P_j = P + R_4 \begin{bmatrix} 0 \\ 0 \\ l_4 \end{bmatrix} \tag{4.4}$$

where $R_4 = R_x(\varphi_{4x}) R_y(\varphi_{4y})$ and $\begin{bmatrix} 0 & 0 & l_4 \end{bmatrix}^T$ is position of P_j with respect to P in $O_4 x_4 y_4 z_4$ coordinate system. Now "palm angle" φ_1 is computed

$$\varphi_1 = tan^{-1}\left(\frac{y_{P_j}}{x_{P_j}}\right) \tag{4.5}$$

where (x_{P_j}, y_{P_j}) is the coordinate of joint P_j in Oxy plane as shown in Fig. 4.3. Once φ_1 is determined, P_2 can be deduced by

$$P_2 = R_z(\varphi_1).[l_1 cos(\varphi_{in})\ 0\ l_1 sin(\varphi_{in})]^T \tag{4.6}$$

It can be seen in Fig. 4.3 that there are two possible solutions, P_3 and P_3', which are two intersection points of two circles with their centers are at P_2 and P_j. Using a temporal frame
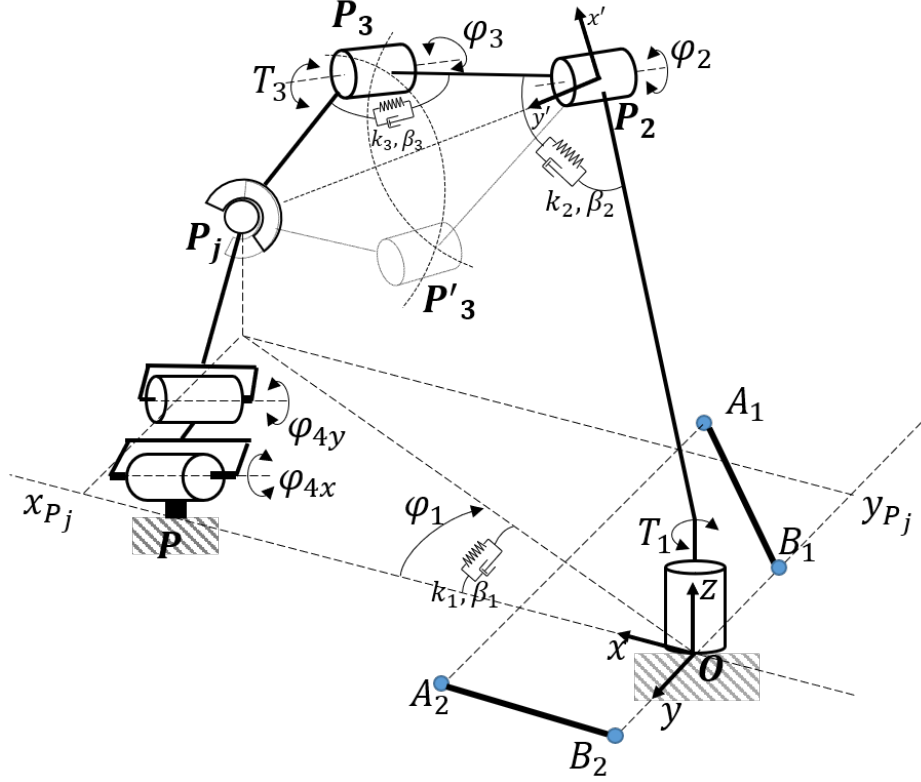
Figure 4.3: Two possible configuration for a given position of joystick

$P_2 x' y'$ on the plane of the first three links as in Fig. 4.3, the selected P_3 is the intersection points with $y_{P_3} > 0$ because it is mimic the real posture of hand fingers. Once P_3 is found, by defined $P_{32} = P_3 - P_2$ and $P_{j3} = P_j - P_3$, φ_2 and φ_3 are obtained from

$$\varphi_2 = tan^{-1}\left(\frac{z_{P_{32}}}{\sqrt{x_{P_{32}}^2 + y_{P_{32}}^2}}\right) \;\; and \;\; \varphi_3 = tan^{-1}\left(\frac{z_{P_{j3}}}{\sqrt{x_{P_{j3}}^2 + y_{P_{j3}}^2}}\right) \tag{4.7}$$

4.3.2 Motion equations of multibody system

For a given position of the joystick, only two of the three angles of hand model φ_1, φ_2 and φ_3 are necessary to completely define the system's position. The first link of the proposed model mimics the ulnar and radial deviation motions of the palm by rotating about z-axis. These motions in reality are caused by traction forces from many forearm muscles. In this model, we consider the whole effects of these forces by an equivalent external torque T_1 which acting on the first link of the proposed robot-arm as shown in Fig. 4.3. Similarly, the motions of second and third links simulate the flexion and extension motions of fingers on hand which are under

Table 4.1: Torques acting on the links of hand-joystick interaction model

Link 1	$\begin{bmatrix} 0 \\ 0 \\ T_1 - k_1\varphi_1 - b_1\dot{\varphi}_1 \end{bmatrix}$
Link 2	$\begin{bmatrix} 0 \\ -k_2\varphi_2 - b_2\dot{\varphi}_2 \\ 0 \end{bmatrix}$
Link 3	$\begin{bmatrix} 0 \\ T_3 - k_3(\varphi_3 - \varphi_2) - b_3(\dot{\varphi}_3 - \dot{\varphi}_2) \\ 0 \end{bmatrix}$
Link 4	$\begin{bmatrix} -k_4\varphi_{4x} - b_4\dot{\varphi}_{4x} \\ -k_4\varphi_{4y} - b_4\dot{\varphi}_{4y} \\ 0 \end{bmatrix}$

actions of many flexor and extensor muscles in reality. We model the effects of these muscles by an equivalent external torque T_3 which acts on the third link as shown in Fig. 4.3. This is due to the fact that flexor and extensor muscles are attached to the intermediate and distal phalanges which are modelled by the third link in this model. Two external torques T_1, T_3 come from hand muscle models which will be presented in the next sections.

In addition, springs-damping elements are essential to reflect the real movement of the hand. In this model, there are four spring-damping elements, each of them has spring stiffness k_i and damping coefficient β_i, located at the joints O, P_2, P_3 and P, respectively. Spherical joint at P_j which simplified the contact between the user's hand and the joystick handle is supposed to be free from this spring-damping elements. The torques acting on the links are summarized, as shown in Table 4.1, under the form of vectors with respect to the link's own coordinate frame.

We adopted the Newton-Euler approach which had been well documented in [71] to analyze the dynamical performance of the proposed hand-joystick interaction model. The orientation of each link with respect to the global coordinate system is expressed by three Euler angles combination. The general coordinate q is chosen as $q = [\varphi_1 \ \varphi_2 \ \varphi_3 \ \varphi_{4x} \ \varphi_{4y}]^T$. Kinematic constraints at the joints are expressed by algebraic equations as

$$\Phi(q) = 0 \tag{4.8}$$

57

The second derivative of (4.8) with respect to time yields

$$\Phi_q \ddot{q} = \gamma \tag{4.9}$$

where Φ_q is the Jacobian matrix of the constraint equations, $\ddot{q}$ is the acceleration vector and γ is a vector that depends on the velocities of the system links. The motion equations of this constrained multibody system are written as

$$M\ddot{q} = T + T_c \tag{4.10}$$

where M is the mass matrix of the system. In this case, there are only the rotation motions that are concerned in this system and thus M includes only the elements of the moment of inertia of links. T denotes for the generalized force vector, which includes the external torques acting on the links of the system as shown in Table 4.1. T_c is the vector of reaction forces that come from the kinematic constraints and it can be expressed using the Jacobian matrix of constraint equations and Lagrange multipliers λ as follow

$$T_c = -\Phi_q^T \lambda \tag{4.11}$$

Rewrite (4.9), (4.10) and (4.11) yields

$$\begin{bmatrix} M & \Phi_q^T \\ \Phi_q & 0 \end{bmatrix} \begin{bmatrix} \ddot{q} \\ \lambda \end{bmatrix} = \begin{bmatrix} T \\ \gamma \end{bmatrix} \tag{4.12}$$

The solution for this differential-algebraic equations system are delivered by [72]

$$\ddot{q} = M^{-1}\Phi_q^T \left(\Phi_q M^{-1}\Phi_q^T\right)^{-1}\left(\bar{\gamma} - \Phi_q M^{-1}T\right) + M^{-1}T \tag{4.13}$$

where $\bar{\gamma} = \gamma - 2\alpha\dot{\Phi} - \beta^2\Phi$ with α and β are the stabilization coefficients according to Baumgarte's stabilization method. To finish this hand-joystick interaction model, the hand muscle torques T_1 and T_3 will be presented in the next sections.

4.4   Muscle model

In general, manipulating the joystick of powered wheelchair requires the participation of many hand and forearm muscles or even some arm and shoulder muscles depending on the posture and degree of impairment of the users. Therefore, in this research, a lumped-model of hand muscles based on the Hill type model of contraction dynamics will be adopted from [67]. As we discussed earlier, there are two links, the first and the third links, are motorized and each link can rotate in two directions. The motion of the first link is supported by two musculotendon units, implements the ulnar and radial deviation movements while the third link supports the flexion and extension movements thanks to two other musculotendon units.

Each musculotendon unit is composed of a contractile element (CE) and a parallel passive element (PE) [67]. The tendon is considered rigid and therefore the length of the tendon is considered as constant. In [66], the pennation angles of the flexor and extensor muscles of wrist and fingers are summarised where their values vary only from 0° to about 15°. Only two of thumb muscles have pennation angles larger than 20°. The dorsal interosseous muscles have large pennation angles [73] but their contribution on the extension and flexion motions of fingers are less than the extensor and flexor muscles. Therefore in this research we neglect the effects of muscle pennation angles to the contraction properties of musculotendon unit. Each unit produces a contraction force $F = F_c + F_p$. The CE produces the force F_c which depends on the peak active force that can provide F_{c_0}, on its length L_c, on its activation level a $(0 < a < 1)$ and on shortening velocity v_c.

$$F_c = F_{c_0} f(L_c) f(v_c) a \tag{4.14}$$

$$f(L_c) = 1 - \frac{(L_c - L_{c_0})^2}{w^2 L_{c_0}^2} \tag{4.15}$$

$$f(v_c) = \frac{v_{c_0} - v_c}{v_{c_0} + \frac{v_c}{c}} \tag{4.16}$$

where L_{c_0} and v_{c_0} are the optimal fibre length and maximum shortening speed of contractile

element, respectively. The parameters of this model are obtained from [67] where v_{c_0} can be chosen by $0.1L_{c_0}$, w which defines the effectiveness range where the contractile element can produce force is set to 0.5, and the hyperbolic shape coefficient c is set to 0.25. The parallel passive element, with its elastic stiffness K_{pe}, produces the force F_p only when its length exceeds optimal contractile length L_{c_0}

$$F_p(L_c) = K_{pe}(L_c - L_{c_0}) \tag{4.17}$$

Muscle forces in the hand-joystick model are denoted F_{11}, F_{12}, for the ulnar and radial deviation movements, and F_{31}, F_{32}, for the flexion and extension movements, respectively. The corresponding moments are deduced as follows

$$T_1 = F_{11}r_{11} + F_{12}r_{12} \tag{4.18}$$

$$T_3 = F_{31}r_{31} + F_{32}r_{32} \tag{4.19}$$

where r_{11}, r_{12}, r_{31} and r_{32} denote the moment arms of muscle forces. While $L_{c_0}, v_{c_0}, F_{c_0}, K_p$ are constants, the other variables L_c, v_c and r must be determined based on the motions of system links.
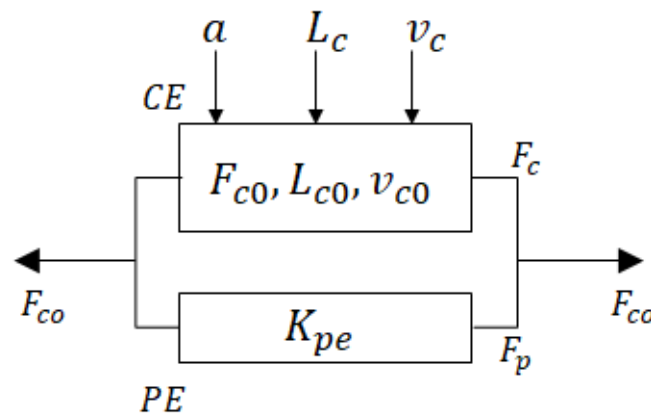
Figure 4.4: Hill type model of contraction dynamics of muscles

As can be seen in Fig. 4.3 the two points $A1, A2$ are fixed with respect to the first link coordinate system $O_1x_1y_1z_1$ where the tendons of the ulnar and radial muscles attach to the first

link. Two other points B_1, B_2 are fixed in the global frame so that the lines A_1B_1 and A_2B_2 are the direction of ulnar and radial forces. This configuration is inspired from real anatomy of the human hand. Moment arms of ulnar and radial forces are the distances from rotation center O to the lines A_1B_1 and A_2B_2, respectively, which can be described as

$$r_{11} = \frac{\|(A_1 R_z(\varphi_1) - B_1) \times (O - B_1)\|}{\|A_1 R_z(\varphi_1) - B_1\|} \tag{4.20}$$

$$r_{12} = \frac{\|(A_2 R_z(\varphi_1) - B_2) \times (O - B_2)\|}{\|A_2 R_z(\varphi_1) - B_2\|} \tag{4.21}$$

In this research, the tendons of musculotendon units acting on the third link are considered passing by the sides of the P_3 joint and the moment arms of their corresponding forces are considered as constants, $r_{31} = r_{32} = constant$. Other variables of musculotendon units are deduced from the motions of hand-joystick interaction model based on its geometrical properties.

4.4.1 Control system

As can be seen in Fig. 4.1, two types of controllers were required to complete this user model: *i*) a low-level controller which directly regulates the activation levels of each muscle to follow the reference joystick position, and *ii*) a path-following controller which chooses an appropriate pair of (v_{ref}, ω_{ref}) to follow user's preferred path. For the low-level control, each of active links (the first and the third links) is performed by a simple PD controller which has the form

$$a = -K_P \left(\varphi - \varphi_{ref}\right) - K_I \dot{\varphi} \tag{4.22}$$

where a is the activation level of muscles, φ are the real position of the link while φ_{ref} is its reference position which come from the inverse geometric calculation (4.5) (4.7).

For the path following controller, we adopt dynamic feedback linearisation tracking control for a unicycle mobile robot which has been well documented in our paper [19] and will not be discussed here.

Table 4.2: Parameters of muscles participating in lumped-model of the hand-joystick interaction model

Motion	Related muscle	Parameters		
		$L_{c_0}(mm)$	$F_{c_0}(N)$	$K_{pe}(\frac{N}{m^2})$
Radial deviation	Abductor Pollicis Longus	59	64	54
	Flexor Carpi Radialis			
	Extensor Carpi Radialis Longus			
	Extensor Carpi Radialis Brevis			
Ulnar deviation	Extensor Carpi Ulnaris	46	74	140
Flexion	Flexor Digitorum Profundus Index	91	55	25
Extension	Extensor Digitorum Index	44	23	67
	Extensor Indicis			

4.5 Results

Firstly, the proposed wheelchair user model was validated by numerical simulations. Then, a comparison between the simulated proposed model and published experimental results was conducted. The parameters of Hill's type muscle model are given in Table 4.2 [66]. Each parameter of these lumped model in this table is the mean value of the related muscles corresponding parameters which contribute to those motions of the hand. The maximum isometric force is found by $F_{c_0} = PCSA.k$ where $PCSA$ stands for Physiological Cross-Sectional Area given in [66] and $k = 30\left(\frac{N}{cm^2}\right)$ is a typical value for the specific tension of human muscles. For the sake of simplicity, in this research, we assume that the initial lengths of muscles are their optimal lengths. The parameters of interaction hand-joystick model are given in Table 4.3 based on the inertial properties and lengths of hand bones which are given in [74]. The length of "palm" l_1 is the mean value of the distance from wrist to metacarpophalangeal joints. The lengths of phalanges l_2, l_3 are also the means of the phalanges lengths in [74]. J_2 is the sum of inertia moments of the proximal phalanges while J_3 is that of the distal and middle phalanges. The spring-damping parameters are obtained from [75] while joystick properties are deduced from [76].

Table 4.3: Parameters of the hand-joystick interaction model

Parameter (unit)	Value	Parameter (Unit)	Value
$l_1(m)$	0.075	$k_3(N.m^{-1})$	0.5
$l_2(m)$	0.05	$k_4(N.m^{-1})$	0.5
$l_3(m)$	0.04	$J_1(g.cm^2)$	4200
$l_4(m)$	0.035	$J_2(g.cm^2)$	153
$b_1(N.m^{-2})$	0.0142	$J_3(g.cm^2)$	30
$b_2(N.m^{-2})$	0.0142	$J_{4x}(g.cm^2)$	40
$b_3(N.m^{-2})$	0.0142	$J_{4y}(g.cm^2)$	40
$b_4(N.m^{-2})$	0.0142	A_2	$[0.03\ 0.03\ 0]^T$
$\varphi_{in}(\deg)$	45	A_1	$[0.03\ -0.05\ 0]^T$
$k_1(N.m^{-1})$	0.5	P	$[0.1\ 0.017\ 0]^T$
$k_2(N.m^{-1})$	0.5	$B2$	$[-0.01\ -0.02\ 0]^T$
$k_3(N.m^{-1})$	0.5	$B1$	$[-0.01\ 0.02\ 0]^T$

4.5.1 Simulation results

In this simulation, the powered wheelchair should follow a predefined path with the desired speed $0.75m/s$ in an office environment as in Fig. 4.5 where the path is given by a series of points along with the corresponding curvatures at each point. This task requires users to be able to go straight, turn 90 degrees with different turning radius. Fig. 4.6 shows the positions of the joystick and its displacement in the two axes with respect to time during powered wheelchair driving.
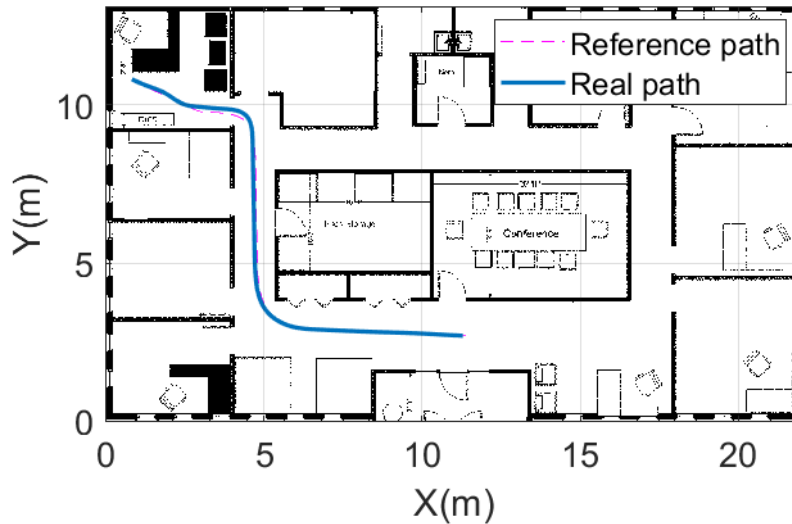
Figure 4.5: Path following results in an office environment.

It can be seen that the joystick is moved the most when the wheelchair follows a curve with a significant curvature (from 15 to $20sec$). To show the position of the joystick, reference

longitudinal velocity and yaw rate are normalized by dividing each value of these variables by their maximum value. The distribution of joystick position also intuitively shows that the joystick was operated in a reasonable way. The activation of muscles in Fig. 4.7 shows that the phalanges extensor muscles are always active to maintain the longitudinal speed while the wrist muscles only intervene when the turning is required. The phalanges flexor muscles are not activated in this test because the deceleration phase (from 15 to 17.5*sec*) is performed by the spring-damping units of the joystick. The simulation results also show that the level of muscle activation is rarely exceeding 20% except for turning on the path with high curvature. It should be noted that these results are based on the assumption that the muscles in this model are normal and without physical impairment. By varying the muscle's parameters, this model may reflect the physical limitation of disabled users in maneuvering powered wheelchair.
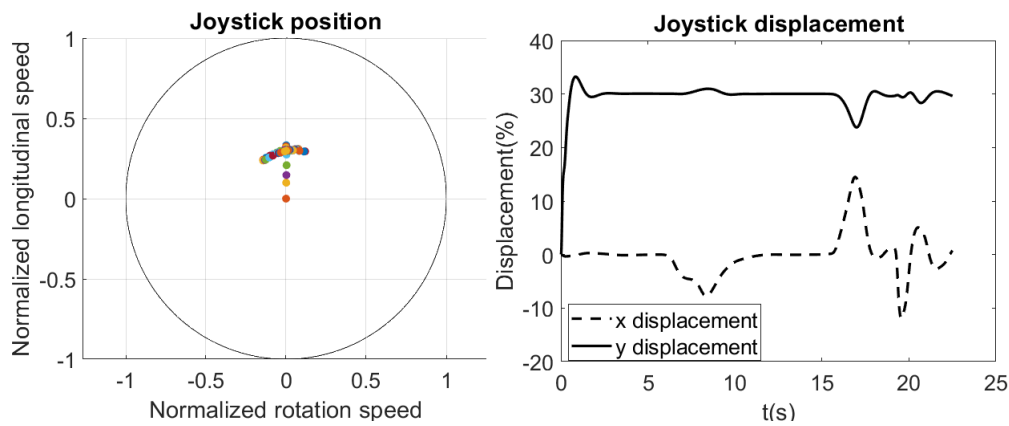
Figure 4.6: Position and displacement of joystick during the wheelchair manoeuvring.

4.5.2 Comparison to published experimental results

In this section, we compare our simulation results to the experiment results which have been well presented in [77]. In these experiments, the authors assessed the degree of proficiency in operating a powered wheelchair by assessing the recorded joystick control data. Two groups of participants, novice and expert have been required to perform some driving tests drawn from Wheelchair Skills Test manual [78] such as rolls backward 5m, turns 90°, maneuvers sideways, turns 180° in place. The joystick movements during these tests are recorded. Only the turning 90° test data was presented explicitly in that paper and therefore is chosen to compare with the

simulation results here.
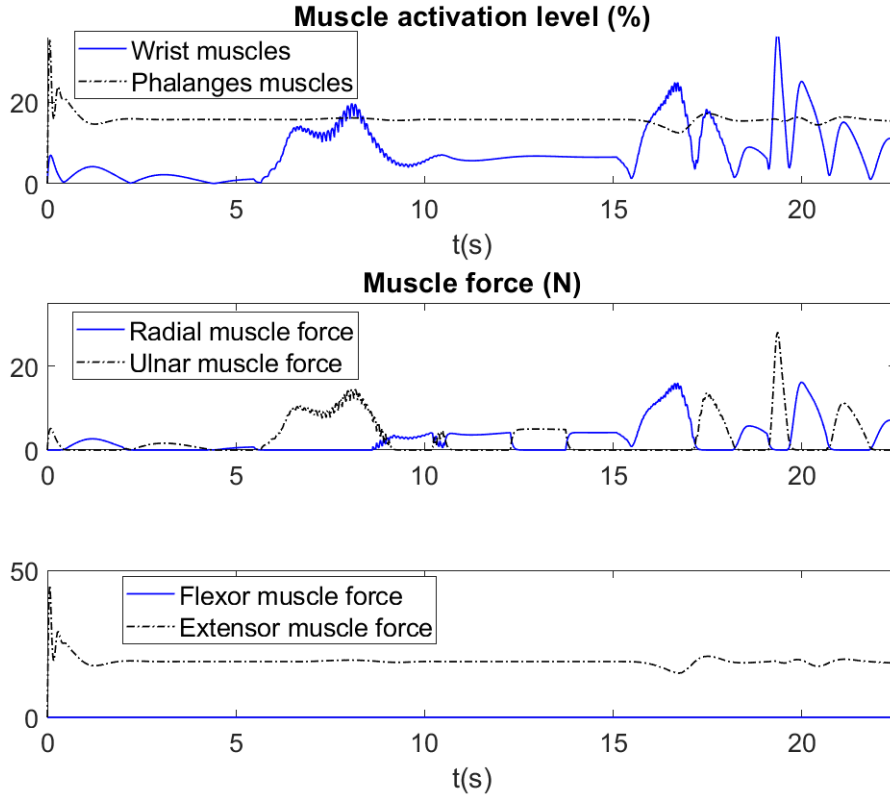
Figure 4.7: Muscle activation level and force produced during the wheelchair manoeuvring

Fig. 4.8 shows the experiment and simulation results in joystick movements including $x-$displacement, $y-$displacement and joystick excursion during turns 90° test. The longitudinal velocity is predefined so that the simulation result of the y-displacement using the proposed wheelchair user model is well consistent with the experiment result. The simulation results of x-displacement and joystick excursion are coherent with the real ones. The real movements oscillate much more than those in simulation because in numerical simulation, position of wheelchair, obstacles and reference path are known prior and therefore the control action is smooth. In contrast, in reality these positions can be estimated relatively by wheelchair user and that leads to the oscillation in control actions which try to correct the position errors.

Fig. 4.9 presents the muscle activation levels of the wheelchair user in two cases. In the first case, we suppose that the user has full capacity to manipulate the joystick (F_{c_0} has the same value as in Table 4.2), only about 44% muscle capacity is activated. On the other hand, in the second case, we suppose that the human experiences a muscle weakness problem (F_{c_0} is only 20% of the value in Table 4.2), and the user has to activate nearly full of his capacity
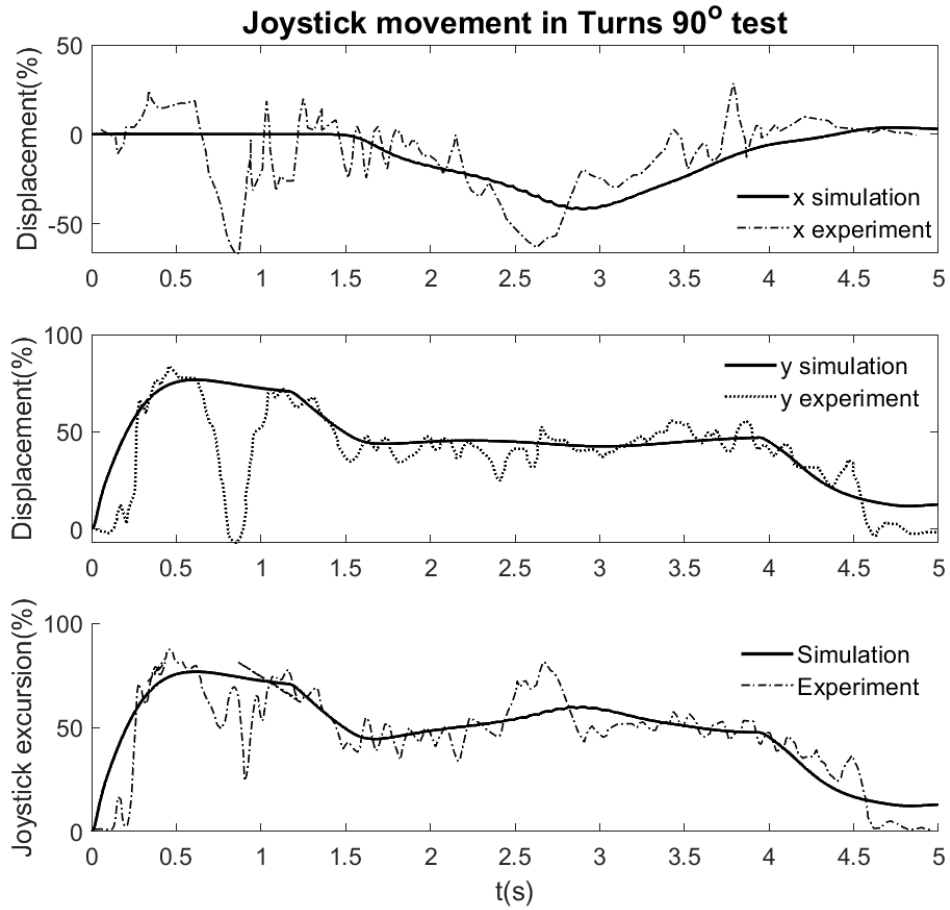
Figure 4.8: Simulation and experimental results of joystick excursion and displacement in Turns 90° test.
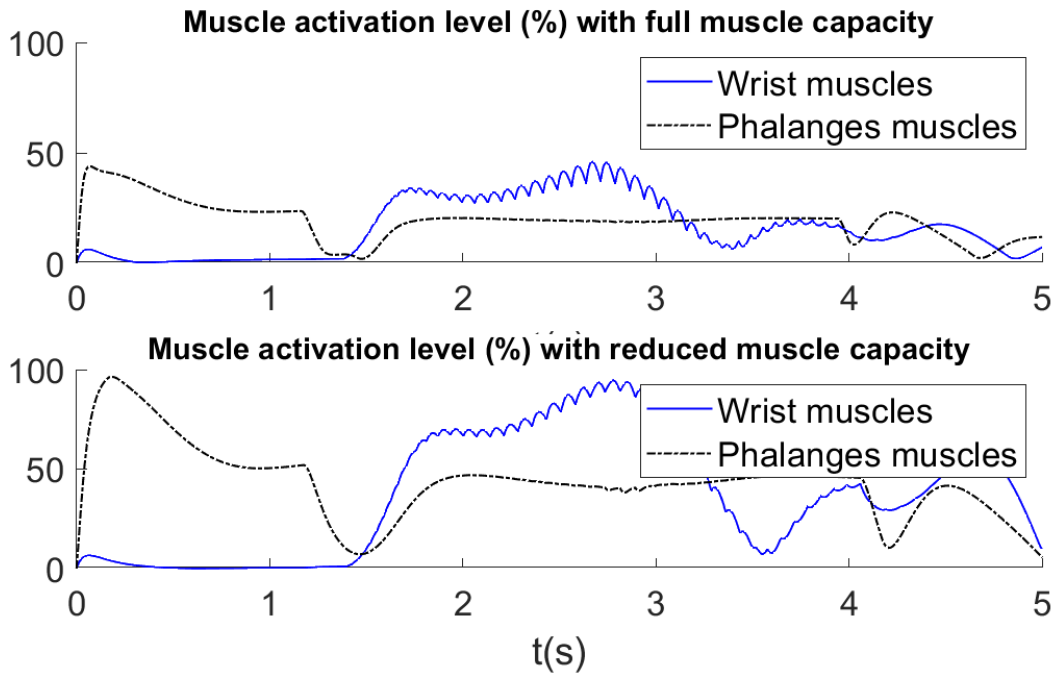
Figure 4.9: Simulation results of muscle activation in both cases: with and without muscle reduced capacity

to manipulate the joystick. These results show that the biomechanical parameters representing the muscle's capacity can be integrated into the model of wheelchair users to take into account their motor difficulties in driving EPW. While each user has different impairment conditions, these biomechanical parameters can be used to personalized the assistance system.

4.6   Conclusions

This chapter presents an original model of powered wheelchair user at the operational level based on a robotic model of interaction hand-joystick and Hill's type muscle model. The interaction hand-joystick is considered as a 3D robot arm with 5 bars closed-chain mechanism. This model is operated by four lumped-parameter musculotendon units of Hill's type model. Simulation results show the reasonableness of the joystick movements as well as muscle's activities while manipulating the powered wheelchair.

The future work of this research is to identify the model's parameters, especially the muscle parameters, based on the directly measuring muscle activities using electromyography (EMG). The obtained parameters will allow personalizing the user model based on the different levels of physical impairment among different groups of the powered wheelchair user. From this model, a new assistance strategy could be developed based on the haptic interaction hand-joystick.

Chapter 5

Shared control-based assistance system for EPW

Contents

This chapter presents a novel approach to design a shared control-based assistance system for EPW users through a joystick haptic force feedback using a model-based control approach. Firstly a general shared-control architecture is presented to show our methodology about how the controller can assist humans efficiently. This architecture has three main parts: (i) Normal driving assistance mode; (ii) Obstacle avoidance assistance mode; and (iii) Conflict management. This chapter will focus on the first part while the second and third ones will be addressed in the next chapter. After introducing the general architecture, we present the observer/controller design tools which will be applied throughout this chapter. Then an augmented dynamic model of the wheelchair-user is developed to take into account human behaviour in the controller design. To assure the applicability of the proposed approach, unknown input observers are designed to estimate some unmeasured states of the system. When all states are known, we design a group of optimal controllers to provide assistance torque to wheelchair users through the haptic joystick. Finally, simulation results will show the effectiveness of the proposed approach.

The content of this chapter has been accepted at the IEEE International Conference on Systems, Man and Cybernetics (SMC) in 2020.

5.1 Shared control architecture

We design here an assistance system like a co-operator who drives the EPW simultaneously with the wheelchair user in the navigation task using the joystick. In normal driving conditions (without risk of collision) this co-operator will try to predict the intention of the user and reduce his effort when driving the wheelchair. However, when a risk of collision is detected, the co-operator will find an optimal solution to prevent that collision and, the most important thing, communicate that solution to the user intuitively through a haptic force at the joystick. The main goal of this communication is that the user can perceive the intention of his co-operator. At this step, we can find two possible scenarios. If the user agrees with the suggestion from his co-operator (no conflict), both of them will follow that proposed optimal solution. In contrast,

if the user rejects that suggestion, he will act on the joystick in the way he wants. Now the co-operator, in his turn, has to detect the conflict and accept the user's decision. The assistance torques now are provided to the user so that he can understand the action of his co-operator. During the whole process of cooperation between user and assistance system, it can be seen that the user is always involved in the control-loop as the final decision-maker. In short, three main goals of the proposed assistance system are:

(i) involving the user continuously during manipulating the wheelchair,

(ii) reducing the effort of the user in manipulating the joystick during the navigation tasks and

(iii) assisting EPW user in obstacle avoidance tasks while maintaining his role as the final decision-maker.

Fig. 5.1 presents more detail about our methodology in designing this assistance system. The user perceives the surrounding environment and drives the wheelchair through hand torques applied to the joystick. The assistance system unit consists of two observer-controller systems and two special blocks related to the risk management and conflict management functions. The normal driving assistance block, which will be addressed in this chapter, is designed to assist the user in normal driving mode (without considering the risks of collisions). This block, therefore, includes a "user intention estimation" block and an optimal controller which is designed with the user behavior model inside. In contrast, the obstacle avoidance assistance block represents a "virtual driver" who has its own decision based on the information from the risk management function. This block is used when a risk of collision is detected and the assistance system should communicate its intention to the user by providing the assistance torques. The risk management block is in charge of evaluating the risk of accidents, looking for an optimal path to eliminate this risk and communicating it to the conflict management block. Then this latter compares the human torque estimated and assistance torques to provide appropriate output torques to assist the user.

.
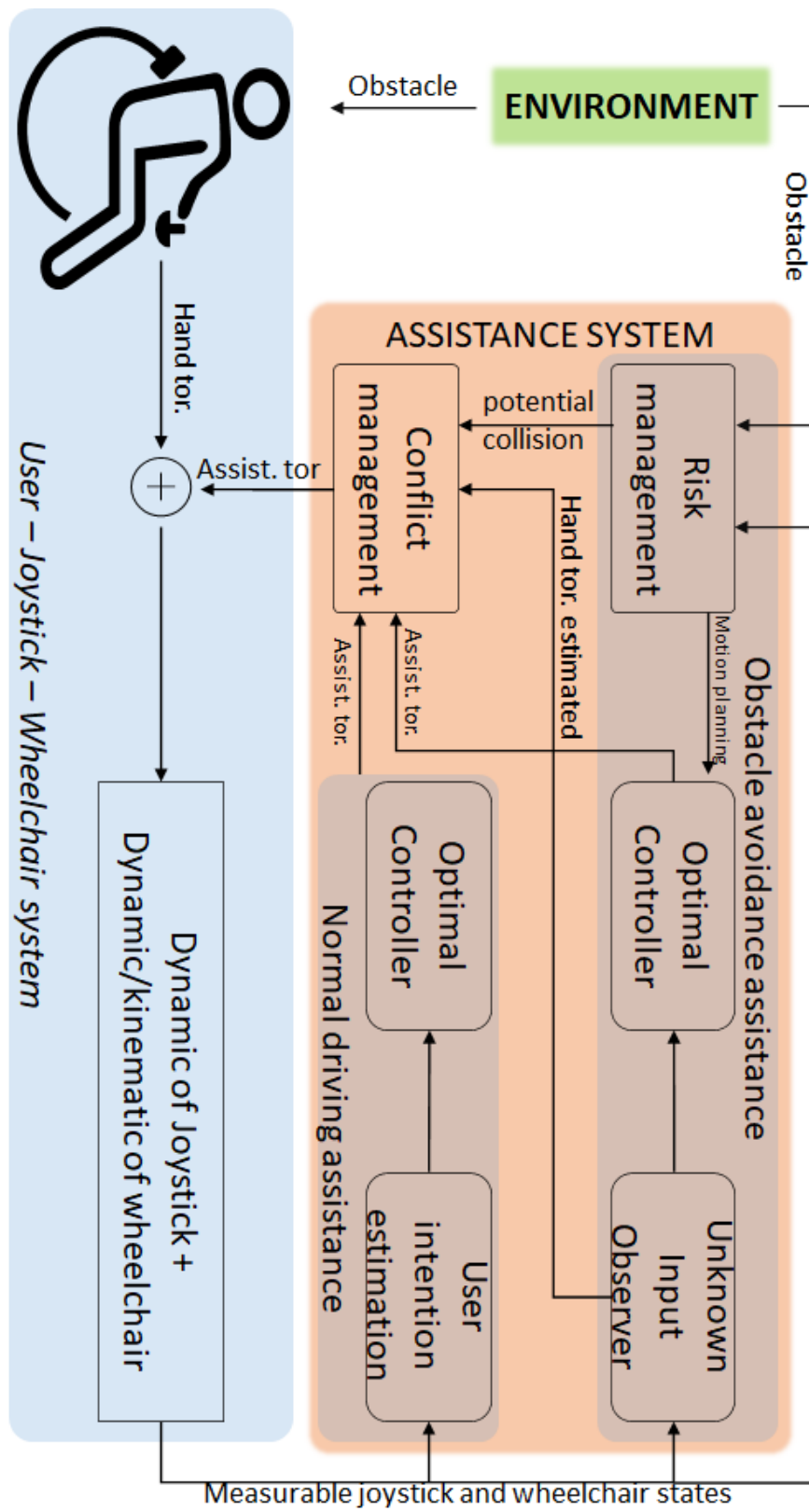
Figure 5.1: General architecture of the proposed assistance system

5.2 Observer-based shared control design

This part gives an introduction to the necessary tools to implement our proposed assistance system. Firstly, we present the Tagaki-Sugeno fuzzy model (T-S model) which is an useful tool for representing a nonlinear system. Then, the design conditions of a fuzzy optimal controller under Linear Matrix Inequalities forms will be presented. Finally, Unknown Input Observer for the linear system will be also included.

5.2.1 TS model representation

In this thesis, we consider the dynamical system model which has the form

$$
\begin{cases}
\dot{x}(t) = f\left(z(t)\right) x(t) + g\left(z(t)\right) u(t) \\
y(t) = h\left(z(t)\right) x(t)
\end{cases}
\tag{5.1}
$$

where $f\left(z(t)\right), g\left(z(t)\right)$ and $h\left(z(t)\right)$ are the smooth nonlinear matrix functions depending on the scheduling variable vector $z(t)$ that may depend on state variable vector $x(t)$ and time t. $u(t)$ and $y(t)$ are the input and output vectors, respectively. This model can be represented under T-S form as

$$
\begin{cases}
\dot{x}(t) = \sum_{i=1}^{r} h_i(z) \left(A_i x(t) + B_i u(t)\right) \\
y(t) = \sum_{i=1}^{r} h_i(z) C_i x(t)
\end{cases}
\tag{5.2}
$$

with system matrices with appropriate dimensions $A_i, B_i, C_i, i = \{1, ..., r\}$ represent the set of r local linear subsystems. For simplicity, the explicit time-dependence of the variables will be omitted. The scalar membership functions $h(z)$ satisfy the following convex sum property

$$
\sum_{i=1}^{r} h_i(z) = 1, \ \ h(z) \geq 0, \ \ i = \{1, ..., r\}
\tag{5.3}
$$

To construct a T-S model from a given nonlinear system, there are generally two methods [79]. The first one is based on the system identifications algorithm which uses the input-output data of the original system. On the contrary, the second approach is based on the concept of

sector nonlinearity or local approximation. This method gives a simple and systematic way to get the T-S representation of a given nonlinear system. We summary here only the second method which will be applied to obtain the T-S representation of the nonlinear user-joystick-wheelchair system.

Suppose that there are k nonlinear terms $nl_i(z), i = 1,..,k$ in system (5.1) and each term is bounded $nl_i \in [nl_{imin}, nl_{imax}]$. Then each term can be expressed by its bounded values as

$$nl_i = wf_i^0 nl_{imin} + wf_i^1 nl_{imax} \tag{5.4}$$

where the two weighting functions wf_i^0, wf_i^1 are given by

$$wf_i^0 = \frac{nl_{imax} - nl_i}{nl_{imax} - nl_{imin}} \qquad ; \qquad wf_i^1 = \frac{nl_i - nl_{imin}}{nl_{imax} - nl_{imin}} \tag{5.5}$$

It can be seen that the weighting functions are normalized, and satisfy convex sum property for any value of nl_i, $wf_i^0 + wf_i^1 = 1$. Then, the membership functions corresponding to the ith local linear model is obtained by

$$h_i(z) = \prod_{j=1}^{k} W_{ij}(z) \tag{5.6}$$

where W_{ij} can be wf_i^0 or wf_i^1 depending on which weighting function is used to obtain the ith local model. It should be noted that the membership functions also verify the convex sum property. The system matrices A_i, B_i and C_i of the i_{th} local model can be obtained by substituting the corresponding values nl_{imin}, nl_{imax} to the nonlinear terms in the matrix functions $f(z), g(z)$ and $h(z)$ in (5.1).

Remark 1. *Firstly, the T-S representation of a given nonlinear system is not unique. By choosing the different premise variables, we can obtain different T-S models. In addition, the number of local linear system r increases exponentially with the number of nonlinear terms k in the nonlinear model, $r = 2^k$. The more number of the local system, the greater complexity to be*

solved efficiently by the actual numerical solvers. Therefore, if the number of nonlinear terms in the nonlinear model is too large, although the T-S representation can be found, designing a controller for this fuzzy system may become impractical.

.

5.2.2 Parallel Distributed Compensator

Once the nonlinear model is presented in T-S model (5.2), the problem now is to find a control law u so that this system is stable. A state-feedback law named Parallel Distributed Compensator (PDC) which was proposed in [80] can be used. Firstly the state feedback law is developed for each rule:

$$u = F_i x, \quad i = 1, 2, ...; r. \tag{5.7}$$

where F_i is the feedback gain matrix of the ith rule. Then the overall fuzzy controller is represented by sharing the same membership functions as T-S model

$$u = \sum_{i=1}^{r} h_i(z) F_i x \tag{5.8}$$

It should be noted that although the PDC is built from the local design structure, the feedback gain matrices F_i should be designed in the global design conditions. This can be done by considering the stability conditions of global system. Substituting control law (5.8) into model (5.2), the closed-loop system of the T-S model becomes:

$$\begin{cases} \dot{x} = \sum_{i=1}^{r} \sum_{j=1}^{r} h_i(z) h_j(z) \left(A_i + B_i F_j \right) x \\ y = \sum_{i=1}^{r} h_i(z) C_i x(t) \end{cases} \tag{5.9}$$

We consider a quadratic Lyapunov function $V(x) = x^T P x$ with P is a positive definite matrix. The time derivative of this Lyapunov function along the trajectories of the system (5.9) yields:

$$\dot{V}(x) = \left(\sum_{i=1}^{r} \sum_{j=1}^{r} h_i(z)h_j(z)(A_i + B_iF_j)x \right)^T Px + x^T P \left(\sum_{i=1}^{r} \sum_{j=1}^{r} h_i(z)h_j(z)(A_i + B_iF_j)x \right) \quad (5.10)$$

$$= x^T \left(\sum_{i=1}^{r} \sum_{j=1}^{r} h_i(z)h_j(z) \left((A_i + B_iF_j)^T P + P(A_i + B_iF_j) \right) \right) x \quad (5.11)$$

The stabilization problem now is transformed to find a positive definite matrix P so that the time derivative of Lyapunov function is negative:

$$\sum_{i=1}^{r} \sum_{j=1}^{r} h_i(z)h_j(z) \left((A_i + B_iF_j)^T P + P(A_i + B_iF_j) \right) < 0 \quad (5.12)$$

The next section will present the "Linear Matrix Inequalities (LMIs)" which is a powerful tool and is used very often to find the solution for the inequalities, for example (5.12).

5.2.3 Introduction to Linear Matrices Inequalities

Definition 5.2.1. [79] A LMI is a matrix inequality of the form

$$F(x) = F_0 + \sum_{i=1}^{m} x_i F_i < 0 \quad (5.13)$$

where $x^T = (x_1, x_2, ..., x_m)$ is the variable and the symmetric matrices $F_i = F_i^T \in \mathbb{R}^{n \times n}, i = 0, ..., m$ are given. The inequality symbol > 0 means that $F(x)$ is positive definite.

The set of solution of (5.13), denoted by $S = \{x | x \in \mathbb{R}^>, F(x) > 0\}$ is a convex set. It can be seen that the matrix inequalities (5.13) are naturally a system of linear algebra inequalities that are rewritten into LMI form. Finding a solution of (5.13) is a convex optimization problem. A well-known example of the application of LMI in control theory is given by necessary and sufficient conditions to stabilize an autonomous system $\dot{x} = Ax$. These conditions can be expressed as finding a positive definite matrix P which satisfies the Lyapunov inequality

75

$$A^T P + PA < 0 \tag{5.14}$$

In general, there are three generic LMI problems [81] which are relevant for the analysis and the synthesis of control system:

1. the feasibility problem

   Find $x \in \mathbb{R}^m$ such that $F(x) < 0$

2. the linear program under LMI constraints

   Minimize $c^T x$ subject to $F(x) < 0$

3. the generalized eigenvalue minimization problem under LMI constraints

   Minimize λ subject to $\begin{cases} \mathbb{C}(x) > 0 \\ \mathbb{B}(x) > 0 \\ \mathbb{A}(x) < \lambda \mathbb{B}(x) \end{cases}$

The LMI problems can be solved efficiently with many numerical solvers such as SEDUMI, SDPT3, LMILAB within Matlab LMI control toolbox [81], or YALMIP toolbox [82]. However, while the LMI problem does not appear "naturally" in control design conditions, it is necessary to transform the control problems into LMI form before using the appropriate solvers. For example, we will transform the stabilization problem (5.12) into LMI expression. It can be seen that this inequality contains the nonlinear terms PB_iF_j and $F_j^T B_i^T P$. Using the changes of variable $X = P^{-1}$ and then $M_j = F_j X$, we now obtain the LMI expression of the stabilization condition

$$\sum_{i=1}^{r} \sum_{j=1}^{r} h_i(z)h_j(z) \left(XA_i^T + A_iX + M_j^T B_i^T + B_iM_j \right) < 0 \tag{5.15}$$

There are some well-known useful lemmas for recasting controller design condition into LMI forms which will be summarized here.

Lemma 1. *Congruence*

Given two matrices P and Q, Q is invertible. Then $P > 0$ equivalent to $QPQ^T > 0$.

Lemma 2. *Schur complement*

Given two symmetric matrices $P \in \mathbb{R}^{m \times m}, Q \in \mathbb{R}^{n \times n}$ and matrix $X \in \mathbb{R}^{m \times n}$. Then the following statements are equivalent:

1. $\begin{bmatrix} Q & X^T \\ X & P \end{bmatrix} > 0$

2. $\begin{cases} Q > 0 \\ P - XQ^{-1}X^T > 0 \end{cases}$

3. $\begin{cases} P > 0 \\ Q - XP^{-1}X^T > 0 \end{cases}$

Lemma 3. *[83]*

Given $X, Y \in \mathbb{R}^{m \times n}$, $F \in \mathbb{S}^m$, $F > 0$, and $\delta > 0$ be a scalar, then

$$X^T FY + Y^T FX \leq \delta X^T FX + \delta^{-1} Y^T FY$$

Based on LMI optimization problem, the next section will present the LMI conditions for designing the optimal fuzzy controller which will be applied throughout this chapter.

5.2.4   Optimal Fuzzy Control

We consider the following T-S fuzzy model [84]

$$\begin{cases} \dot{x}(t) = \sum_{i=1}^{r} h_i(z) \left(A_i x(t) + B_i u(t) \right) \\ \mu(t) = \sum_{i=1}^{r} h_i(z) C_{\mu i} x(t) \\ y(t) = \sum_{i=1}^{r} h_i(z) C_i x(t) \end{cases} \tag{5.16}$$

where x is the system state vector, u is the control input vector, y is the vector of outputs, μ is the vector of performance outputs and z is the vector of premise variable. The system

matrices with an appropriate dimensions $A_i, B_i, C_i, C_{\mu i}, i = \{1, ..., r\}$ represent the set of r local linear subsystems. The scalar membership functions $h_i(z)$, which is from now denoted by h_i for simplicity, satisfy the convex sum property (5.3). The fuzzy state feedback controller is designed based on the following parallel distributed compensation law:

$$u(t) = \sum_{i=1}^{r} h_i F_i x(t), \quad i = \{1, ..., r\} \tag{5.17}$$

where F_i is the feedback gain matrix corresponding to i^{th} subsystem. The control problem are formulated as follow.

Problem Given W, R is the weighting matrix with appropriate dimensions. $W = W^T > 0$ and $R = R^T > 0$. Find the gain matrices F_i in the parallel distributed compensation law (5.17) to minimize the performance index

$$J = \int_0^\infty \left(\mu^T(t) W \mu(t) + u^T(t) R u(t) \right) dt \tag{5.18}$$

along the solution of (5.16).

The following theorem gives conditions for the design of an optimal controller which solves the above control problems .

Theorem 4. *Given positive scalar $\gamma > 0$, two matrices W, R with appropriate dimensions. The T-S model system (5.16) is stabilizable with PDC control (5.17) if there exists a matrix $Q > 0$ and Y_i, $i = \{1, ..., r\}$ such that the LMI condition (5.19)(5.20)(5.21) are satisfied [84]. And the performance index J will be less than γ. The feedback gain matrix of PDC controller are given by $F_i = Y_i Q^{-1}$ and the Lyapunov function is $V(x) = x^T Q^{-1} x$.*

$$\begin{bmatrix} 1 & x^T(0)) \\ x(0)) & Q \end{bmatrix} > 0 \tag{5.19}$$

$$\begin{bmatrix} -A_iQ - QA_i^T - B_iY_i - Y_i^TB_i^T & QC_{\mu i}^TW^{1/2} & Y_i^TR^{1/2} \\ W^{1/2}C_{\mu i}Q & \gamma I & 0 \\ R^{1/2}Y_i & 0 & \gamma I \end{bmatrix} > 0 \qquad (5.20)$$

$$\begin{bmatrix} T & QC_i^TW^{1/2} & QC_j^TW^{1/2} & Y_i^TR^{1/2} & Y_j^TR^{1/2} \\ W^{1/2}C_iQ & \gamma I & 0 & 0 & 0 \\ W^{1/2}C_jQ & 0 & \gamma I & 0 & 0 \\ R^{1/2}Y_i & 0 & 0 & \gamma I & 0 \\ R^{1/2}Y_j & 0 & 0 & 0 & \gamma I \end{bmatrix} > 0 \qquad (5.21)$$

with $T = -A_iQ - A_jQ - QA_i^T - QA_j^T - B_iY_j - Y_j^TB_i^T - B_jY_i - Y_i^TB_j^T$, $i,j = \{1,...,r\}$, $j > i$.

Proof. We consider the Lyapunov function $V = x^TPx$. Assuming that the closed-loop system is asymptotically stable. Then if the condition

$$\frac{dV}{dt} < -\left(\mu^T(t)W\mu(t) + u^T(t)Ru(t)\right) \qquad (5.22)$$

is justified, then by integrating both sides of (5.22) from 0 to ∞ the following inequality is obtained

$$J < V(0) = x(0)^TPx(0) \qquad (5.23)$$

It can be seen that the cost function J is upper bounded by the initial value of Lyapunov function $V(x(0))$ under the above assumptions. We now design the controller optimizing $V(x(0))$ instead of J. Therefore the original optimization problem now is transformed to the following problem:

Problem   Find the gain matrices F_i for controller (5.17) to minimize γ subject to

$$J < V(0) = x(0)^T P x(0) < \gamma.$$

Define $Q = \gamma P^{-1}$ the above problem can be recast into LMI expression thanks to Schur complement as

$$\begin{bmatrix} 1 & x(0)^T \\ x(0) & Q \end{bmatrix} \geq 0 \qquad (5.24)$$

The closed loop system with control law (5.17) is given by

$$\dot{x} = \sum_{i=1}^{r} \sum_{j=1}^{r} h_i h_j (A_i + B_i F_j) x = \sum_{i=1}^{r} h_i^2 G_{ii} x + 2 \sum_{i=1}^{r} \sum_{j=i+1}^{r} h_i h_j \frac{G_{ij} + G_{ji}}{2} x \qquad (5.25)$$

where $G_{ij} = A_i + B_i F_j$.

The time derivative of the Lyapunov function can be described as:

$$\begin{aligned} \frac{dV}{dt} &= \sum_{i=1}^{r} h_i^2 x^T \left(G_{ii}^T P + P G_{ii} \right) x \\ &+ 2 \sum_{i=1}^{r} \sum_{j=i+1}^{r} h_i h_j x^T \left[\left(\frac{G_{ij} + G_{ji}}{2} \right)^T P + P \left(\frac{G_{ij} + G_{ji}}{2} \right) \right] x \end{aligned} \qquad (5.26)$$

So if

$$G_{ii} P + P G_{ii} + C_{\mu i}^T W C_{\mu i} + F_i^T R F_i < 0 \qquad (5.27)$$

$$\left(\frac{G_{ij} + G_{ji}}{2} \right)^T + P \left(\frac{G_{ij} + G_{ji}}{2} \right) + \frac{C_{\mu i}^T W C_j + C_{\mu j}^T W C_i}{2} + \frac{F_i^T R F_j}{2} + \frac{F_j^T R F_i}{2} < 0 \qquad (5.28)$$

Then

$$\frac{dV}{dt} < -x^T \left[\sum_{i=1}^{r} h_i^2 \left(C_{\mu i}^T W C_{\mu i} + F_i^T R F_i \right) \right] x$$

$$- x^T \left[2 \sum_{i=1}^{r} \sum_{j=i+1}^{r} h_i h_j \left(\frac{C_{\mu i}^T W C_{\mu j} + C_{\mu j}^T W C_{\mu i}}{2} + \frac{F_i^T R F_j + F_j^T R F_i}{2} \right) \right] x \qquad (5.29)$$

It can be seen that the right side of the above inequality is identical to $\mu(t)^T W \mu(t) + u(t)^T R u(t)$. Therefore we have

$$\frac{dV}{dt} < -\mu(t)^T W \mu(t) - u(t)^T R u(t) \qquad (5.30)$$

which justifies the assumption in (5.22). We now need to transform the two conditions (5.27) and (5.28) to LMI forms. Define $Y_i = F_i Q$, (5.27) can be rewritten as below

$$A_i Q + Q A_i^T + B_i Y_i + Y_i^T B_i^T + \gamma^{-1} Q C_{\mu i}^T W C_{\mu i} Q + \gamma^{-1} Y_i^T R Y_i < 0 \qquad (5.31)$$

which can be recast into LMI form thanks to the Schur complement

$$\begin{bmatrix} -A_i Q - Q A_i^T - B_i Y_i - Y_i^T B_i^T & Q C_{\mu i}^T W^{1/2} & Y_i^T R^{1/2} \\ W^{1/2} C_{\mu i} Q & \gamma I & 0 \\ R^{1/2} Y_i & 0 & \gamma I \end{bmatrix} > 0 \qquad (5.32)$$

From Lemma 3, it can be seen that

$$C_{\mu j}^T W C_{\mu i} + C_{\mu i}^T W C_{\mu j} \le C_{\mu i}^T W C_{\mu i} + C_{\mu j}^T W C_{\mu j}$$

$$Y_j^T W Y_i + Y_i^T W Y_j \le Y_i^T W Y_i + Y_j^T W Y_j$$

Apply these equalities to (5.28) we obtain

$$A_iQ + QA_i^T + B_iY_j + Y_j^T B_i^T + A_jQ + QA_j + B_jY_i + Y_i^T B_j^T + \gamma^{-1}QC_{\mu i}WC_{\mu i}Q$$

$$+ \gamma^{-1}QC_{\mu j}WC_{\mu j}Q + \gamma^{-1}Y_i^T RY_i + \gamma^{-1}Y_j^T RY_j < 0 \tag{5.33}$$

or in equivalent LMI form

$$\begin{bmatrix} T & QC_i^T W^{1/2} & QC_j^T W^{1/2} & Y_i^T R^{1/2} & Y_j^T R^{1/2} \\ W^{1/2}C_iQ & \gamma I & 0 & 0 & 0 \\ W^{1/2}C_jQ & 0 & \gamma I & 0 & 0 \\ R^{1/2}Y_i & 0 & 0 & \gamma I & 0 \\ R^{1/2}Y_j & 0 & 0 & 0 & \gamma I \end{bmatrix} > 0 \tag{5.34}$$

with $T = -A_iQ - A_jQ - QA_i^T - QA_j^T - B_iY_j - Y_j^T B_i^T - B_jY_i - Y_i^T B_j^T$, $i,j = \{1,...,r\}$, $j > i$.

$\square$

Remark 2. *Theorem 4 is given based on the assumption that $J < V(x(0)) = x^T(0)Px(0)$ and therefore solving LMI conditions (5.19) (5.20) (5.21) gives a sub-optimal solution which minimizes the upper bound $V(x(0))$ of the cost function J instead of J.*

5.2.5 Unknown Input Observer for Linear system

In this part, the PI-Observer developed in [85] is briefly introduced. We consider a class of linear system with unknown input described by

$$\begin{cases} \dot{x}(t) = Ax(t) + Bu(t) + Nd(x,t) \\ y(t) = Cx(t) \end{cases} \tag{5.35}$$

where the system matrices $A \in R^{n \times n}, B \in R^{n \times l}, C \in R^{m \times n}, N \in R^{n \times r}$ are assumed known and matrix A is stable. $d(x,t)$ is unknown input vector which need to be estimated. The idea behind

PI-Observer is to replace $d(x,t)$ by an integral term

$$d(t) \approx Hv(t) \text{ with } \dot{v}(t) = Vv(t)$$

where H, V are the appropriate matrices which calibrate the relation between $d(t)$, $v(t)$ and $\dot{v}(t)$. According to [85], $V = 0$ and $H = I$ are sufficient to obtain very good results in estimation and control applications. Adding new variable $v(t)$ to (5.35) leads to a reduced system

$$\begin{cases} \begin{bmatrix} \dot{x}(t) \\ \dot{d}(t) \end{bmatrix} = \begin{bmatrix} A & N \\ 0 & 0 \end{bmatrix} \begin{bmatrix} x(t) \\ d(t) \end{bmatrix} + \begin{bmatrix} B \\ 0 \end{bmatrix} u(t) \\ y(t) = \begin{bmatrix} C & 0 \end{bmatrix} \begin{bmatrix} x(t)) \\ d(t)) \end{bmatrix} \end{cases} \tag{5.36}$$

In order to estimate extended state $[x(t) \; d(t)]^T$ a proportional term is added to construct observer (5.37)

$$\begin{cases} \begin{bmatrix} \dot{\hat{x}}(t) \\ \dot{\hat{d}}(t) \end{bmatrix} = \underbrace{\begin{bmatrix} A & N \\ 0 & 0 \end{bmatrix}}_{A_e} \begin{bmatrix} \hat{x}(t) \\ \hat{d}(t) \end{bmatrix} + \underbrace{\begin{bmatrix} B \\ 0 \end{bmatrix}}_{B_e} u(t) + \underbrace{\begin{bmatrix} L_1 \\ L_2 \end{bmatrix}}_{L} \left(y(t) - \hat{y}(t) \right) \\ \hat{y}(t) = \underbrace{[C \; 0]}_{C_e} \begin{bmatrix} \hat{x}(t) \\ \hat{d}(t) \end{bmatrix} \end{cases} \tag{5.37}$$

where $L = [L_1 \; L_2]^T$ are the feedback gains of observer which need to be chosen to make estimation errors converge to zero. The condition for PI Observer design is given by

$$rank \begin{bmatrix} \lambda I_n - A & -N \\ 0 & \lambda I_r \\ C & 0 \end{bmatrix} = n + r \tag{5.38}$$

LQR method can be used to design L. For an asymptotic stable observer, if for two positive definite matrices $Q_o = \begin{bmatrix} I_n & 0_{n \times r} \\ 0_{r \times n} & qI_r \end{bmatrix}$ and $R_o = I_m$ with $q > 0$, I_n is identity matrix size of n,

the Riccati equation

$$A_e P + P A_e^T + Q_o - P C_e^T R_o^{-1} C_e P = 0$$

has a unique positive definite solution P, then the observer gain can be found by $L = P C_e^T R_o^{-1}$.

5.3 User-in-the-loop wheelchair dynamic model

To design the optimal controllers for the proposed assistance system using the model-based control approach, it is necessary to develop an augmented dynamic model of the user-joystick-wheelchair system as shown in Fig. 5.1. We propose here a model of this system during the navigation task. This task can be described as follow. Firstly, based on the desired destination and knowledge/experience (is it a known area? sign ...), the user approximately sketches out a "global optimal path" in his head. This step can be classed into the strategy level. The second step is to plan an "optimal local path" which is about a few meters around EPW to avoid the obstacles while orienting to the above "global optimal path". This step belongs to the tactical level. At the operational level, the user manipulates joystick to control EPW following the pre-defined path. More specifically, based on position errors, the neuromuscular system provides traction forces that act on the joystick. By changing joystick positions, the user changes the power delivered to two electric motors which rotate both driven wheels at appropriate speeds. The user continuously verifies the position errors of the wheelchair to make sure that it follows his intention in both strategic and tactical levels. The control loops are now closed as shown in Fig. 5.2. Path planning block corresponds to the tactical level which is not considered in this thesis. We now develop each block of user-joystick-wheelchair augmented model at the operational level.

5.3.1 Kinematic model and user path following controller

Kinematic properties of EPW are considered as a unicycle robot as shown in Fig. 5.3. Assuming that there is not any slipping of the wheels (purely rolling), the motions of the robot can be described by the following system
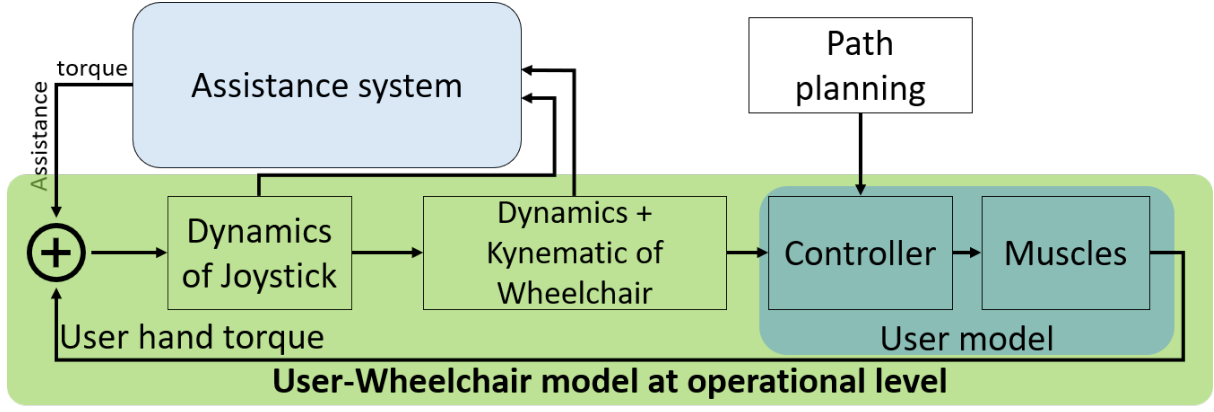
Figure 5.2: Proposed model of user-joystick-wheelchair system at the operational level

$$
\begin{cases}
\dot{x} = v\cos\varphi \\[2mm]
\dot{y} = v\sin\varphi \\[2mm]
\dot{\varphi} = \omega
\end{cases}
\tag{5.39}
$$

where (x, y, φ) is the actual position of the wheelchair in global coordinate system, respectively. v, ω are the longitudinal and angular velocity of the wheelchair. At each moment, the user targets a virtual desired wheelchair position located at point P which belongs to the desired path **C**. v_r, ω_r are the reference longitudinal and rotational velocities related to this virtual desired wheelchair position, respectively. The position errors of point P in the wheelchair body coordinate system are given by

$$
\begin{bmatrix} e_1 \\ e_2 \\ e_3 \end{bmatrix} = \begin{bmatrix} cos(\varphi) & -sin(\varphi) & 0 \\ sin(\varphi) & cos(\varphi) & 0 \\ 0 & 0 & 1 \end{bmatrix} \begin{bmatrix} x_P - x \\ y_P - y \\ \varphi_P - \varphi \end{bmatrix}
\tag{5.40}
$$

where (x_P, y_P, φ_P) is the reference position.

As shown in Fig.5.3, e_1 represents the look-ahead distance which is the distance between wheelchair center of gravity CG and the reference point P in the longitudinal direction. This distance depends on how long the user predicts wheelchair motions in the future and therefore depends subjectively on the user behavior. e_2, e_3 are the lateral and angular errors, respectively,
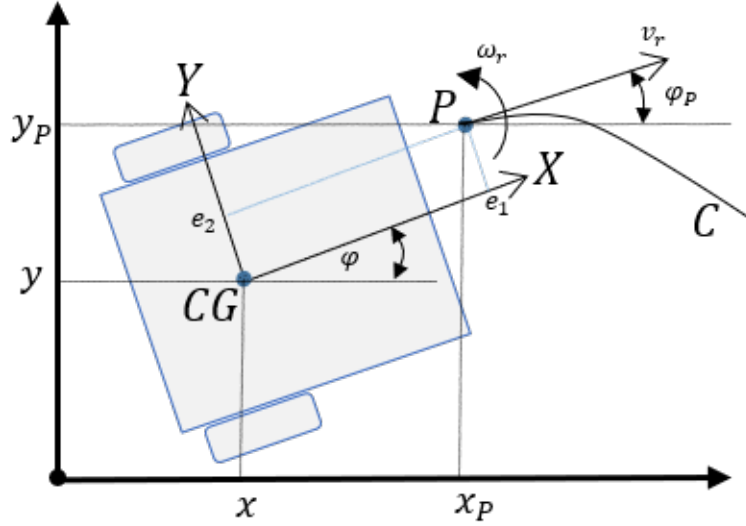
Figure 5.3: Kinematic model of EPW

which human controller tries to minimize. e_1, e_2, e_3 can be interpreted as how the user predicts the wheelchair's motion in the next few moments. This approach is similar to the trajectory tracking method. However, in trajectory tracking, the location of point P is pre-described by a function of time which is independent from wheelchair motion. In contrast, in this approach the location of point P is defined as follow: at each moment, the user selects on the desired path the nearest point to the wheelchair, then the reference point P is located in front of the wheelchair at a certain distance from this nearest point on the desired path. Note that the reference point P is always on the desired path and maintains a relatively fixed distance to the wheelchair.

Path following and trajectory tracking are well-known problems in the robotic area. While the motions in trajectory tracking are described by time, the path-following method needs to precise the geometry properties of the desired path independent from time. Although both these methods can archive human-like motions, their complexity leads to limitations in modeling user behavior for controller synthesis purposes. Besides, both methods based on the kinematic model of the unicycle robot with control signals that are longitudinal and angular speed, neglect the actions at the operational level. Motivated from this problem, we propose here a simple user path-following controller with human muscle forces as control signals which act on wheelchair's joystick to follow a pre-described path based on coordinate systems in Fig. 5.3. This controller consists of two parts: longitudinal and angular parts. During following

a reference path, users tend to have a preferable longitudinal velocity which depends on their capacity, curvature of the path, surrounding environment (obstacle, incline surface ...). The longitudinal part of the proposed controller is in charge of realizing the desired forward speed of human users. It is a proportional-integral controller-based as follow

$$F_l = k_p e_v + k_i \int e_v \tag{5.41}$$

where $e_v = v_r - v_{real}$ is the velocity error, v_{real} is the real velocity of wheelchair, k_p, k_i are the coefficients of the controller and F_l denotes the human hand force applied on the joystick in the longitudinal direction. The desired velocity v_r in general may vary depending on user situation, surrounding environment and user's desired trajectory. In this research, we consider a simple model of desired velocity v_r depending linearly on the lateral and angular errors as

$$v_r = v_0 \left(1 - k_{ve2} |e_2| - k_{ve3} |e_3|\right) \tag{5.42}$$

Formula 5.42 allows reducing the desired speed of the wheelchair user when he finds that the lateral and angular errors increase.. v_0 is the desired speed when wheelchair is on a right position ($e_2 = e_3 = 0$). $k_{ve2}, k_{ve3} > 0$ are the coefficients which reflect how the human negotiate their speed to adapt the position errors. Normally wheelchair users tend to reduce their speed or even stop when they find a big error in their position. The angular part of human path-following controller tries to minimize the lateral and angular errors e_2, e_3 by a simple proportional controller

$$F_a = k_{re2} e_2 + k_{re3} e_3 \tag{5.43}$$

where F_a is the human hand force applied on the joystick in lateral direction. k_{re2} and k_{re3} are the parameters which represent the effort of user in changing wheelchair direction. These parameters, along with k_{ve2}, k_{ve3} allow to simulate the user's driving behaviour during navigation task.

5.3.2 Neuromuscular-joystick-wheelchair dynamic model

Dynamics model of muscles attracted much attention from biomechanical researchers who try to describe the force creating mechanism of muscles by its properties [86]. In the point of view of control engineering, neuromuscular dynamics is often modeled as a first-order transfer function to take into account the delay in a human neuromuscular reaction as

$$\dot{F}_{m,i} = -\frac{1}{\tau_m}\left(F_{m,i} + F_i\right) \tag{5.44}$$

where $i = l, a$ denotes for longitudinal and angular components. τ_m is the time constant which represents the delay in processing, transmitting information of users and the response of muscles.

Joystick is the most popular interface used in EPW [5] [9]. However, in literature, to the best of author's knowledge, dynamics of the hand-joystick system is often neglected in researches on assistance system for EPW. To develop a joystick force feedback-based assistance system for EPW, we consider here a hand-joystick dynamic model which is represented by a second-order system as in (5.45). It should be noted that joystick can rotate about its two axes $x-axis$ and $y-axis$ which are in the same direction to the body coordinate system of the wheelchair. Longitudinal hand force $F_{m,l}$ makes joystick rotate about $y-axis$ and makes wheelchair go forward and reverse while lateral hand force $F_{m,a}$ makes joystick rotate about $x-axis$ and makes wheelchair turn.

$$\ddot{\theta}_i = \frac{1}{J}\left(T_{h,i} + T_{a,i} - K_j\theta_i - B_j\dot{\theta}_i\right) \tag{5.45}$$

where $i = l, a$. $T_{h,a} = F_{m,a}l_j, T_{h,l} = F_{m,l}l_j$, are hand torques acting on the joystick in longitudinal and rotational directions which are equal to hand forces multiplied by the joystick's length l_j (suppose that the hand force vectors are always perpendicular to joystick). θ_i are rotation angles of joystick. J, K_j, B_j are the moment of inertia, stiffness and viscosity equivalent of hand-joystick systems, respectively. Since both joystick and human hand move during manipulating, hand-wrist stiffness and viscosity have to be considered in the corresponding equivalent values of hand-joystick system. $T_{a,a}, T_{a,l}$ are assistance haptic torques applied on joystick in both

directions.

The low-level controller of EPW provides electric energy to the wheelchair motors by varying the voltages based on the position of joystick θ_i. The dynamics of electric motors are considered much faster than that of a wheelchair and therefore is negligible. Thanks to this simplification, the dynamic of the wheelchair can be generally reduced to the first-order system.

$$\dot{v}_{real} = -\frac{1}{\tau_{yv}}v_{real} + k_{yv}\theta_l + d_v \tag{5.46}$$

$$\dot{\omega}_{real} = -\frac{1}{\tau_{x\omega}}\omega_{real} + k_{x\omega}\theta_a + d_\omega \tag{5.47}$$

where $k_{yv}, k_{x\omega}$ are coefficients related to power amplifier characteristics of joystick. $\tau_{yv}, \tau_{x\omega}$ are time constants of the wheelchair dynamic response. d_v, d_ω denote the external disturbances to the wheelchair performance (incline surface, misalignment of front wheels, ...).

5.3.3 Model state-space representation

From (5.40), lateral errors dynamics can be deduced

$$\dot{e}_2 = -e_1\omega_{real} + v_r\sin e_3 \tag{5.48}$$

where ω_{real} is the rotation speed of the wheelchair. To simplify this model, e_3 is supposed small and therefore $\sin e_3 = e_3$. The dynamics of the longitudinal speed error is given by $\dot{e}_v = \dot{v}_r - \dot{v}_{real}$. For sake of simplicity, we suppose that $\dot{v}_r = 0$ and therefore

$$\dot{e}_v = -\frac{1}{\tau_{yv}}e_v - k_{yv}\theta_l + \frac{1}{\tau_{yv}}v_r - d_v \tag{5.49}$$

From (5.49), (5.46) and (5.44), the longitudinal part can be represented in the following form

$$\begin{cases} \dot{x}_l = A_l x_l + B_l T_{a,l} + B_{u,l} v_r + B_{d,l} d_v \\ y_l = C_l x_l \end{cases} \qquad (5.50)$$

where $x_l = \begin{bmatrix} \int_0^t e_v & e_v & \theta_l & \dot{\theta}_l & F_{m,l} \end{bmatrix}^T$ is the system state vector and the system matrices are given by

$$A_l = \begin{bmatrix} 0 & 1 & 0 & 0 & 0 \\ 0 & \frac{-1}{\tau_{yv}} & -k_{yv} & 0 & 0 \\ 0 & 0 & 0 & 1 & 0 \\ 0 & 0 & -\frac{K_j}{J} & -\frac{B_j}{J} & \frac{l_j}{J} \\ \frac{K_i}{\tau_m} & \frac{K_p}{\tau_m} & 0 & 0 & -\frac{1}{\tau_m} \end{bmatrix}, B_l = \begin{bmatrix} 0 \\ 0 \\ 0 \\ \frac{1}{J} \\ 0 \end{bmatrix}, B_{u,l} = \begin{bmatrix} 0 \\ \frac{1}{\tau_{yv}} \\ 0 \\ 0 \\ 0 \end{bmatrix}, B_{d,l} = \begin{bmatrix} 0 \\ -1 \\ 0 \\ 0 \\ 0 \end{bmatrix}.$$

It can be seen from the state-space representation that the human desired velocity v_r and external disturbance d_v now are considered as the unknown inputs. However, both appear together in the dynamics of the second state and therefore we cannot estimate both simultaneously. Assume that $d_v = 0$, v_r now is the unique unknown input needed to be estimated. The assistance haptic torque $T_{a,l}$ plays the role of the control input. In general, only the joystick position θ_l is available for measurement on the real wheelchair and therefore the output matrix is given as $C_l = \begin{bmatrix} 0 & 0 & 1 & 0 & 0 \end{bmatrix}$.

The angular part of this human-wheelchair model has the same form

$$\begin{cases} \dot{x}_a = A_a x_a + B_a T_{a,a} + B_{u,a} \omega_r + B_{d,a} d_\omega \\ y_a = C_a x_a \end{cases} \qquad (5.51)$$

where $x_a = \begin{bmatrix} e_2 & e_3 & \omega_{real} & \theta_a & \dot{\theta}_a & F_{m,a} \end{bmatrix}^T$ is the system state and the system matrices are given by

$$A_a = \begin{bmatrix} 0 & v_r & -e_1 & 0 & 0 & 0 \\ 0 & 0 & -1 & 0 & 0 & 0 \\ 0 & 0 & -\frac{1}{\tau_{x\omega}} & k_{x\omega} & 0 & 0 \\ 0 & 0 & 0 & 0 & 1 & 0 \\ 0 & 0 & 0 & -\frac{K_j}{J} & -\frac{B_j}{J} & \frac{l_j}{J} \\ \frac{K_{re2}}{\tau_m} & \frac{K_{re3}}{\tau_m} & 0 & 0 & 0 & \frac{-1}{\tau_m} \end{bmatrix}, B_a = \begin{bmatrix} 0 \\ 0 \\ 0 \\ 0 \\ \frac{1}{J} \\ 0 \end{bmatrix}, B_{u,a} = \begin{bmatrix} 0 \\ 1 \\ 0 \\ 0 \\ 0 \\ 0 \end{bmatrix}, B_{d,a} = \begin{bmatrix} 0 \\ 0 \\ 1 \\ 0 \\ 0 \\ 0 \end{bmatrix}$$

In this model, desired rotation speed of the user ω_r and external disturbance d_ω are considered as unknown inputs while assistance feedback torque $T_{a,a}$ is the control input. For this system, only the joystick position θ_a and the real yaw rate ω_{real} can be directly measured and therefore the output matrix is $C_a = \begin{bmatrix} 0 & 0 & 1 & 0 & 0 & 0 \\ 0 & 0 & 0 & 1 & 0 & 0 \end{bmatrix}$.

5.4 Normal driving assistance

5.4.1 Observer - controller architecture

"Normal driving mode" is defined as driving EPW without risk of collision/accident with the surrounding environment. In this mode, the main mission of the assistance system is to reduce the user effort in manipulating the joystick while maintaining the initiative of the user in wheelchair control. To this end, it is necessary to estimate the user intention allowing to provide a haptic assistance torque through joystick according to the user demand. We propose here a novel structure of shared control for those purposes as shown in Fig. 5.4. In this context, user intention is defined by the lateral and angular errors e_2, e_3, desired longitudinal speed v_r, and desired angular speeds ω_r. Two unknown input observers (UIO) are used for estimating these informations as unknown inputs $(v_r, \omega_r, d_\omega)$ and system states (e_2, e_3). In the next step, two controllers, for longitudinal and angular motions, are used to provide assistance torques $T_{a,l}, T_{a,a}$ to the user through joystick force feedback. It should be noted that this system requires only standard measurements (joystick positions and wheelchair's rotation speed) which

are available on the CAN-bus system of commercial electric wheelchair [4] and therefore no additional physical sensor is required.
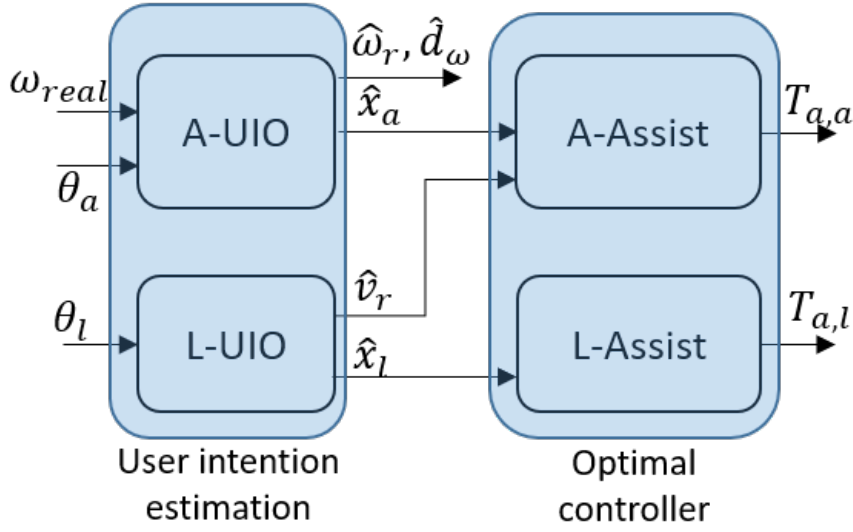
Figure 5.4: Structure of proposed assistance system based on unknown input observers and optimal controllers

L-UIO is the unknown input observer for the longitudinal system (5.50) which estimates the state $\hat{x}_l$ and the desired velocity $\hat{v}_r$ based on the longitudinal movement θ_l of the joystick. A-UIO estimates the desired rotation speed ω_r, external disturbance d_ω and the state $\hat{x}_a$ based on the joystick angle θ_a and the yaw rate ω_{real} of the wheelchair. In this research, both observers are Proportional-Integral (PI) Observer type which was presented in section 5.2 . System (5.50) is a linear time-invariant (LTI) system and therefore we adopt here a simple Linear-Quadratic Regulator (LQR) method to design the L-Assist block. In contrast, system (5.51) is a linear parameter varying (LPV) system because it is nonlinear according to the user's desired velocity v_r considered here as a time-varying parameter. In section 5.4.3, we will present this system under the form of the Tagaki-Sugeno fuzzy model to deal with this non-linearity and then an optimal fuzzy control scheme will be adopted to design the A-Assist block.

5.4.2 User intention estimation

User intention is defined by the position errors e_2, e_3 and desired speeds ω_r, v_r. It can be verified that the linear system (5.50) satisfies rank condition (5.38) and therefore PI-observer technique

can be applied to estimate desired velocity v_r of the user from the longitudinal position of the joystick. In contrast, system (5.51) is non-linear with two time-variant parameters v_r, e_1. To facilitate observer design, v_r in the model (5.51) is assumed a constant at $0.2m/s$ [4]. This value is chosen based on analyzing published data in [4] where a group of fourteen EPW users, including 12 persons with different diseases (cerebral palsy, Duchenne muscular dystrophy, multiple sclerosis, brain injury, etc.) was required to follow a course as rapidly as possible without any collision with obstacles. The data shows that participants finish a course of $10.5m$ within about $61s$. In practice e_1 is also changed with position errors e_2, e_3 and v_r. To simplify observer design, $e_1 = 0.1m$ is chosen as half of the distance traveled in 1 second. With fixed v_r, e_1 values, model (5.51) becomes linear system and PI-Observer can be used to estimate desired rotation speed of user ω_r based on wheelchair's yaw rate ω_{real} and joystick lateral position θ_a and satisfies rank condition (5.38). With above assumption ($v_r = 0.2m/s$ and $e_1 = 0.1m$) user's intention in this context is *short-term intent*. It means that we try to estimate what human want in the next about one second.

5.4.3 Optimal controller design

To design the L-Assist block for delivering longitudinal assistance torque $T_{a,l}$, a simple LQR controller is presented. Given LTI system (5.50) where the states are available from observer L-UIO block, and two weighting matrices Q_a, R_a, the state feedback law $T_{a,l} = -R_a^{-1}B_l Px$ minimizes the cost function

$$J = \frac{1}{2}\int_0^\infty \left(x_l^T Q_a x_l + R_a T_{a,l}^2\right) dt \qquad (5.52)$$

where P is the solution of Algebraic Ricatti Equation

$$A_l^T P + PA_l + Q_a - PB_l R_a^{-1} B_l^T P = 0 \qquad (5.53)$$

To design the A-Assist block, model (5.51) is converted to T-S fuzzy model (5.16) with v_r is the unique premise variable while $e_1 = 0.1m$ is fixed. Because v_r cannot be measured directly,

the membership functions will be calculated based on the estimated value $\hat{v}_r$ from L-UIO block in Fig. 5.4 which is bounded $\hat{v}_{min} \leq \hat{v}_r \leq \hat{v}_{max}$ with $\hat{v}_{min} = 0.05 m/s$ and $\hat{v}_{max} = 0.3 m/s$. The membership functions are

$$h_1 = \frac{\hat{v}_{max} - \hat{v}_r}{\hat{v}_{max} - \hat{v}_{min}} \quad h_2 = \frac{\hat{v}_r - \hat{v}_{min}}{\hat{v}_{max} - \hat{v}_{min}} \tag{5.54}$$

In this research, position errors of wheelchair and human effort should be minimized and therefore the performance matrix is defined as

$$C_{\mu i} = \begin{bmatrix} 1 & 0 & 0 & 0 & 0 & 0 \\ 0 & 1 & 0 & 0 & 0 & 0 \\ 0 & 0 & 0 & 0 & 0 & 1 \end{bmatrix}$$

Theorem 4 now can be applied to T-S model of wheelchair-user model to design the state feedback controller (5.17) in the A-Assist block.

Remark 3. *The LMI conditions in Theorem 4 can be solved numerically with available solvers. In this work, the feedback gains $F_i, \ i = 1,...,r$, are computed with SeDuMi solver version 1.3 and YALMIP toolbox for MATLAB [82].*

5.5   Simulation results

Table 5.1 summaries the parameters used in this work. The time constants $\tau_{yv}, \tau_{x\omega}$ are adopted from experiment results in [87] with a small reduction to reflect the fact that voltage applied to electric motors on these experiments was quite small ($\pm 1V$). τ_m is given in [88]. Values of $k_{yv}, k_{x\omega}$ are calculated based on the technical parameters of electric motor for EPW in [89]. Note that these values can be varied depending on the operation modes of the wheelchair. When driving in a confined environment, lower values of $k_{yv}, k_{x\omega}$ help the user to get a finer control while higher ones are suitable for outdoor space [4]. Moment of inertia, viscosity, and stiffness equivalent coefficients of the lumped hand-joystick system are estimated by using the mass, dimensions of the joystick in [76] and muscle viscoelastic properties of the human wrist

Table 5.1: Parameters of the proposed joystick - wheelchair model

Parameter	Value	Parameter	Value
τ_{yv}	0.3	J	$5.10^{-4} \; kg.m^2$
$\tau_{x\omega}$	0.3	K_j	$0.62 \; Nm/rad$
τ_m	0.11	B_j	$0.022 \; Nms/rad$
k_{yv}	5.7	$k_{x\omega}$	-4.3
k_{ve2}	1	k_{ve3}	1.27

Table 5.2: Parameters of the path following-like human controller

Parameter	Value	Parameter	Value
Without shared control-based assistance			
k_p	0.62	k_i	2.5
k_{re2}	7.5	k_{re3}	7.5
With shared control-based assistance			
k_p	0.31	k_i	1.25
k_{re2}	4.5	k_{re3}	4.5

in [90] [91]. The other parameters of the human path-following controller can be varied to reflect different behaviors and motor impairments of users in driving their wheelchair using a joystick interface. Table 5.2 shows the parameters of the path following-like human model. In assistance mode, the navigation task is shared between humans and controller, therefore the model of humans should be changed correspondingly. Table 5.3 summarises the chosen matrices for controller and observer design.

The simulation results will show the effectiveness of the proposed assistance system through two main goals: (i) estimate user intention (position errors) and, (ii) reduce user efforts in maneuvering joystick by providing assistance torque. We design here two simulation scenarios: (i) Go straight with external disturbance and (ii) Follow an arbitrary path.

Table 5.3: Matrices chosen for synthesizing controller and observer

A-UIO	L-UIO	A-Assit	L-Assit
$q = 10^3$	$q = 10^3$	$W = \begin{bmatrix} 10 & \mathbf{0} \\ \mathbf{0} & I_2 \end{bmatrix}$	$Q_a = \begin{bmatrix} I_4 & \mathbf{0} \\ \mathbf{0} & 80 \end{bmatrix}$
$R_o = I_2$	$R = 1$	$R = 1$	$R_a = 1$
		$\gamma = 0.1$	

5.5.1 Go straight with external disturbance

This scenario is motivated by the fact that when getting around outdoor, the EPW user may suffer an unexpected inclined surface that can make a wheelchair go in the wrong direction and therefore need the correction from the human. In this simulation, EPW user is required to follow a straight line and an unexpected external turning torque $d_\omega = 0.9rad.s^{-2}$ will be applied to wheelchair in $10sec$, from $t = 6sec$ to $t = 16sec$.

5.5.1.1 User intention estimation results
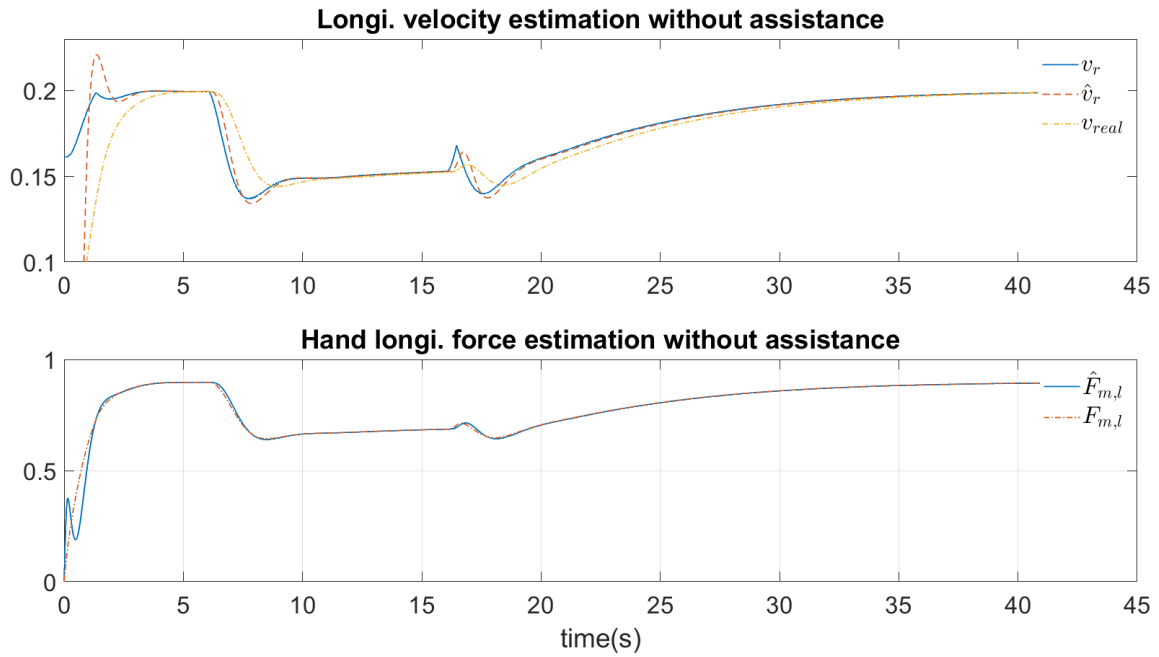
Figure 5.5: Estimation results of L-UIO block in the case of **without** assistance

Fig. 5.5 and Fig. 5.6 show the estimation results in both cases, with and without assistance, where the unknown input observer well estimates the desired longitudinal velocity of human. Fig. 5.7 and Fig. 5.8 present the estimation results of A-UIO block which estimates well the error position e_2, e_3, the human hand torque $F_{m,a}$ and unknown inputs ω_r. In the case with assistance, the estimation error e_3 is small while one of e_2 larger than the case without assistance. The external disturbance d_ω is well estimated in both case with and without assistance as shown in Fig. 5.9.

Figure 5.6: Estimation results of L-UIO block in the case of **with** assistance

Figure 5.7: Estimation results of A-UIO block in the case of **without** assistance
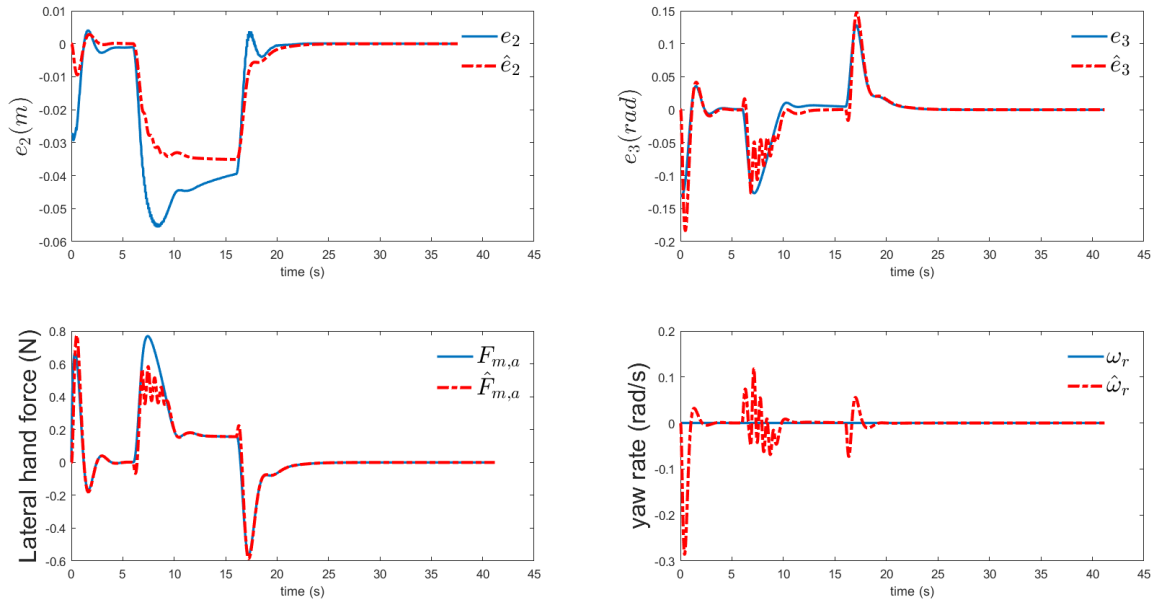
Figure 5.8: Estimation results of A-UIO block in the case of **with** assistance
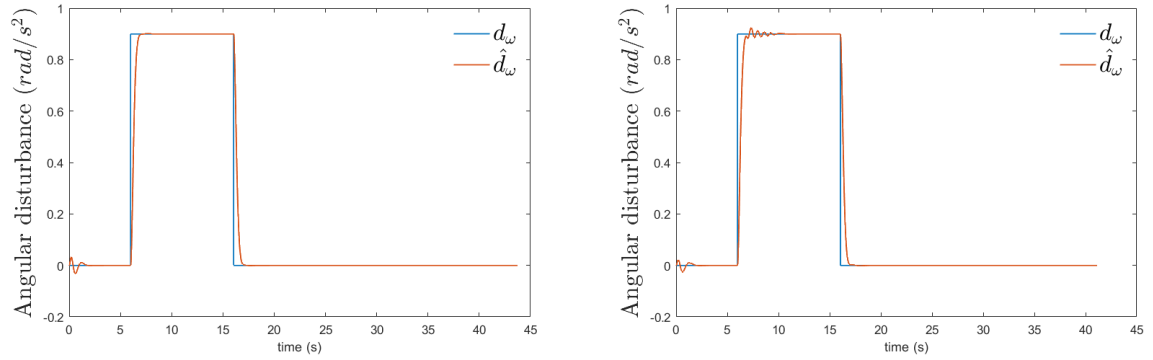
Figure 5.9: Disturbance estimation results in both case of **with and without** assistance
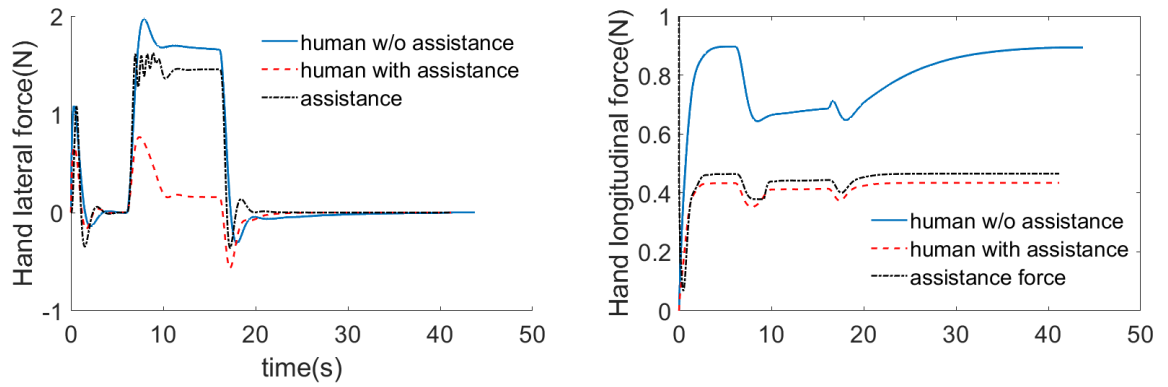
Figure 5.10: User hand force and assistance force in both cases with and without assistance

98

5.5.1.2 Haptic force feedback

Fig. 5.10 shows the evolutions of the longitudinal and lateral force of EPW user and assistance system. In the longitudinal direction, the user and system shared nearly the same amount of force and therefore reduce about 50% user hand force. In the lateral direction, it can be seen that the assistance system provides nearly the total required force to manipulate the joystick. The effectiveness of this assistance system can be seen in Fig. 5.11 where position errors of a wheelchair with assistance is much less than the case without assistance.
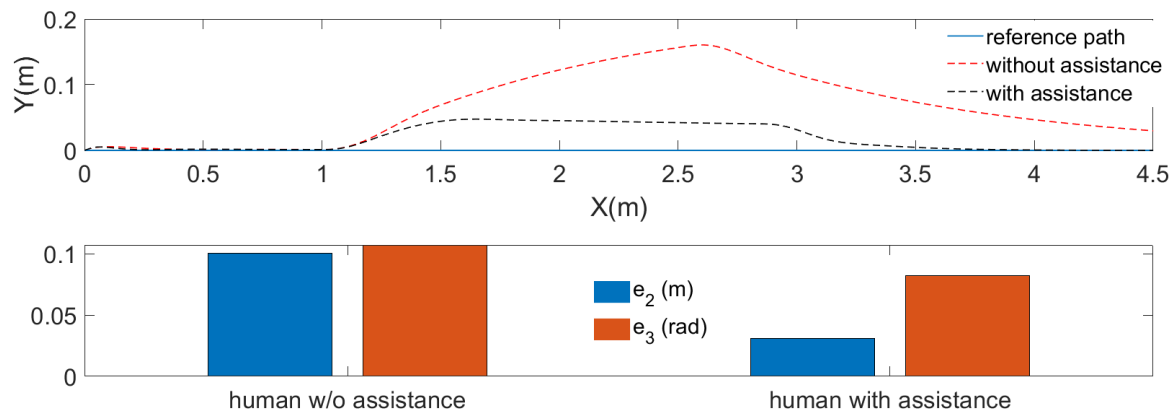
Figure 5.11: Path following results and mean position errors in both cases with and without assistance system

5.5.2 Follow an arbitrary path

In this simulation, EPW is required to follow an arbitrary pre-defined path which is considered as the desired path of the user (blue line in Fig. 5.16). This ideal path is a series of points which is naturally a 4th-order B-spline curve created by authors. The minimum turning radius of this path is $0.4m$ to represent the movement of the wheelchair in a confined environment. The position of wheelchair is initialized at the first point of this path with an initial heading angle error $\pi/12$. The simulation is conducted in two cases: with and without shared-control based assistance.
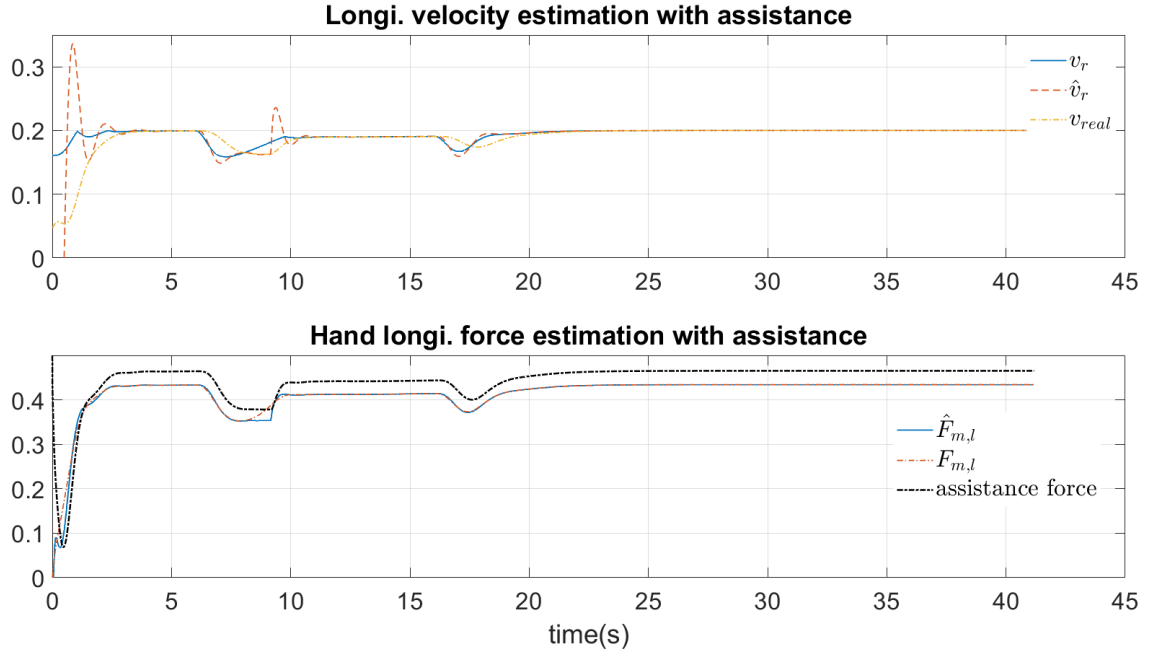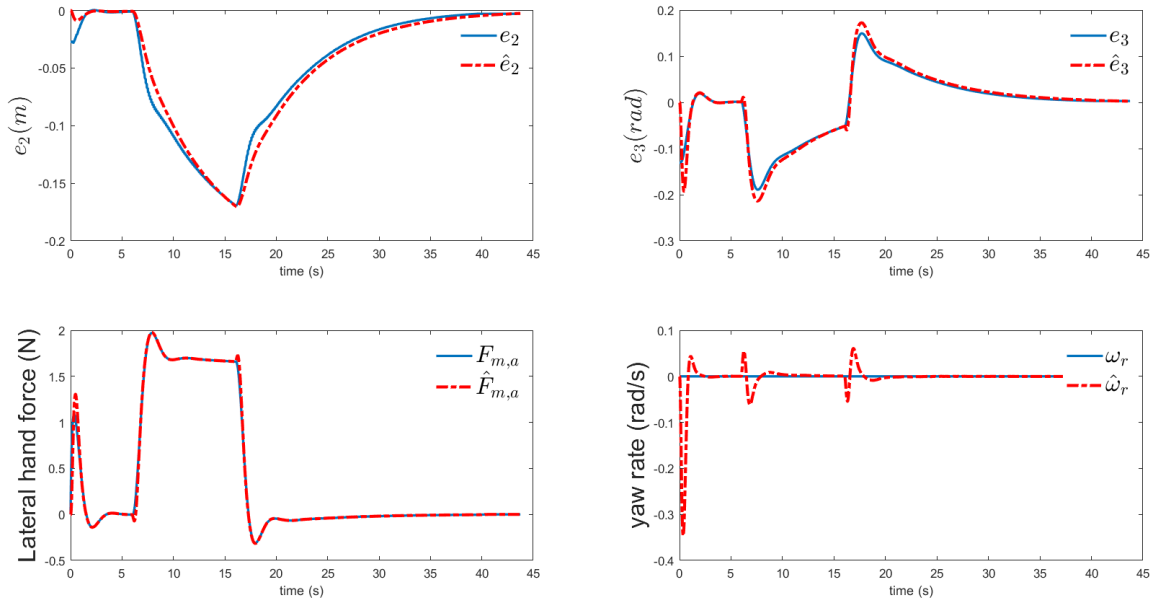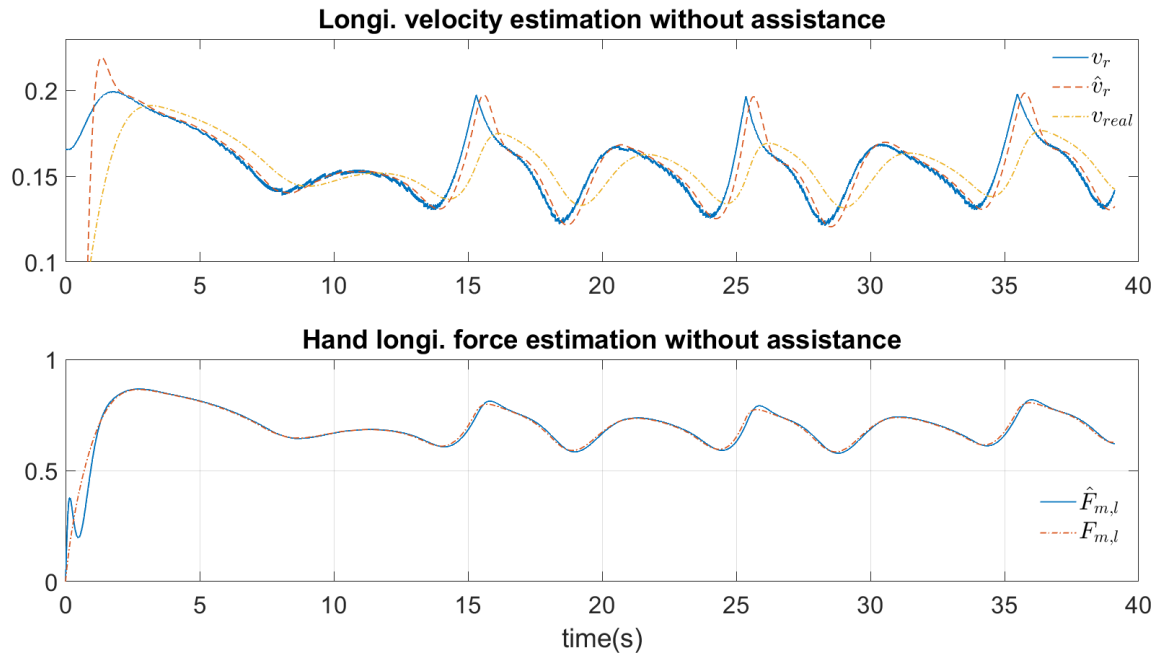
Figure 5.12: Estimation results of L-UIO block in the case of **without** assistance
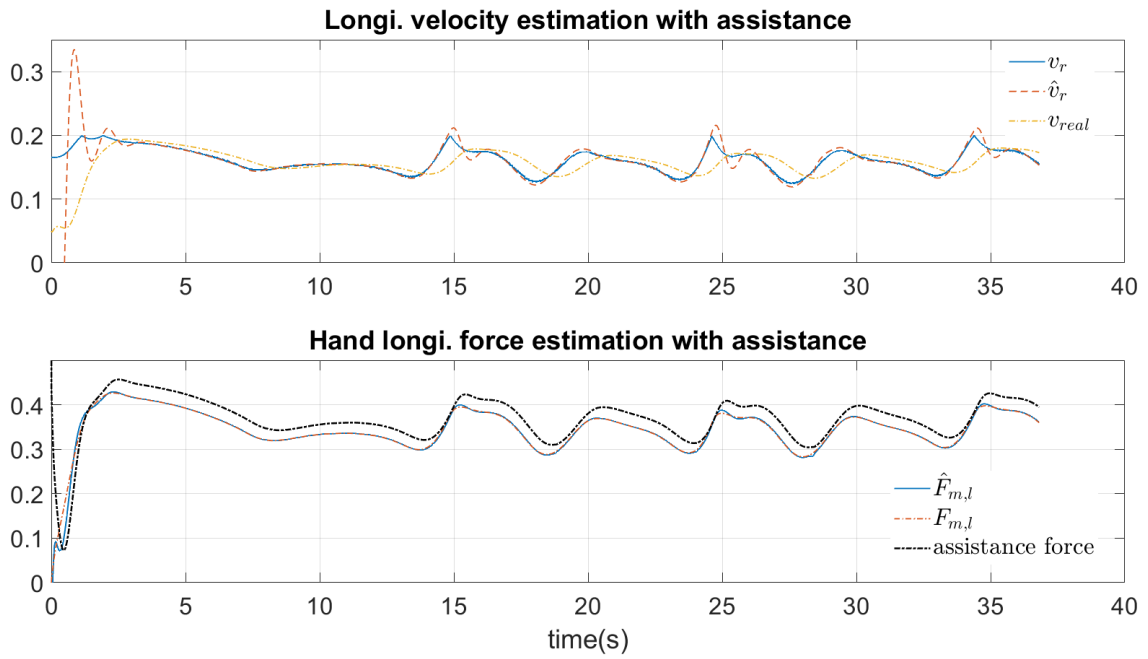
Figure 5.13: Estimation results of L-UIO block in the case of **with** assistance

5.5.2.1   User intention estimation results

Fig. 5.12 and Fig. 5.13 present the states and unknown input estimation results in longitudinal direction in both scenarios. It can be seen that from the longitudinal motion θ_l of the joystick, the proposed PI-Observer estimates well the desired velocity v_r and the hand longitudinal force $F_{m,l}$. The convergence time of the observer is about 1s. The estimated value of longitudinal velocity $\hat{v}_r$ is a little bit slower than the real one because the UIO supposes that the user desired velocity is constant which is not valid in reality.

The estimation results of the A-UIO block are shown in Fig. 5.14 and Fig. 5.15 where human hand torque, heading angle error and desired yaw rate, are well estimated based on the joystick position. The estimated lateral error $\hat{e}_2$ in the first 10*sec* is different from the real one. This is because the beginning of the desired path is quite linear and therefore the assumption $e_1 = 0.1$ is no longer valid. When the wheelchair turning, $\hat{e}_2$ follows the real ones. The estimation errors mostly come from the simplifying assumption of the system model.
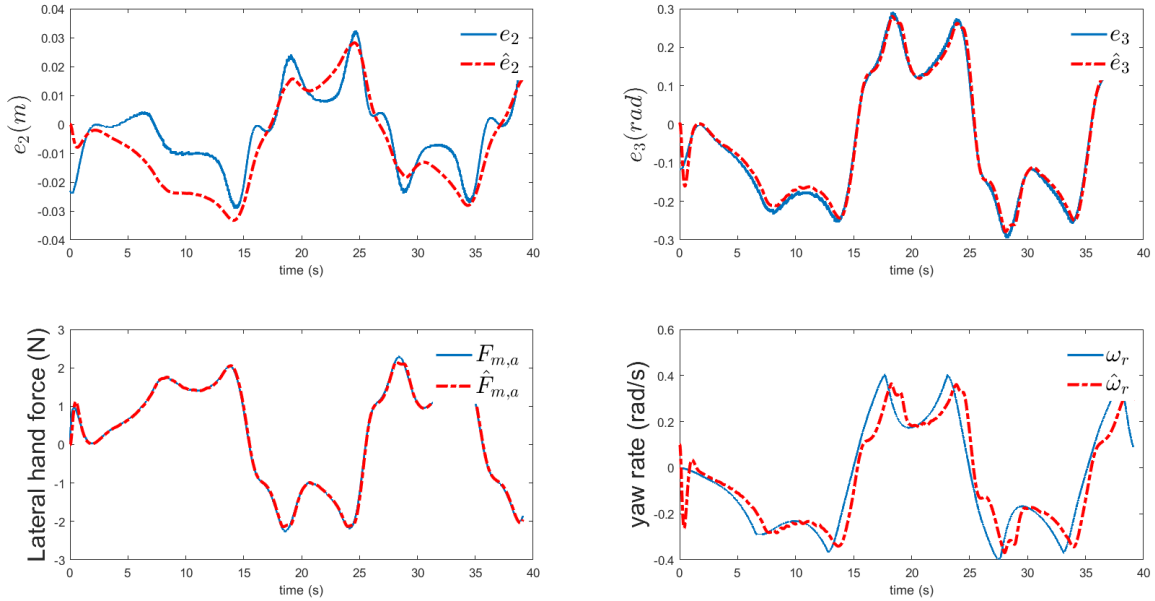
Figure 5.14: Estimation results of A-UIO block in case without assistance

5.5.2.2   Haptic force feedback

Fig. 5.16 presents the paths of a wheelchair in two cases: with and without assistance. It can be seen that in both cases mean position errors are small ($e_2 < 0.02m$ and $e_3 < 0.2rad$). Fig. 5.17
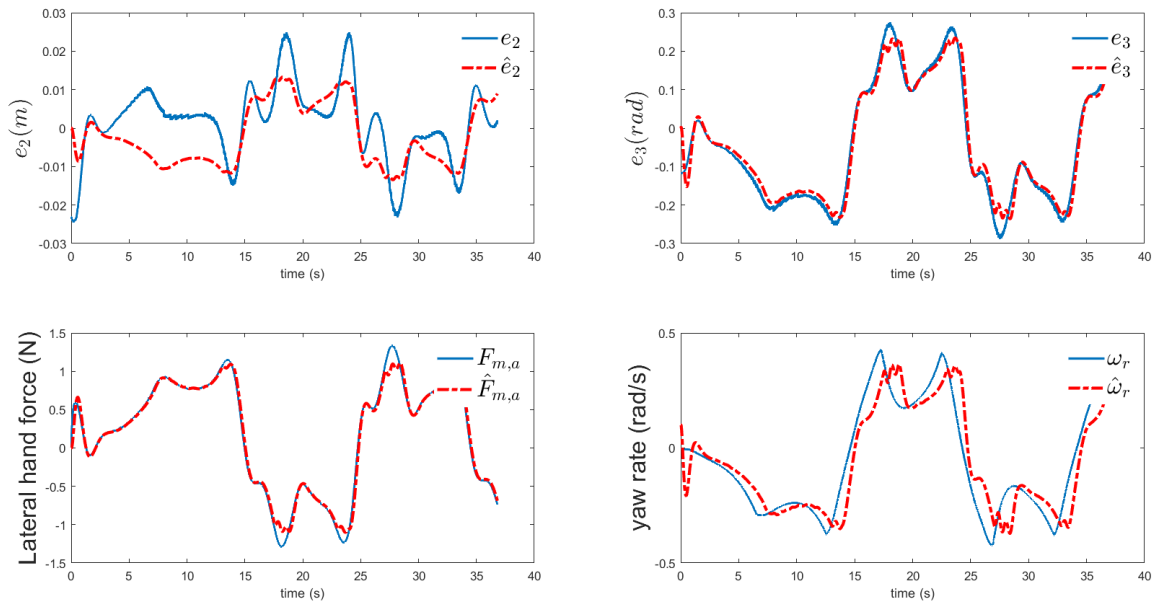
Figure 5.15: Estimation results of A-UIO block in case with assistance
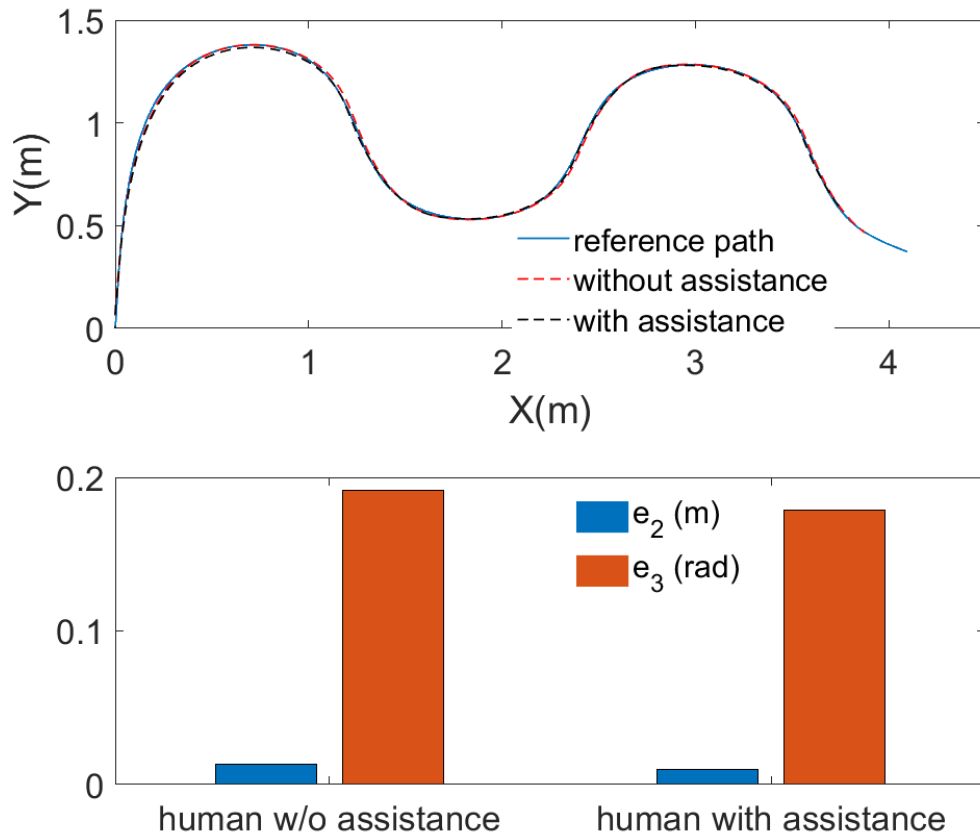
Figure 5.16: Path following results and position errors

shows that with assistance system, wheelchair user provides only about 50% of the necessary lateral force, about maximum $1.1N$ in comparison to the case without assistance with $2N$. Fig. 5.13 also shows that user effort is also reduced in manipulating joystick in the longitudinal direction where the assistance system provides about the same force as the user. It can be seen in Fig. 5.14, Fig. 5.15 and Fig. 5.16 that the assistance system maintains a good path following performance while reducing the user efforts in the navigation task.
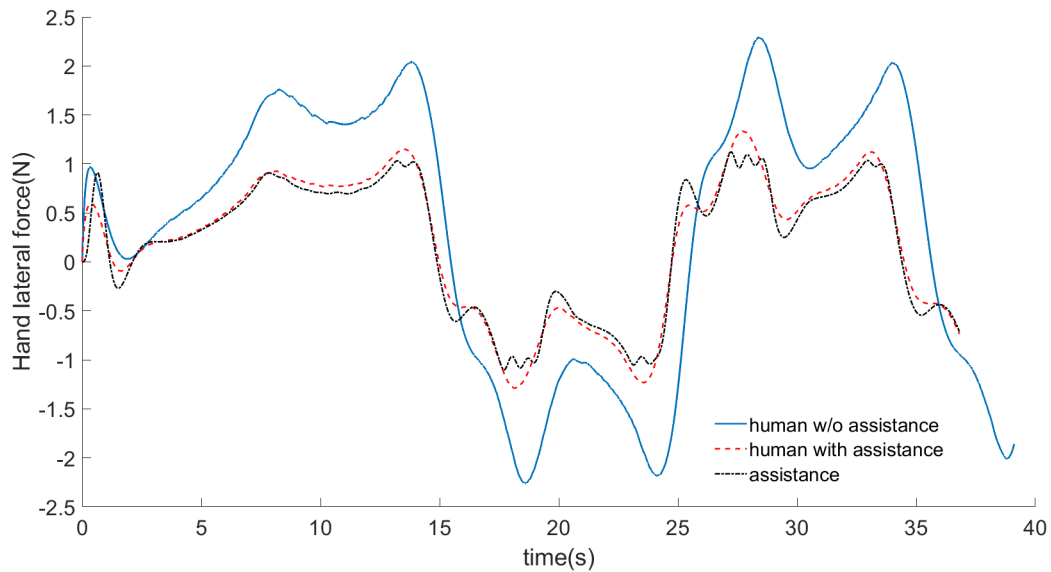
Figure 5.17: Wheelchair user lateral hand force and assistance force

5.6 Conclusion

This chapter presents the application of model-based control to design the assistance system to the EPW user in the navigation task through a haptic joystick force feedback. The assistance forces are provided by the optimal controllers which are designed based on an augmented dynamics model of user-joystick wheelchair system. This method allows us to estimate the user's intention and provides the haptic force to reduce the user efforts in manoeuvring joystick. Simulation results show that the proposed assistance system can predict the position errors of power wheelchair and assist the user to correct them by providing haptic forces to the joystick. Furthermore, this is done keeping a very good trajectory following performance, this performance

being even better in assisted mode than in non assisted mode. The user hand torques are reduced significantly thanks to the haptic torques and therefore the user comfort can be improved. One important aspect of this approach is that it does not require more special sensors but uses only joystick positions and wheelchair standard measurement signals to calculate the assistance force to the wheelchair user.

Chapter 6

Navigation assistance: obstacle avoidance and conflict management

Contents

The previous chapter presented the general shared control architecture (Fig. 5.1) of the proposed assistance system for power wheelchair users via a joystick force feedback and designed the assistance system in normal driving assistance mode. This chapter is devoted to design the

remaining parts in this architecture (Fig. 6.1) including the obstacle avoidance assistance mode (risk management functions and path-following controller) and conflict management function. The goal of these parts are:

- to inform/communicate to the user the potential collision/accident, the nearby obstacles to enhance the user situation awareness through the haptic force feedback joystick.

- to provide the appropriate assistance to help/guide the user to avoid the obstacles or prevent potential accidents through the haptic force feedback joystick so that the user can understand the suggestions/intentions of the system.

- to manage conflict between the user's actions/decisions and the suggestions from the system to assure the final decision maker role of the user.

As shown in the last chapter, when there is no risk of collision, the assistance system estimates the user's desired motions and provides haptic torques to reduce human effort. However, the desired path of humans may have a potential accident due to the wrong estimation of the distance to obstacles or incorrect predictions of the wheelchair motions. Therefore the first mission of the risk management block is to detect the potential collision. Once the potential collisions are detected, this block finds an alternative optimal free-collision path and transfer it to the path following controller. At this moment, the conflict management block activates the obstacle avoidance mode of the assistance system which expresses the proposed optimal path to the user through the haptic torques at the joystick. Now the joystick - wheelchair system is controlled by two independent "drivers", user and assistance system. The conflict management block makes sure that the user has the final decision role and fully understands the suggestion from the assistance system.

Firstly we design the path following controller of obstacle avoidance assistance system based on the dynamics model of joystick-wheelchair system and do not consider the human behavior model. Then the risk management block which manages the risk of accident is designed. To make sure that the wheelchair user is always the final decision-maker, the conflict management block is designed so that the assistance system follows the user decisions. Building a virtual wheelchair simulator platform in the next section is necessary to validate our proposed assistance system. Finally, the experimental results in a virtual environment will be presented.

6.1 Path following controller

The mission of the path-following controller in the obstacle avoidance assistance mode is to follow a predefined path with a predefined desired linear velocity by manipulating the haptic joystick without intervention from the users. Fig. 6.1 shows the structure of the assistance system in this mode. There are two controllers for longitudinal and angular movements. The path planning block provides the positions errors e_2, e_3, and the reference longitudinal and rotational velocities v_r, ω_r instead of estimating from joystick movements as in normal driving assistance mode. The conflict management block will choose which assistance torque, in normal driving assistance mode or obstacle avoidance assistance mode, will be applied to the joystick based on the risk of accident and conflict situation. We now focus on designing the controllers and observers in autonomous driving mode.
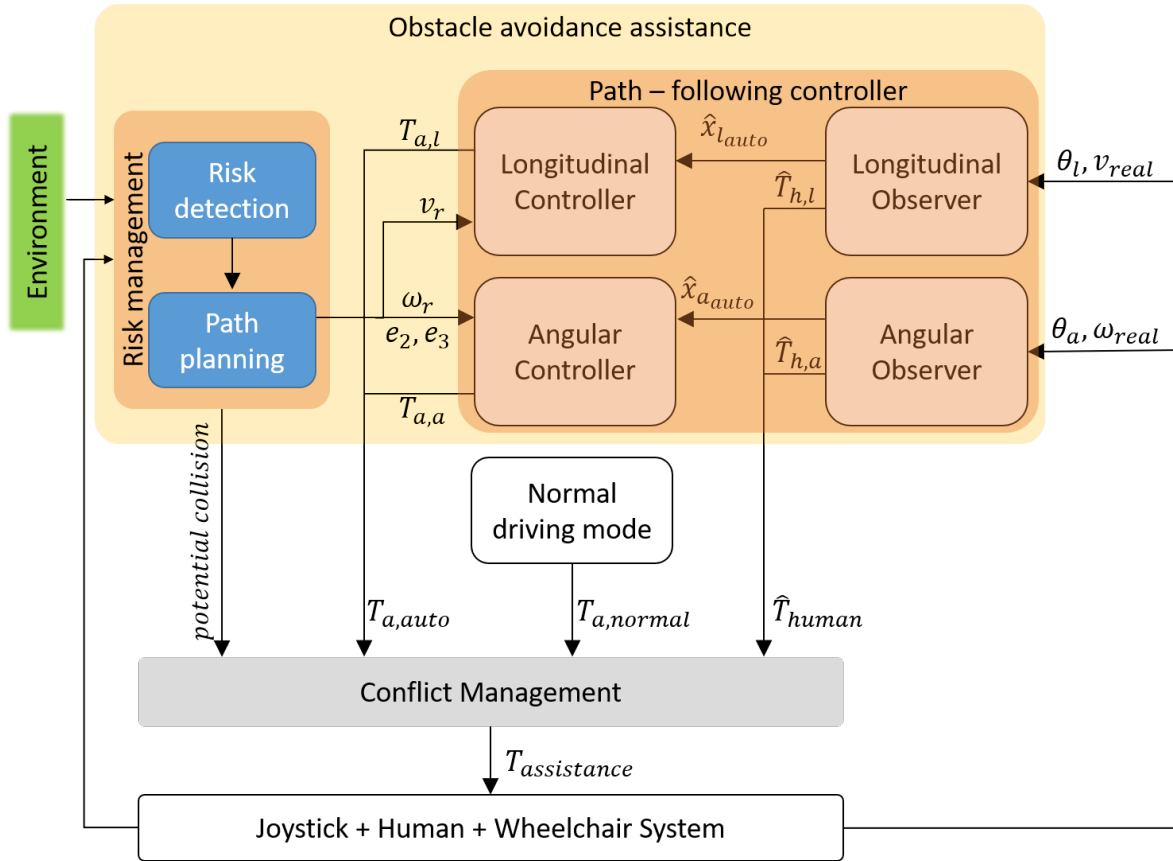
Figure 6.1: Structure of assistance system in obstacle avoidance assistance mode

6.1.1 Longitudinal and angular controller

To develop the path-following controller for the obstacle avoidance assistance mode of the assistance system, we keep the whole model presented in section 5.3 but remove the human model part. As a result, the dynamical model of the joystick-wheelchair system is now made of two parts: longitudinal and angular parts without human hand torque components. Without a human behavior model inside, the wheelchair operates in the autonomous mode. However, it should be noted that the wheelchair user always manipulates the joystick even in obstacle avoidance assistance mode. Therefore the model of the system in obstacle avoidance assistance mode cannot neglect the influence of user hand torques but considers them as the known inputs which will be estimated by the observers in the next sections. The dynamical model of the longitudinal part is

$$
\begin{cases}
\dot{x}_{l_{auto}} = A_{l_{auto}} x_{l_{auto}} + B_{l_{auto}} T_{a,l} + B_{h,l_{auto}} T_{h,l} + B_{d_{l_{auto}}} d_v \\
y_{l_{auto}} = C_{l_{auto}} x_{l_{auto}}
\end{cases}
\tag{6.1}
$$

where $x_{l_{auto}} = \begin{bmatrix} v_{real} & \theta_l & \dot{\theta}_l \end{bmatrix}^T$ is the system state vector and the system matrices are given by

$$
A_{l_{auto}} = \begin{bmatrix} \frac{-1}{\tau_{yv}} & k_{yv} & 0 \\ 0 & 0 & 1 \\ 0 & -\frac{K_j}{J} & -\frac{B_j}{J} \end{bmatrix}, \quad B_{l_{auto}} = B_{h,l_{auto}} = \begin{bmatrix} 0 \\ 0 \\ \frac{1}{J} \end{bmatrix}, \quad B_{d,l} = \begin{bmatrix} 1 \\ 0 \\ 0 \end{bmatrix}.
$$

The longitudinal motion model of EPW is a linear system with the control input being the assistance torque $T_{a,l}$. The longitudinal controller has to drive the wheelchair to track the reference velocity from the risk management block. It can be seen that the system (6.1) is linear and therefore a simple reference tracking controller is used by using the pole placement method as below.

Given a dynamical system :

$$
\begin{cases}
\dot{x}(t) = Ax(t) + Bu(t) \\
y(t) = Cx(t)
\end{cases}
\tag{6.2}
$$

The output $y(t)$ should track the reference input $r(t)$ as in Fig. 6.2. A solution for this tracking problem is

$$u(t) = Nr(t) - Kx(t) \tag{6.3}$$

The closed-loop system is

$$\begin{cases} \dot{x}(t) = (A - BK)x(t) + BNr(t) \\ y(t) = Cx(t) \end{cases} \tag{6.4}$$

The problem is choosing the appropriate matrices K, N so that the closed loop system is stable and $y(t) = r(t)$ as $t \to \infty$. Feedback gain matrix K can be calculated by the Ackermann's Formula [92] to put the poles of closed loop system at the desired positions. The extra gain N which scales the input reference can be computed [92]

$$N = -\left(C(A - BK)^{-1}B\right)^{-1} \tag{6.5}$$
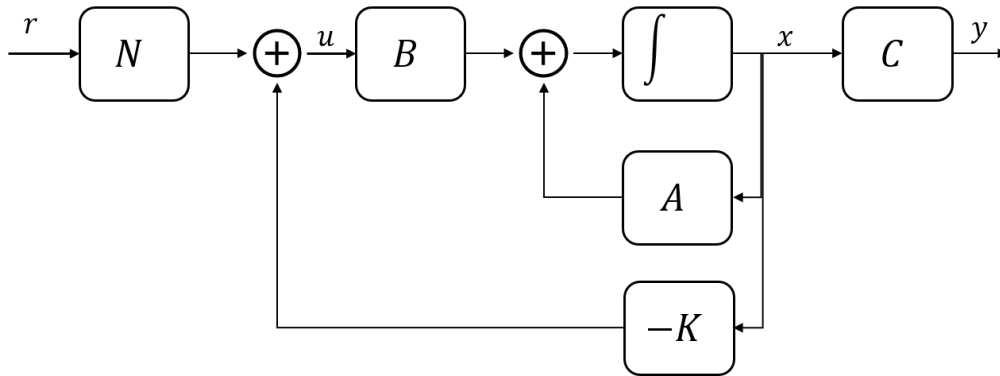
Figure 6.2: Tracking control for linear system

The longitudinal controller is designed by applying the controller (6.3) and (6.5) to the system (6.1).

The angular part of the joystick-wheelchair system is given by

$$\begin{cases} \dot{x}_{a_{auto}} = A_{a_{auto}}x_{a_{auto}} + B_{a_{auto}}T_{a,a} + B_{h,a_{auto}}T_{h,a} + B_{u,a_{auto}}\omega_r + B_{d,a_{auto}}d_\omega \\ y_{a_{auto}} = C_{a_{auto}}x_{a_{auto}} \end{cases} \tag{6.6}$$

where $x_{a_{auto}} = \begin{bmatrix} e_2 & e_3 & \omega_{real} & \theta_a & \dot{\theta}_a \end{bmatrix}^T$ is the system state and the system matrices are given by

$$A_{a_{auto}} = \begin{bmatrix} 0 & v_r & -e_1 & 0 & 0 \\ 0 & 0 & -1 & 0 & 0 \\ 0 & 0 & -\frac{1}{\tau_{x\omega}} & k_{x\omega} & 0 \\ 0 & 0 & 0 & 0 & 1 \\ 0 & 0 & 0 & -\frac{K_j}{J} & -\frac{B_j}{J} \end{bmatrix}, B_{a_{auto}} = B_{h,a_{auto}} = \begin{bmatrix} 0 \\ 0 \\ 0 \\ 0 \\ \frac{1}{J} \end{bmatrix}, B_{u,a_{auto}} = \begin{bmatrix} 0 \\ 1 \\ 0 \\ 0 \\ 0 \end{bmatrix}, B_{d,a_{auto}} = \begin{bmatrix} 0 \\ 0 \\ 1 \\ 0 \\ 0 \end{bmatrix}$$

In this model, desired rotation speed ω_r is given by a predefined path curvature. The external disturbance d_ω is the unknown input while assistance feedback torque $T_{a,a}$ is the control input. To design the controller for above model, we adopted the T-S representation as in 5.2.1 to deal with the nonlinear term v_r in this system. In this fuzzy model, v_r is still the premise variable which varies within a range $\begin{bmatrix} v_{r_{min}} & v_{r_{max}} \end{bmatrix}$. Then the optimal fuzzy controller can be designed as in 5.2.4 to minimize the errors positions e_2, e_3 with the performance output matrix as

$$C_{\mu i} = \begin{bmatrix} 1 & 0 & 0 & 0 & 0 \\ 0 & 1 & 0 & 0 & 0 \end{bmatrix}$$

It should be noted that the human hand torque inputs are not considered in designing these above controllers. Generally, it is reasonable to design a robust controller that rejects the effect of noise/disturbance to obtain the desired system performance. However, in this case, the main purpose of these above controllers is not to reject the human actions but to communicate to the user the intention of the assistance system. If the assistance system rejects the user's torques, it can make them feel confused when suddenly feeling a large reverse torque. Therefore the above controller design did not consider the "external disturbance" of human hand torques.

6.1.1.1 Simulation results

This part shows the efficiency of the proposed path following controller for EPW. The parameters of the joystick + wheelchair system model are the same as Table 5.1. The EPW is required to follow the reference path as in Fig. 5.16 with the reference longitudinal velocity given by 5.42. The desired longitudinal velocity is set to $0.2m/s$. The initial position of EPW is off the reference path of about $0.25m$. Table 6.1 summary the chosen matrices for synthesizing the path following controllers.
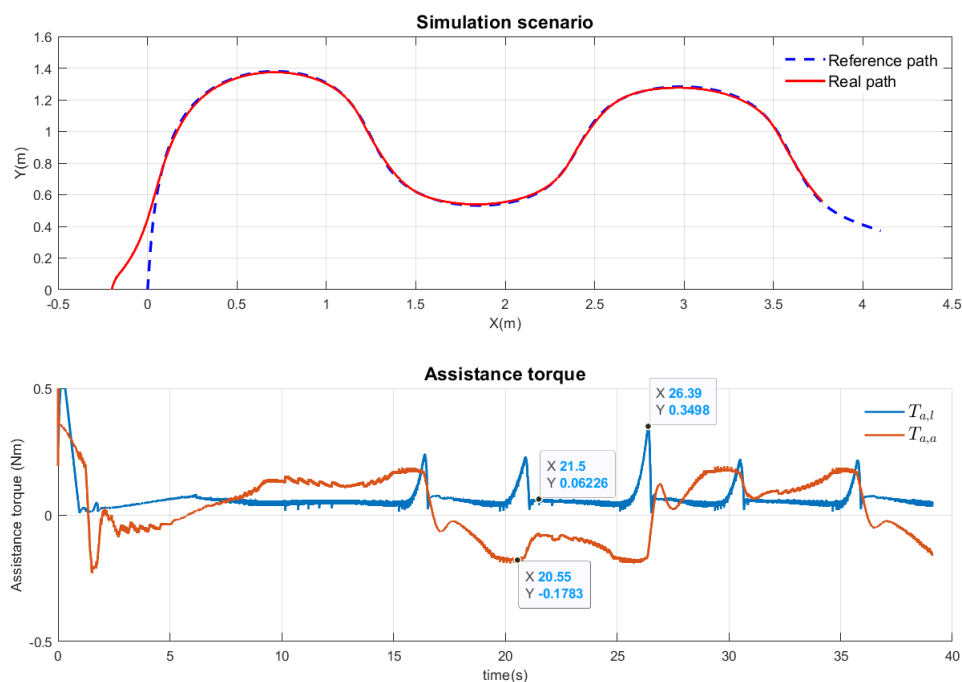
Figure 6.3: Simulation scenario and assistance torques in the path following task. $T_{a,l}$ and $T_{a,a}$ are the assistance torques in the longitudinal and lateral directions, respectively.

Fig. 6.3 shows the simulation results where the EPW follows well the reference path. The longitudinal joystick torque increases when the EPW reaches a linear segment of the path and reduces considerably when following a segment with high curvature. The lateral assistance torque is maximum about $0.17Nm$ which is consistent with the human torque to control the joystick in Fig. 5.17. Fig. 6.4 presents the joystick position distribution and EPW's velocities during the path following task. It can be seen that the longitudinal velocity follows well the reference one except for some moments ($16s, 21s, 27s, 31s$, and $36s$). This can be explained by the mechanical limitations of the EPW and the joystick [4]. Since the joystick can rotate inside
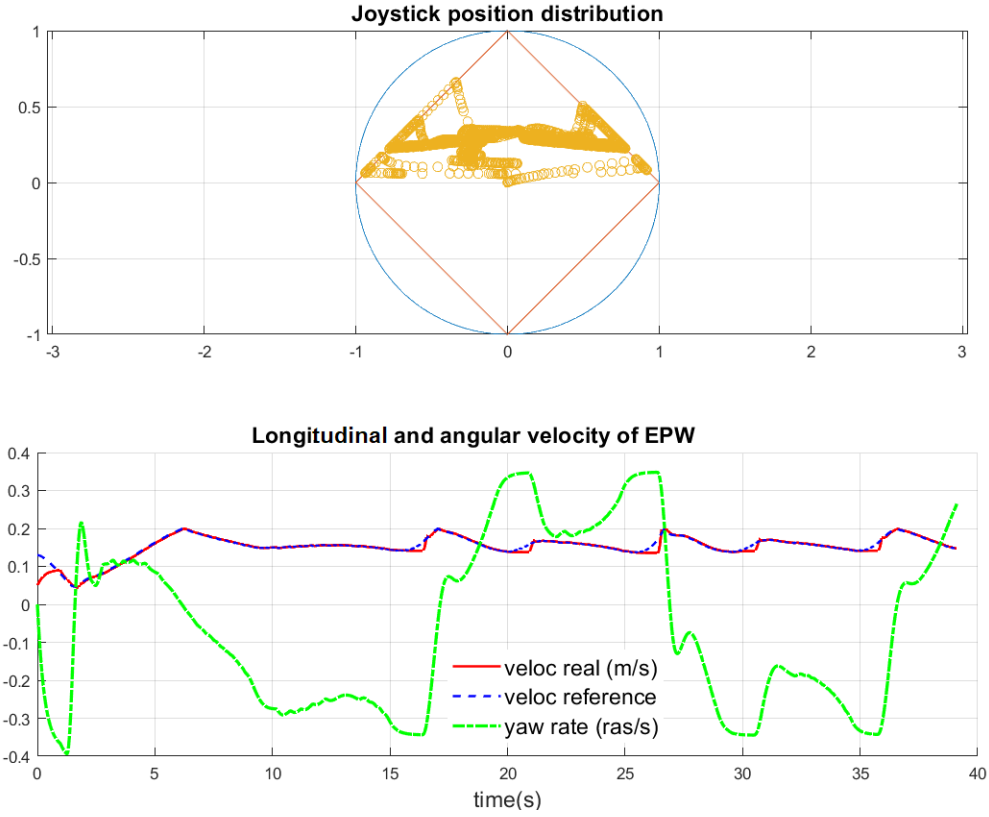
Figure 6.4: Joystick position distribution and EPW velocities

the circle, the longitudinal and angular velocities of EPW are constrained inside the square as shown in Fig. 6.4. Therefore, as the above moments, while the velocity tracking controller wants to increase speed due to the small position errors e_2, e_3, the angular path still needs to maintain the yaw rate of EPW to follow the path. As a result, the longitudinal velocity cannot increase until the yaw rate reduces correspondingly.

When these controllers are applied to assist the wheelchair user, it is expected that the user feels the haptic torques that represent the intentions of the assistance system. To make these assistances not only follow the optimal path (section 6.2.1.2) but also adapt their behaviours to the risk situation (section 6.2.1.1), we design here two modes of longitudinal and angular controllers by changing the design parameters in Table 6.1. The "near" mode will be used when the wheelchair is too near the obstacles and the assistance torques will be larger than that in the "far" mode where the EPW is still "far" the obstacles. Section 6.2 provides more detail on the operations of this system.

Table 6.1: Matrices chosen for synthesizing controllers

Longitudinal controller	Angular controller
$K = \begin{bmatrix} 8.4843 & 2.8387 & 0.0513 \end{bmatrix}$	$W = \begin{bmatrix} 10 & 0 \\ 0 & 0.1 \end{bmatrix}$
$N = 10.5$	$R = 0.05$

6.1.2   User hand torques estimation

One important function of our proposed assistance system is the conflict management function. It is necessary to estimate the user hand torques to detect the conflicts with assistance system actions. We exploit here the dynamic of the joystick to estimate the hand torques.

$$\ddot{\theta}_i = \frac{1}{J} \left(T_{h,i} + T_{a,i} - K_j \theta_i - B_j \dot{\theta}_i \right) \tag{6.7}$$

where $i = l, a$. θ_i are rotation angles of joystick. J, K_j, B_j are the moment of inertia, stiffness and viscosity equivalent of hand-joystick systems, respectively. $T_{a,a}, T_{a,l}$ are assistance haptic torques applied on joystick in both directions which are considered as the known inputs. To estimate the user torques $T_{h,i}$, we represent system (6.7) by state-space model with the state variable $x_i = \begin{bmatrix} \theta_i & \dot{\theta}_i \end{bmatrix}^T$, then

$$\begin{cases} \dot{x}_i = \begin{bmatrix} 0 & 1 \\ -\frac{K_j}{J} & -\frac{B_j}{J} \end{bmatrix} x_i + \begin{bmatrix} 0 \\ \frac{1}{J} \end{bmatrix} T_{a,i} + \begin{bmatrix} 0 \\ \frac{1}{J} \end{bmatrix} T_{h,i} \\ y_i = \begin{bmatrix} 1 & 0 \end{bmatrix} x_i \end{cases} \tag{6.8}$$

with assumption that only the joystick angles θ_i are measurable. Now the system (6.8) has the same form as (5.35) then we can adapt the unknown input observer presented in section 5.2.5 to design the observer for estimating the user hand torques $T_{h,i}$.

6.2 Risk and Conflict Management

6.2.1 Risk management

As mentioned before, the risk management block has to detect the risk of collision and find the optimal alternative movement solutions. This section details each function of this block.

6.2.1.1 Potential collision detection

In this section, we suppose that the obstacle positions and geometry are known prior. It should be noted that in a real confined environment, a few centimeters can make a big difference in navigation tasks [31]. Therefore we consider also the wheelchair geometry in the detection of potential collisions. Also, the EPW users can change their desired motion very fast, within a second. As a result, a collision detected in the next, for example, $5sec$ has no practical meaning. We consider here a "prediction horizon" varying from $1sec - 1.5sec$ depending on the velocity of EPW.

Firstly to predict the wheelchair motions in the next few seconds, we have two options. The first one is to use the user intention estimation results as in section 5.4.2. While this method can estimate the desired position of the user in the next few moments based on the dynamics of the joystick, it should be noted that this position may not be the future position of the wheelchair. The second option is to use the joystick positions, which are roughly proportional to the linear and angular velocities of the wheelchair, and the kinematic model (5.39). **While this method is purely kinematic and neglects the dynamics of the joystick, it is widely accepted in the prior works**. In this thesis, we will adapt the second approach for predicting the future motions of the wheelchair.

The algorithm 1 details the calculation steps for path-prediction function. Since the obstacle positions are given in the world coordinate system, the future path of the wheelchair has to be transformed accordingly to this system so that the collision check step can be done.

To perform the collision check, we defined all obstacles as connected segments. The wheelchair geometry is simplified by a rectangular box with four corners A, B, C, D as in Fig. 6.5 where we figure out eight collision poses that can occur to the wheelchair in a confined environ-

---
Algorithm 1 Path prediction

1: **function** PATH-PREDICT$(x, y, \varphi, \theta_l, \theta_a)$
2:     $x(1) = x; \quad y(1) = y; \quad \varphi(1) = \varphi$
3:     $v_{real} = k_{yv}\theta_l; \quad \omega_{real} = k_{xw}\theta_a; \quad \Delta t = 0.3;$
4:     **for** $i = 2$ to 6 **do** $\triangleright$ prediction horizon is $(6-1) \times \Delta t = 1.5 sec$
5:        $x(i) = x(i-1) + v_{real}\cos(\varphi(i-1))\Delta t;$
6:        $y(i) = y(i-1) + v_{real}\sin(\varphi(i-1))\Delta t;$
7:        $\varphi(i) = \varphi(i-1) + \omega_{real}\Delta t;$
8:        **Collision Check Algorithm 2 is here**
9:     **end for**
10: **end function**
---

ment. These poses influence the finding of an optimal alternative path which will be addressed in the next sections. The collision check task here is divided into two steps: i) detecting the potential collisions, and ii) finding where is the potential collision point on the wheelchair. The algorithm for this task is detailed in Algorithm 2 where $R_z(\cdot) = \begin{bmatrix} \cos(\cdot) & -\sin(\cdot) \\ \sin(\cdot) & \cos(\cdot) \end{bmatrix}$ is the 2D rotation matrix.
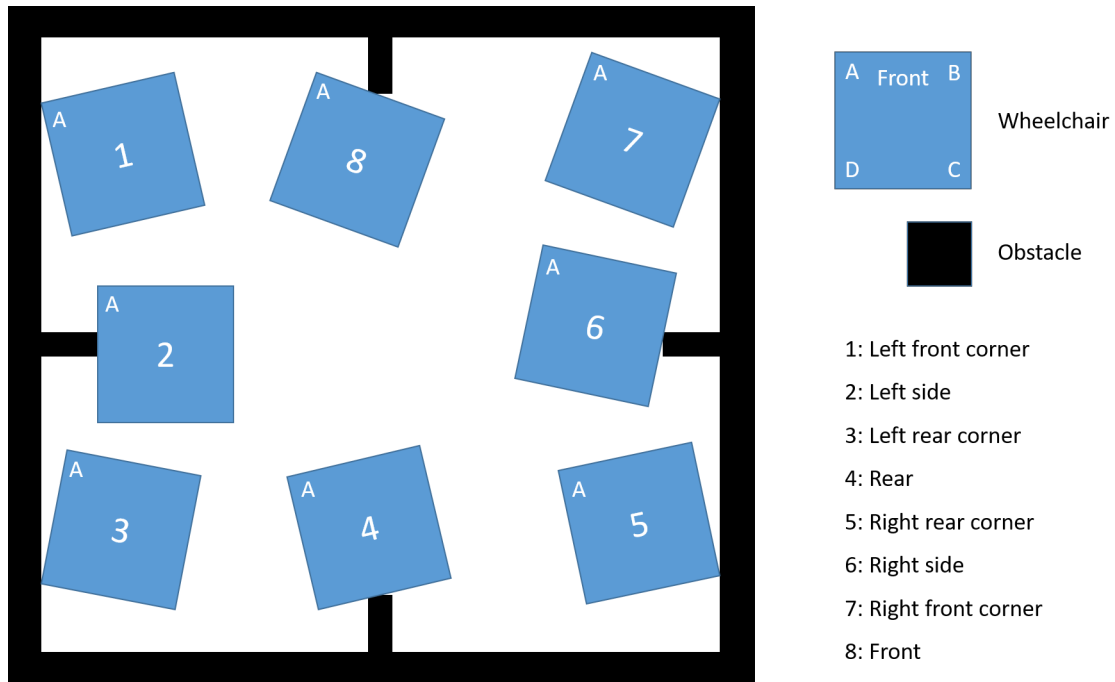
Figure 6.5: Eight typical collision poses of EPW

Algorithm 2 Potential collision detection

1: **function** COLLSION-DETECT(obstacles,(x, y, φ))
2: $\quad (A, B, C, D)_{global} = R_z(\varphi) \times (A, B, C, D)_{local} + \begin{bmatrix} x & y \end{bmatrix}^T$; $\quad \triangleright$ Corners of EPW in global system
3: $\quad$ **for** $j = 1$ to number of obstacles **do**
4: $\quad\quad$ **if** $distance\,(EPW \rightarrow obs(j)) < 1.5$ **then** $\quad\quad \triangleright$ only near obstacles are considered
5: $\quad\quad\quad$ **for** $k = 1$ to 4 **do** $\quad\quad\quad\quad\quad\quad\quad\quad\quad\quad\quad\quad\quad \triangleright$ 4 edges of the EPW
6: $\quad\quad\quad\quad$ **if** $intersection(edge(k), obs(j))$ **then**
7: $\quad\quad\quad\quad\quad$ case $= [1...8]$ $\quad\quad\quad\quad\quad\quad \triangleright$ Detect sides of collision (Fig. 6.5)
8: $\quad\quad\quad\quad\quad$ iscollis = 1;
9: $\quad\quad\quad\quad\quad$ Break;
10: $\quad\quad\quad\quad$ **else**
11: $\quad\quad\quad\quad\quad$ iscollis = 0;
12: $\quad\quad\quad\quad$ **end if**
13: $\quad\quad\quad$ **end for**
14: $\quad\quad$ **end if**
15: $\quad\quad$ **if** $iscollis == 1$ **then**
16: $\quad\quad\quad$ **if** $i < 4$ **then**
17: $\quad\quad\quad\quad$ time_to_risk = 1; $\quad\quad\quad\quad\quad\quad\quad\quad\quad\quad\quad \triangleright$ active "near mode"
18: $\quad\quad\quad$ **else**
19: $\quad\quad\quad\quad$ time_to_risk = 0; $\quad\quad\quad\quad\quad\quad\quad\quad\quad\quad\quad \triangleright$ active "far mode"
20: $\quad\quad\quad$ **end if**
21: $\quad\quad\quad$ Break;
22: $\quad\quad$ **end if**
23: $\quad$ **end for**
24: **end function**

6.2.1.2 Path planning

Once the potential collision is detected, the assistance system has to find an alternative path. This path should avoid the obstacles and remain not too far from the actual future path of EPW so that it is feasible and does not require too much user's effort to be realized. Fig. 6.6 illustrates our idea about the alternative solutions for obstacle avoidance. It can be seen that with the potential collision of the EPW (the red one), there are, for example, two possible substitute solutions. While the yellow one is too far from the intention of the user, the green one is selected as the optimal position of EPW because it satisfies both of the above requirements. It should be noted that we consider here only the obstacles which are near the wheelchair and hence, the proposed path is "optimal" only in this context.

By using the joystick positions which imply a pair of (v, ω), we predict the potential collisions as in Algorithm 2. Now the optimal path finding problem can be reduced to find an
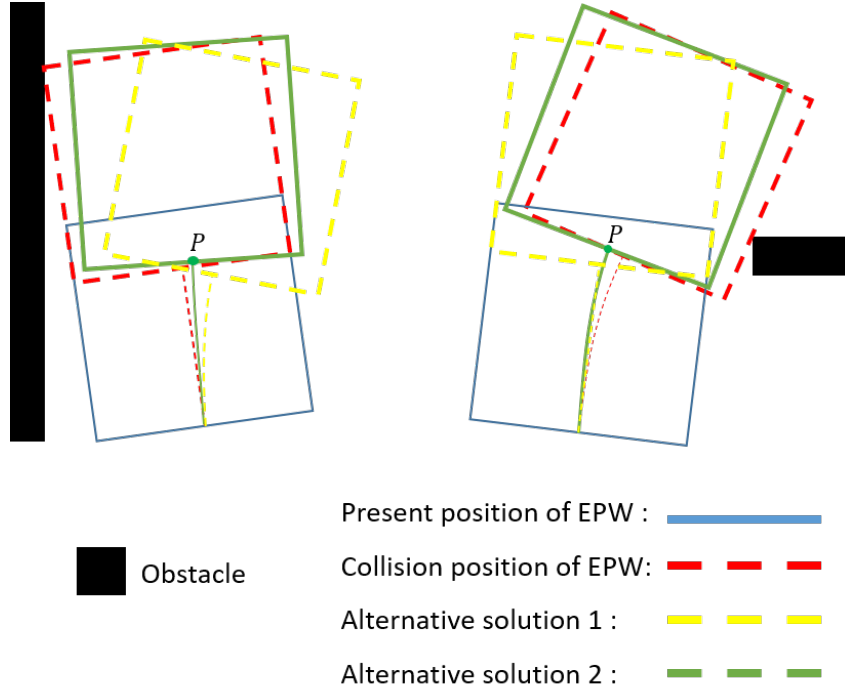
Figure 6.6: Path planning with the multiple choices

optimal pair of (v_{opt}, ω_{opt}) which satisfies these above requirements. We use here a "scan method" which numerically scans all the possible solutions, within mechanical limitations, of the pair (v, ω) to find the "best" one which is not only a free-collision path but also not too far from the actual motions of wheelchair. The algorithm 3 details the steps to implement this method where the cost function at line 36 is used to find the nearest solution to the actual motion of wheelchair. Scanning all possible solutions may practically increase calculation load and therefore influences considerably the performance of the system, or even make it works in an unacceptable way. Therefore, the side and position of potential collisions on the EPW as shown in Fig. 6.5 can be used to reduce the ranges of possible solution pairs (v, ω) as shown in Table 6.2. In this table, v_{max}, v_{min} are the mechanical limitations of v while $\omega_{max}, \omega_{min}$ are those of ω. (v, ω) is the actual velocities of the EPW corresponding to the current position of joystick (θ_l, θ_a). Once the ranges of (v, ω) are done, we repeat the following steps as shown in Algorithm 3: predict the future path with new pair of (v, ω); collision check; if there is not any collision detected, then update the value of (v_{opt}, ω_{opt}); if there is a collision then repeat the loop with another pair of (v, ω). Finally, the output of path planning function is not only (v_{opt}, ω_{opt}) but also the new position errors e_2, e_3 between the optimal EPW's position (the

Table 6.2: Ranges of (v, ω) according to each collision case

Case	1	2	3	4
v	$[v_{min} \quad v]$	$[-|v| \quad |v|]$	$[v \quad v_{max}]$	$[v \quad v_{max}]$
ω	$[\omega_{min} \quad \omega]$	$[-|\omega| \quad |\omega|]$	$[\omega \quad \omega_{max}]$	$[-|\omega| \quad |\omega|]$
Case	5	6	7	8
v	$[v \quad v_{max}]$	$[-|v| \quad |v|]$	$[v_{min} \quad v]$	$[v_{min} \quad v]$
ω	$[\omega_{min} \quad \omega]$	$[-|\omega| \quad |\omega|]$	$[\omega \quad \omega_{max}]$	$[-|\omega| \quad |\omega|]$

green one in Fig. 6.5) and the actual position of wheelchair (see Fig. 6.1). These new position errors are determined at the end of Algorithm 3.

6.2.2 Conflict Management

The mission of this block is to detect the disagreement between user and assistance system expressed through the interaction torques at the haptic joystick. In this research, the conflict between the human and system occurs when the three follow conditions are satisfied:

1. The hand torques $T_{h,i}$ and the assistance torques $T_{a,i}$ are in the opposite directions, $T_{h,i} \cdot T_{a,i} < 0$, $i = l, a$;

2. In both longitudinal and lateral directions, the differences between the hand and assistance torques are greater than a predefined threshold torque T_{cf}, $|T_{a,i} - T_{h,i}| > T_{cf}$, $i = l, a$;

3. Condition 1 and condition 2 occur and maintain for a period greater than a given period of t_{thr}.

While the conflict conditions can be easily detected when the assistance and the hand torques are known by the controllers and observers, the remaining problem is to manage the risk and the conflict so that once the conflict is detected, the assistance system will be changed from the obstacle avoidance assistance mode to the normal driving assistance mode.

Fig. 6.7 shows the detailed operation of this block which is mainly the switches controlled by the control variables. The conflict solving steps are described as follow:

1. Without the risk of accident (*iscollis* $= 0$), the assistance system always stays in normal driving assistance mode, and the conflict variable is set to 0.

Algorithm 3 Path Planning

1: **function** OPTIMAL-PATH-PLANNING(obstacles,(x, y, φ))
2:     $x(1) = x;\quad y(1) = y;\quad \varphi(1) = \varphi;$
3:     $v_{opt} = \omega_{opt} = 0;\quad cost_{initial} = 10;$
4:     **switch** case
5:         $(v_{min}, v_{max}) \leftarrow$ Table 6.2
6:         $(\omega_{min}, \omega_{max}) \leftarrow$ Table 6.2
7:     **endswitch**
8:     **for** $v = v_{min}$ to v_{max} **do**
9:         **for** $\omega = \omega_{min}$ to ω_{max} **do**
10:            **for** $l = 2$ to 6 **do**
11:                $x(l) = x(l-1) + v\cos(\varphi(l-1))\Delta t;$
12:                $y(l) = y(l-1) + v\sin(\varphi(l-1))\Delta t;$
13:                $\varphi(l) = \varphi(l-1) + \omega\Delta t;$
14:                $(A,B,C,D)_{global} = R_z(\varphi) \times (A,B,C,D)_{local} + [x \quad y]^T;$ ▷ Global system
15:                collision = 0;
16:                **for** $m = 1$ to number of obstacles **do**
17:                    **if** $distance(EPW \rightarrow obs(m)) < 1.5$ **then**   ▷ only near obstacles
18:                        **for** $n = 1$ to 4 **do**   ▷ 4 edges of the EPW
19:                            **if** $intersection(edge(n), obs(m))$ **then**
20:                                collision = 1;
21:                                Break;
22:                            **else**
23:                                collision = 0;
24:                            **end if**
25:                        **end for**
26:                        **if** collision == 1 **then**
27:                            Break;
28:                        **end if**
29:                    **end if**
30:                **end for**
31:                **if** $collision == 1$ **then**
32:                    Break;
33:                **end if**
34:            **end for**
35:            **if** $collision == 0$ **then**
36:                cost = $\sqrt{w \cdot (v_{real} - v)^2 + (\omega_{real} - \omega)^2}$
37:                **if** $cost < cost_{intial}$ **then**
38:                    $v_{opt} = v; \omega_{opt} = \omega;$
39:                    $cost_{intial} = cost:$
40:                    $e_2 = x_{P_{/local}};\qquad e_3 = arg(P_{/local});$
41:                **end if**
42:            **end if**
43:        **end for**
44:    **end for**
45: **end function**

2. When a risk of collision appears (*iscollis* = 1), the assistance torques will be switched to the autonomous mode (near mode or far mode is chosen by *time_to_risk* variable as in Algorithm 2) because both inputs of logic gate AND are 1 (*conflict* = 0 and *risk* = 1). The user now is expected to sense the haptic torques which communicate a free-collision path. Then he gives his decision by applying the appropriate torques at the joystick.

    (a) If there is not any conflict between user and assistance torques (*conflict* = 0), it means that the user agrees with the proposed path, the assistance system will stay in the autonomous mode until no risk of collision is detected. Then the control loop is repeated from step 1.

    (b) However, if a conflict is detected (*conflict* = 1), it means that the user does not agree with the proposed path, then assistance is switched to normal driving assistance mode (because one of two inputs of logic gate AND is 0) to follow the user desires. This conflict can be interpreted as: "I do not agree with your suggestion, there is not any risk, I will continue as I want".

3. After re-activating the normal driving assistance mode, it is expected that the conflict will be solved. An edge-detector block is used to detect this event by examining the decrease of the conflict variable. Once the conflict is solved, the edge-detector turns the *risk* variable to 0 to maintain the normal driving assistance mode until no any risk of collision is detected. Then the control loop is repeated from step 1.

6.3 Virtual Reality Simulator platform

To validate the proposed approach, we developed a virtual-reality simulator to integrate the wheelchair user and the joystick force feedback into the control loops. The general architecture of this simulator, as shown in Fig. 6.8, consists of four main elements: a haptic force feedback joystick, an electronic board Arduino Mega 2560, the controllers and observers, a virtual-reality environment.
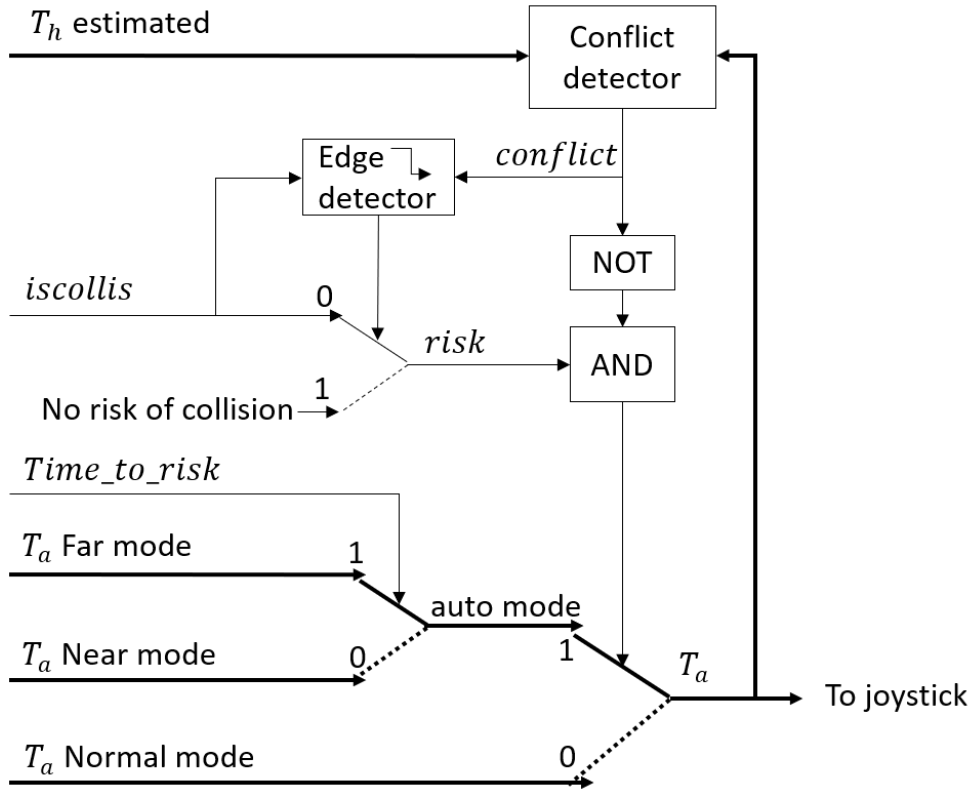
Figure 6.7: Conflict management block is composed of the switches controlled by the variables *conflict*, *iscollis*, *time_to_risk*. Values 0 and 1 present the positions of switches corresponding to these input values of control variables. Switch solid line: default position of switch. Switch dash line: switch position depending on the control variables. AND and NOT are two logic gates.
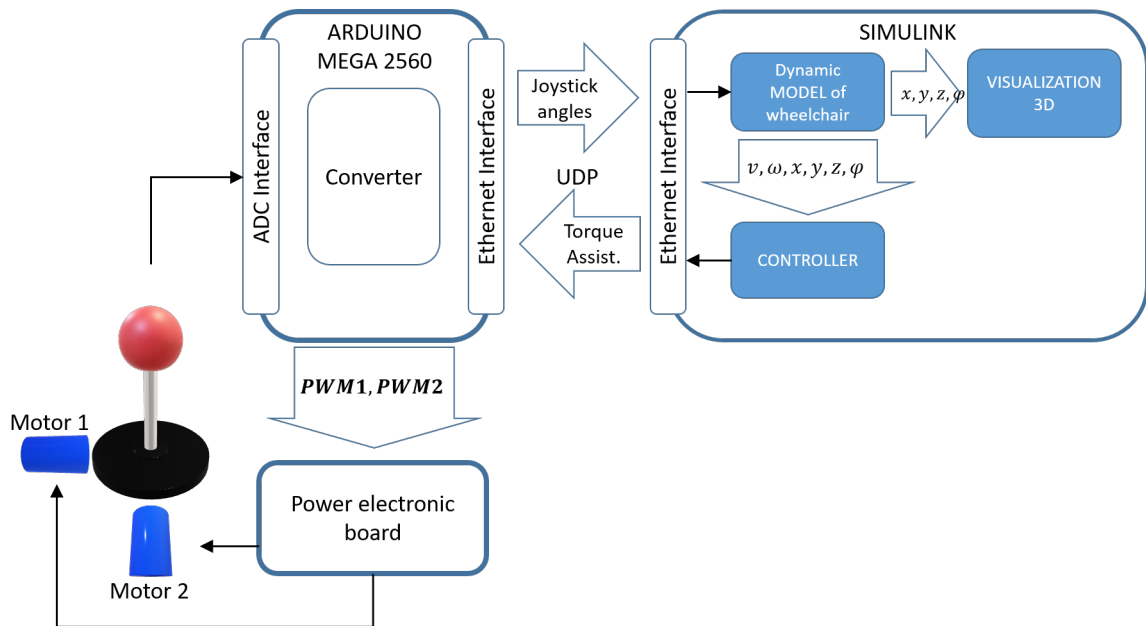
Figure 6.8: Virtual reality simulator for electric wheelchair comprises virtual scenario, force feedback joystick, observers/controllers and electronic boards.

1. The force feedback joystick is a modified version of a commercial joystick. It is equipped with two electric direct current motors which work with a nominal voltage of 12V. Each motor is attached to an axis to provide assistance torque to the user. To control the assistance torques, we use here a dual H-bridge power electronics board and pulse-width modulation (PWM) method. Two potential dividers are used as the joystick positions sensors to measure the rotation angles of the joystick. The maximum rotation angles of this joystick are 20° for each axis. The electronic board and two position sensors are connected to the Arduino Mega 2560 board.
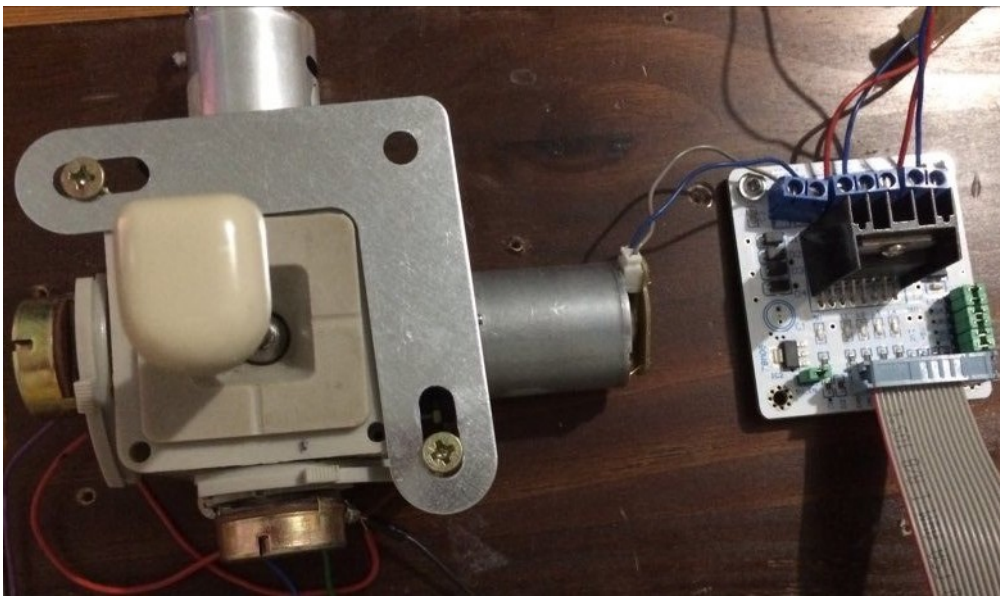
Figure 6.9: Haptic force feedback joystick and H-bridge power electronic board

2. The Arduino board plays an intermediate role in this system. It reads the joystick positions by using its Analog-Digital converters, converts the read values to integer format, and then sends them to Simulink through the UDP connection thanks to its Ethernet shield. It receives the assistance torque values from Simulink through UDP connection, converts them to corresponding PWM values, and realizes these torques by controlling two DC motors using its PWM modules. The source code for these Arduino functions is developed in Simulink thanks to the Arduino Support Package for Simulink. The sample time for the Arduino program is set to $0.01sec$.

3. The observers/controllers designed in chapter 5 and this chapter are implemented in
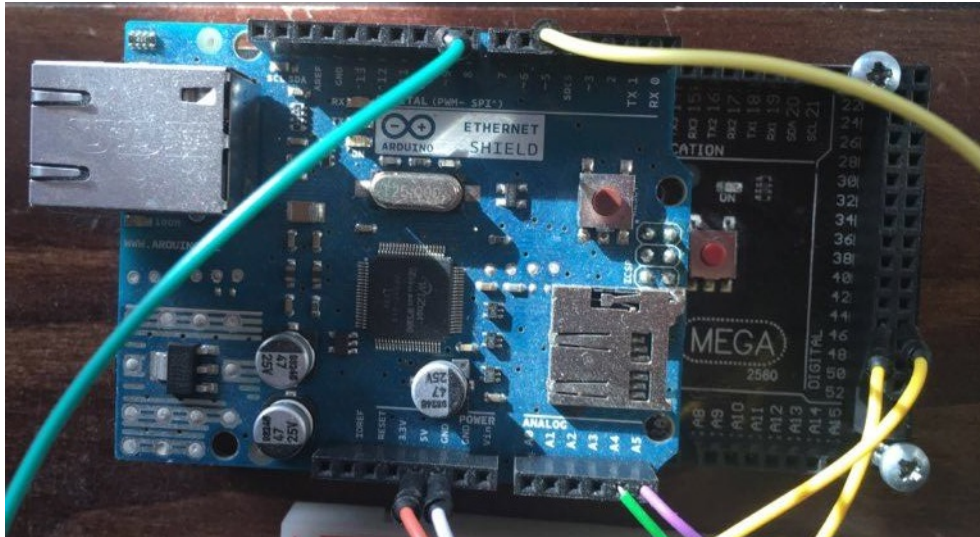
Figure 6.10: Arduino Mega 2560 and Ethernet shield

Simulink Desktop Realtime to work in realtime conditions. The sample time is set to $0.01sec$. The models (5.39), (5.46), (5.47) are used to simulate the motions of wheelchair in the virtual environment.

4. Virtual-reality plays an important role in this system. It simulates the environment so that the user can experience different scenarios to verify the functions of the proposed assistance system. It is designed using the Simulink 3D toolbox as in Fig. 6.11.
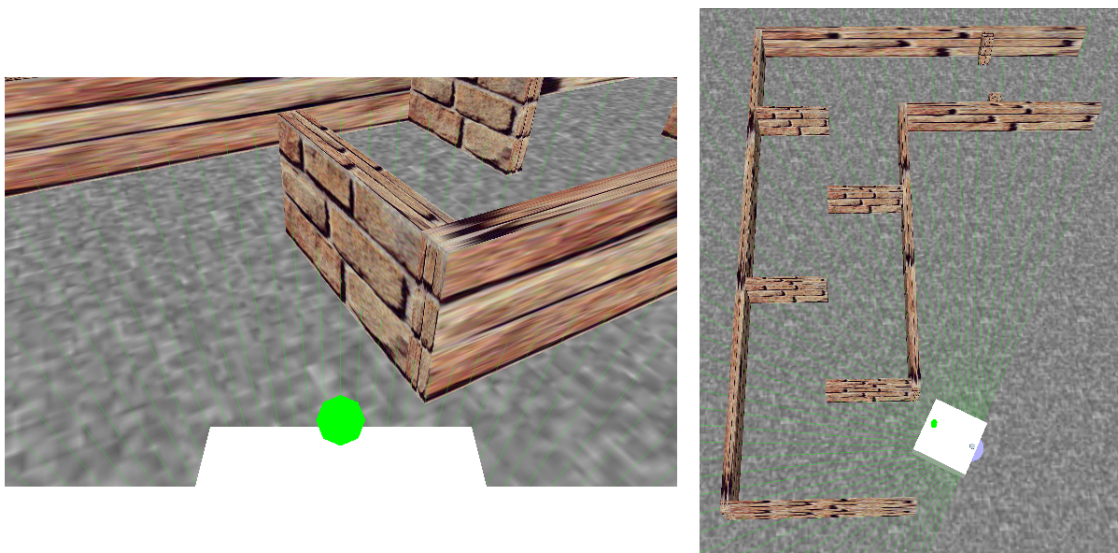
Figure 6.11: Virtual scenario build in Simulink 3D

The virtual-reality simulator now is ready to conduct the validation experiments.

6.4 Experiment and results

In this section, we conduct the experiments with the developed simulator to validate the shared control architecture proposed in chapter 5 and this chapter. Firstly, the user-joystick wheelchair model is validated by identifying the parameters of the proposed models through the measurable input/output variables. Then the shared-control assistance mode in chapter 5 is validated through two aspects: i) user intention estimation, and ii) shared-control assistance torques. Finally, the obstacle avoidance assistance mode is integrated into the tests to verify the efficiency of the proposed system.

6.4.1 User-joystick wheelchair model validation

By using the developed virtual-reality simulator platform, the joystick and wheelchair users are involved in the control loop. The proposed augmented model in section 5.3 consists of the user-path following model and dynamical model of the joystick which are now replaced by the real objects. Therefore, the parameters of these two models need to be identified.

To get data for this parameter identification step, we recruited one participant who is 33 years old and has no problem in manipulating the joystick. The participant gets used to using the joystick to control a wheelchair in a virtual-reality environment before carrying out the experiments. The participant is required to follow a predefined path in a virtual environment as shown by the green dot line from point **S** to point **I** in Fig. 6.12 four times. The obstacles in this scenario are adapted from experiments in [4] where participants commented that this setup is similar to the difficulties in their daily life. We record the wheelchair's position x, y, φ, the position errors e_2, e_3 from the virtual-reality environment, and the joystick angles θ_a, θ_l from the joystick. Then we identify the model parameters by using the Parameter Estimation toolbox in Simulink.

Fig. 6.13 and Fig. 6.14 present the estimation results of the proposed user-joystick model and the real responses of the participant. It can be seen that the responses of the model follow the trend of the real movements. There are some moments, in both cases of velocity and yaw rate, where the simulation responses do not match the real ones. The reasons may come from
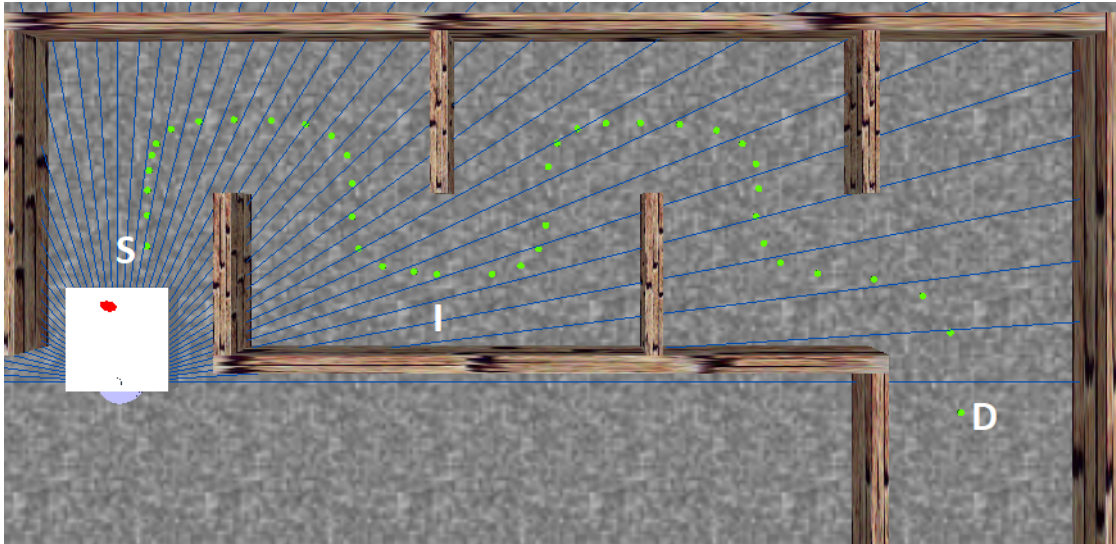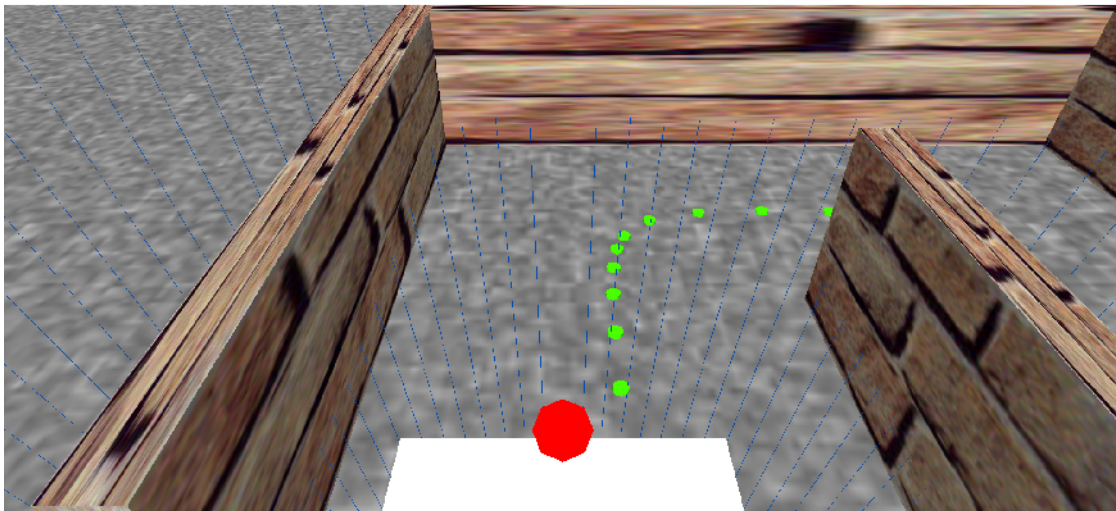
Figure 6.12: *a)* Simulation-experiment scenario. Green dot-line is the predefined reference path. White bloc represents the wheelchair. *b)* View point of participant during the experiments.

the uncertainties in the way the user perceives his position errors and his reactions. While in the proposed model, we suppose that the reference points are located at a fixed distance in front of the wheelchair, the user may choose a different point depending on the future curvature of the path. Table 6.3 summarizes the parameters of the participant identified from the above experiments.
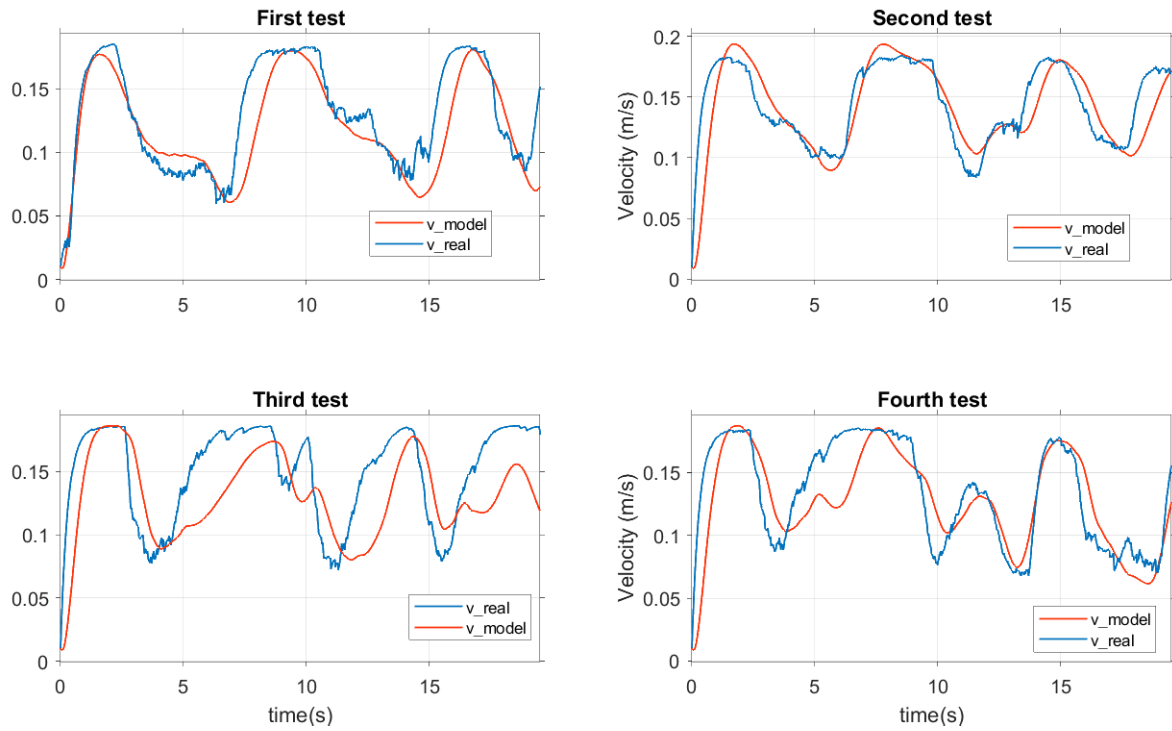
Figure 6.13: *a)* Simulation-experiment results in the four tests to identify the parameters of the longitudinal part of the user model.

6.4.2 Normal driving assistance mode

The experiments in this part are to validate two functions of the system proposed in chapter 5: estimating the user's intention and reducing the user effort in manipulating the joystick. The participant now is required to go from point **S** to point **D** in the virtual environment in Fig. 6.12 two times without collision with virtual walls. The first time is without assistance torques and the second time is with the assistance torques. There is not any predefined path as in section 6.4.1 and the user is free to choose his desired path to avoid the collision.
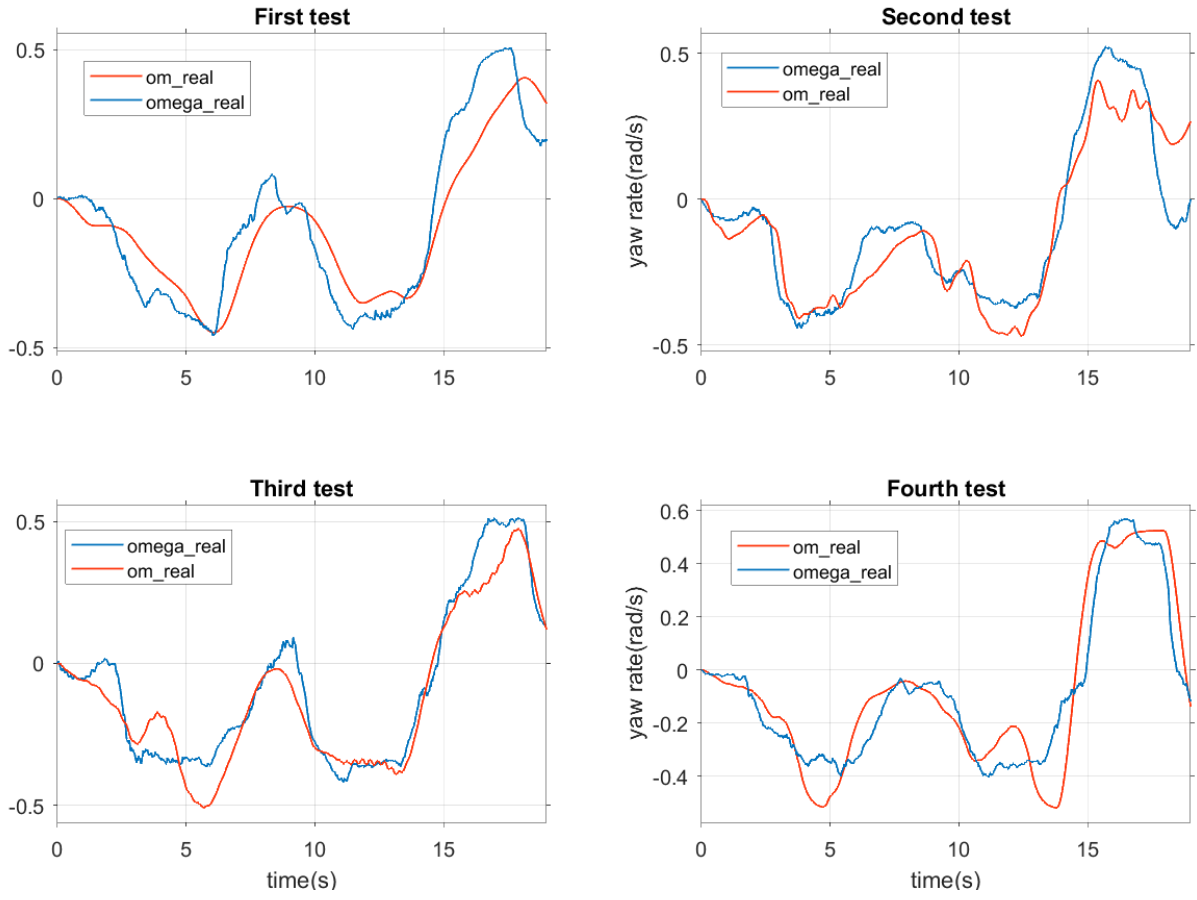
Figure 6.14: *a)* Simulation-experiment results in the four tests to identify the parameters of the rotational part of the user model.

Table 6.3: Identified parameters of user-hand-joystick dynamical model

Participants				1		
Parameters		Test 1	Test 2	Test 3	Test 4	Mean
Hand - Joystick (longi. direction) model	$\beta_{j,lo}$	0.0003	0.0003	0.0001	0.0002	0.0002
	J_{lo}	0.0004	0.0003	0.0006	0.0004	0.0004
	$K_{j,lo}$	0.3509	0.3673	0.3302	0.3795	0.3570
Hand - Joystick (lateral direction) model	$\beta_{j,la}$	0.2861	0.0625	0.0170	0.0104	0.0940
	J_{la}	0.0029	0.0145	0.0062	0.0012	0.0062
	$K_{j,la}$	0.5297	1.8490	2.9626	0.4424	1.4459
User path following controller model	k_{re2}	8.8705	5.5117	35.7740	17.1370	16.8233
	k_{re3}	4.3017	20.2920	26.2800	5.9445	14.2046
	k_{vre2}	0.6857	0.6832	0.2623	0.3437	0.4937
	k_{vre3}	1.7372	1.7374	1.0635	1.4127	1.4877
	k_i	0.3701	0.3837	0.5551	0.3363	0.4113
	k_p	0.6557	0.6646	1.1206	0.7137	0.7886
	τ_m	0.2040	0.1746	0.2269	0.3210	0.2316
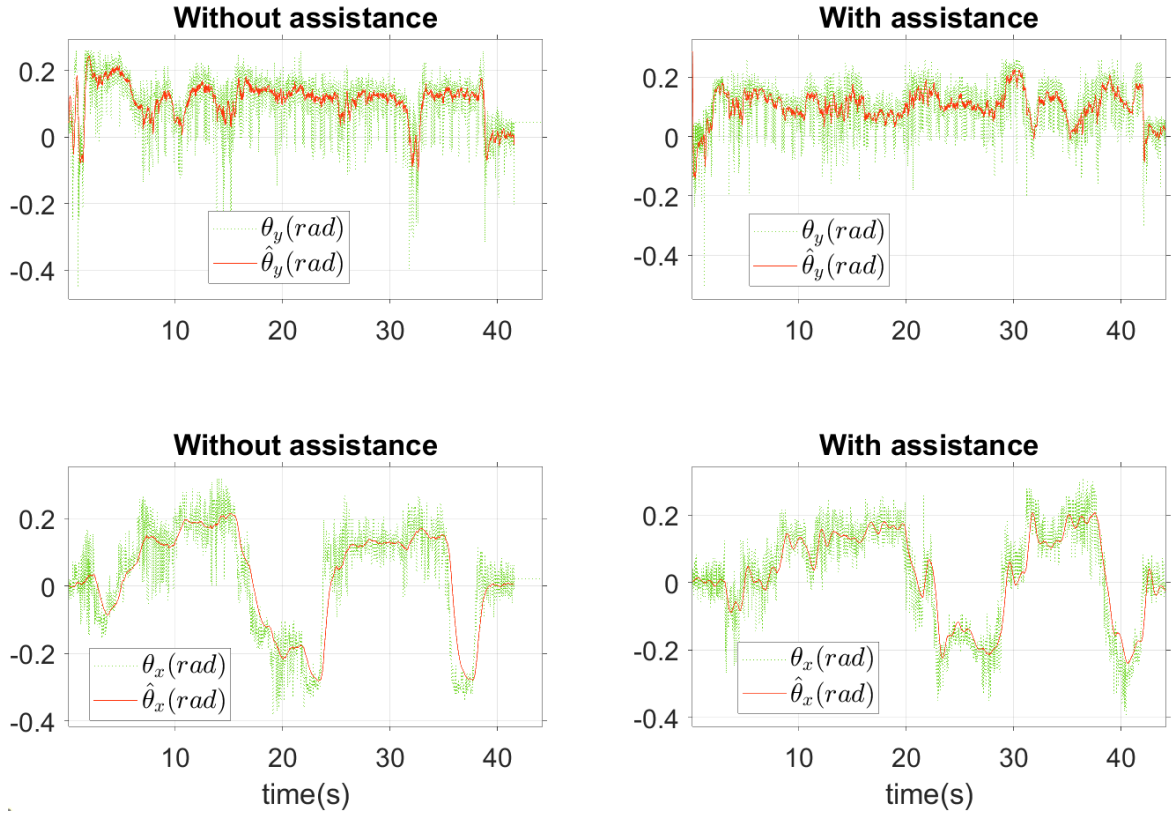
Figure 6.15: Estimation of joystick angles where the observers play the roles of the filters.
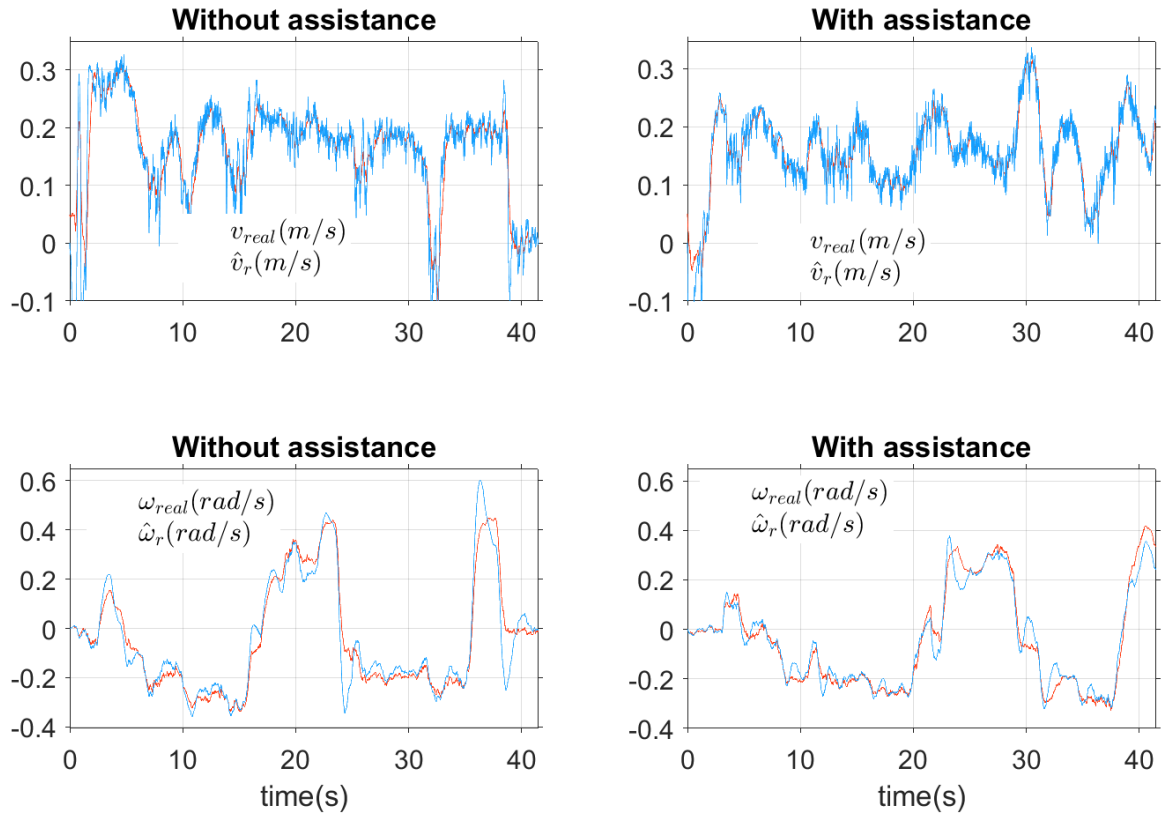
Figure 6.16: Estimation of the user's desired longitudinal velocity and yaw rate.

128

6.4.2.1 User intention estimation

Fig. 6.15 shows the filtered and the raw measurement results of joystick angles during the two tests, with and without assistance. Firstly it can be seen that recorded data is noisy, especially the longitudinal angle of θ_y. The delayed time between the measured and estimated data of these observers is about $0.2sec$ to $0.3sec$.

Fig. 6.16 presents the estimation results of the user's desired motions including longitudinal velocity $\hat{v}_r$ and yaw rate $\hat{\omega}_r$. While these real corresponding values of user cannot be measured explicitly, these estimated results are compared with the real measurements on the wheelchair. It is expected that the estimated user's desired velocity is a little bit faster than the real as in Fig. 5.12. However, the choice of the observer gains is constrained by the convergence speed and the noise sensitivity of estimated results. While increasing these gains can make the estimated ones converge faster as in the simulation, it also makes the estimated results to be too sensitive to the measurement noises as in Fig. 6.16. As a result, the estimation results of the user's desired motions have nearly the same values to the real motions of the wheelchair. Therefore, we can use practically the longitudinal velocity v_{real} of the wheelchair as the premise variable instead of the estimated desired velocity of $\hat{v}_r$ of the user.
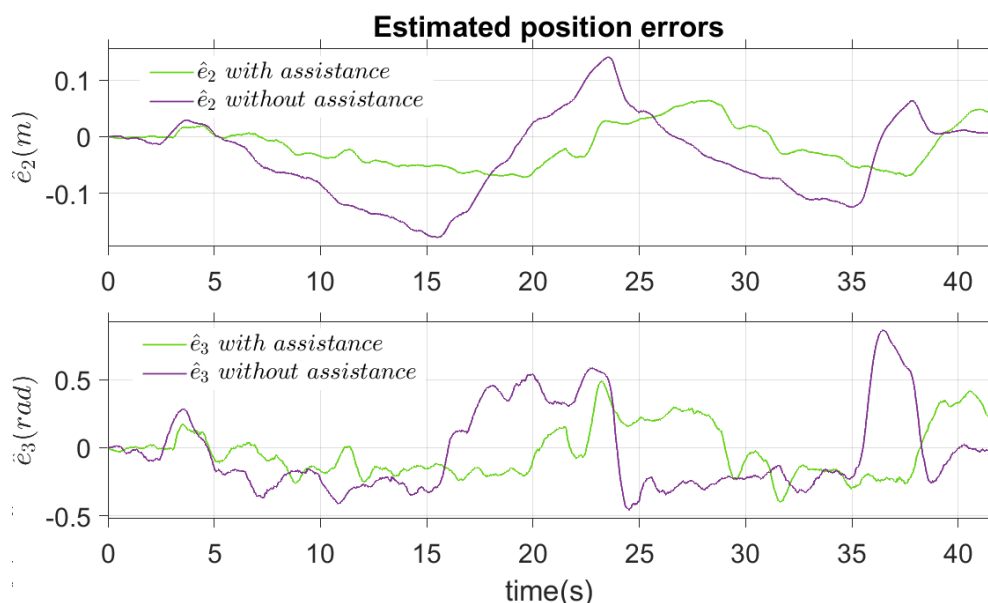
Figure 6.17: Estimation of the positions errors in both cases with and without assistance.

Fig. 6.17 shows the estimated position errors in both cases with and without assistance

torques. It can be seen that the lateral errors $\hat{e}_2$ and the angular errors $\hat{e}_3$ in the case with assistance are reduced considerably compared to the case without assistance.

6.4.2.2 Normal driving assistance mode
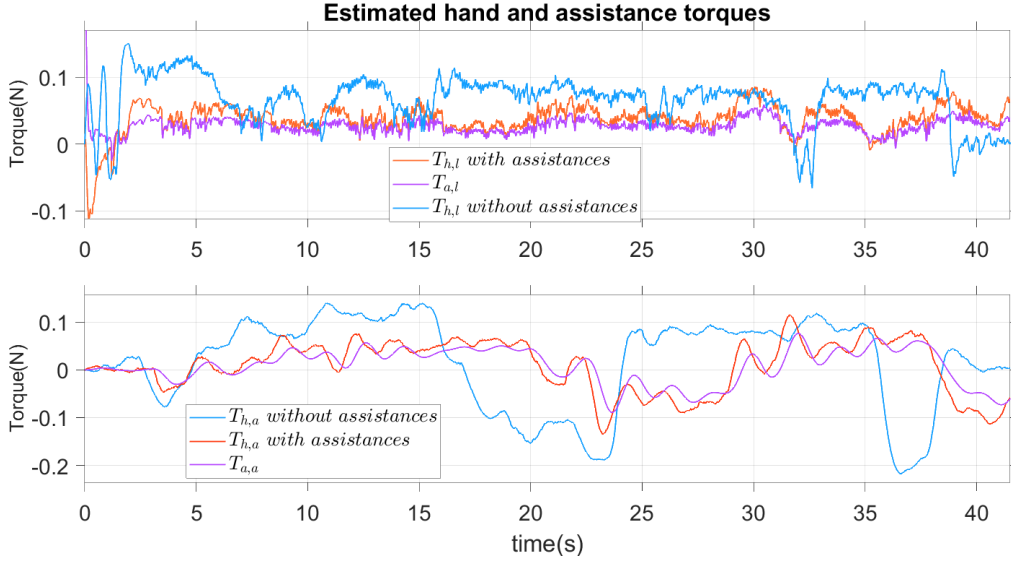
Figure 6.18: Estimation of the user's hand torques and assistance torques.

Fig. 6.18 shows the hand and assistance torques in both cases with and without assistance. It can be seen that in the case with assistance torques, in both longitudinal and angular directions, the user delivered only about a half of necessary torques compared to the cases without assistance.

To adapt the assistance torques to the user's needs (e.g.: they may require more or less assistance depending on their healthy on a specific moment), the assistance should be adjustable. By varying the parameters $k_{re2}, k_{re3}, k_I, k_P$ of the user-path following controller, the proposed assistance system adjusts the assistance torques according to the user's desires. To illustrate this idea, **the participant now is required to repeat the same experiment one more time** while the parameters $k_{re2}, k_{re3}, k_I, k_P$ are reduced to 50% their values in the Table 6.3. As can be seen in Fig. 6.19 the hand torques now are reduced considerably compared to the case in Fig. 6.18. The assistance torques now account for the majority of required torques to manipulate the joystick.

Remark: The assistance torques are delivered thanks to the observer-based controllers.
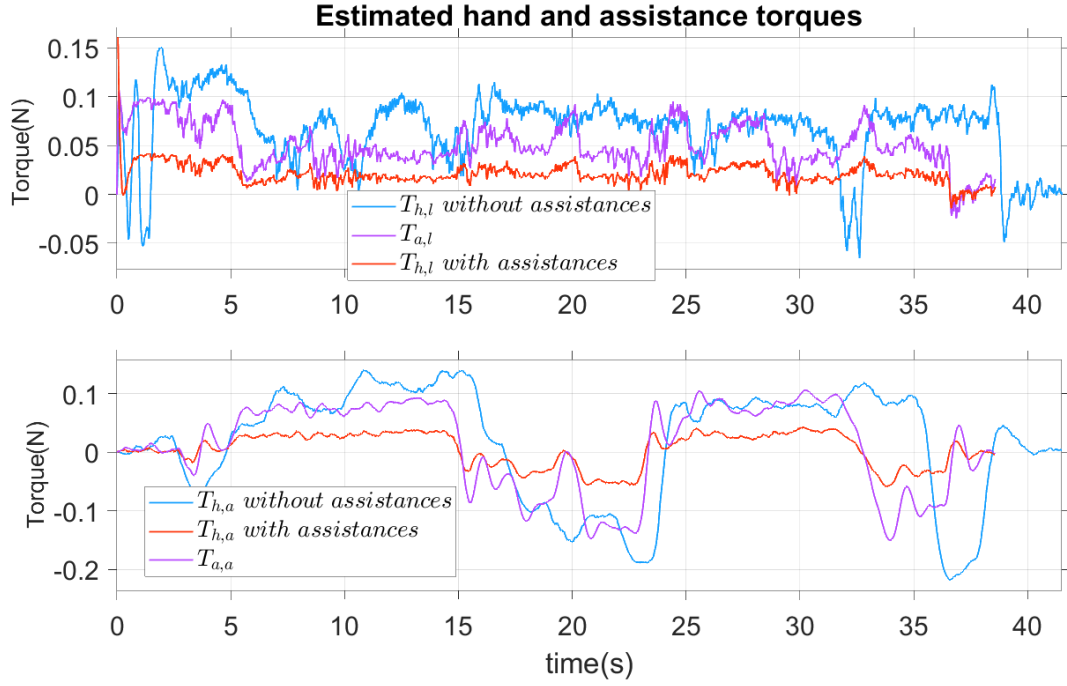
Figure 6.19: Estimation of the user's hand torques and assistance torques where the parameters can be adapted to user need.

Therefore the assistance torques have generally a small delay compared to the real human torques. This phenomenon is reported also by the participant who stated that "while the assistance torques reduce user's efforts, these assistances are delayed at the moment of reversing the joystick movement directions. As a result, the assistance torques become resistant torques at that moment". The faster response to the user's change, the higher the noise sensibility and therefore there is a negotiation in designing the observers.

6.4.3 Obstacle avoidance assistance mode

In this section, we conduct the experiments to validate the proposed assistance system in the obstacle avoidance assistance mode. The participant is required to repeat the same path as in the previous experiment without knowing that an additional obstacle is inserted as in Fig 6.20. This obstacle is invisible to the participant but known by the assistance system. The goal of this setup is to validate the conflict management function of the proposed assistance system. The torque threshold T_{cf} is set to $0.2N$ and t_{thr} is set to $1.5s$.

Fig. 6.21 shows the realized path in the designed scenario and the position of the wheelchair
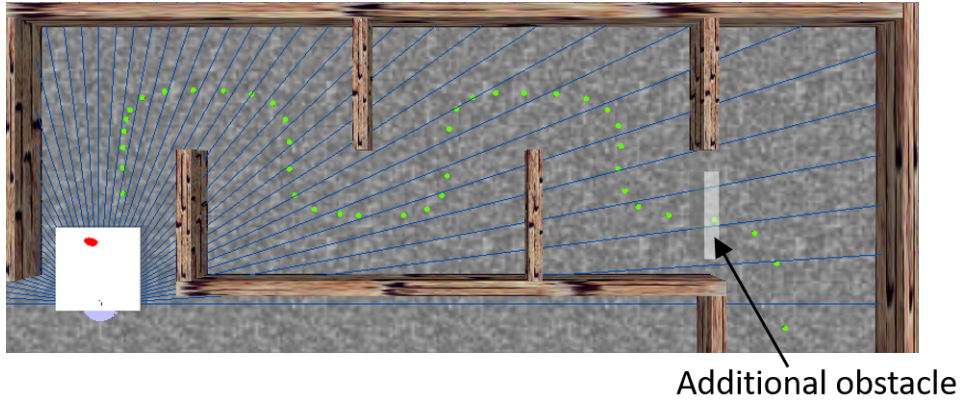
Figure 6.20: Scenario with the additional invisible obstacle.

where the risk of collision is detected. There are 4 times the risk management block detects the potential collision and activates the obstacle avoidance assistance mode. It can be seen that in this experiment all the potential collisions are at the front corners of the wheelchair. Without the risk of collision, the system provides about 50% of the required torques to manipulate the joystick as shown in Fig. 6.22. Otherwise, when a risk of collision appears, the obstacle avoidance assistance mode is activated, at $7.7s, 14s, 22.5s$ and $29s$. The zooming to these moments is presented in Fig. 6.23.

It can be seen that in the longitudinal direction, the wheelchair user seems to always disagree with the assistance torque. In four times of detecting a potential collision, the longitudinal hand torque is always opposite to the assistance one. However, the response of longitudinal velocity agrees with the proposed optimal solution in Fig. 6.22 where the real velocity decreased according to the suggestion from the assistance system.

In the lateral direction, the user is more agreeable to the suggestion of the system where the hand torque has the same direction with the assistance one in the three first times of potential collision detections. While the longitudinal hand and the assistance torques are opposite in these three times, there is not any conflict found between the user and system. The reason is that with the assistance in the lateral direction, the system found that the risk of collision is eliminated and then it changes to the normal driving assistance mode. Fig. 6.22 illustrates these results when only two flags *iscollis* and *risk* are turned on while the flags *conflict* and *solve conflict* are still off.

The conflict between the user's intention and the assistance system is shown clearly at
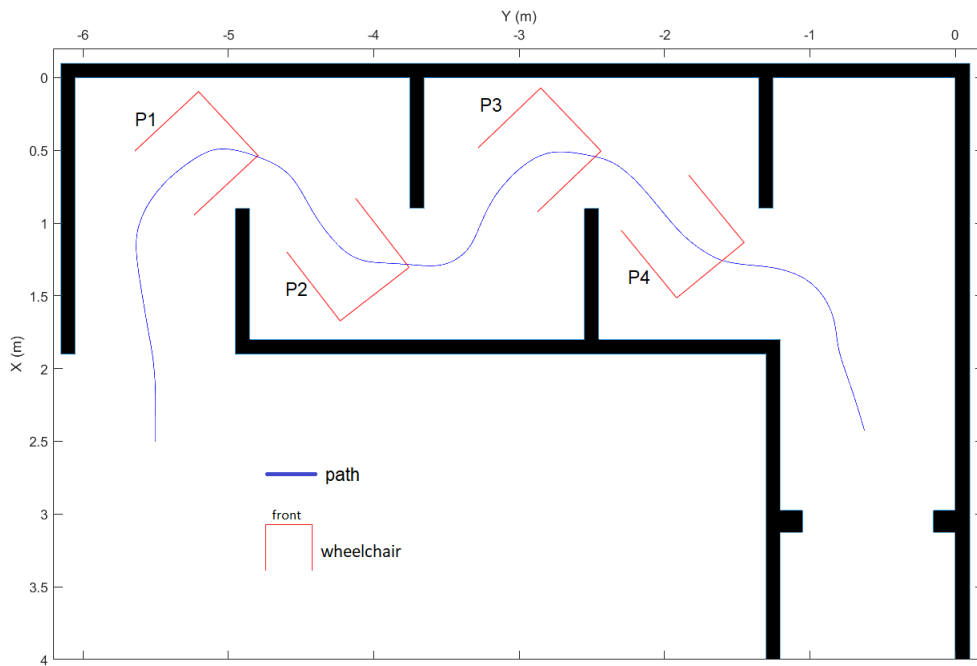
Figure 6.21: Realized path with the position of wheelchair where the assistance for obstacle avoidance is activated when the risk of collision is detected

the point $P4$ in Fig. 6.21 when the wheelchair approaches the additional obstacle which is described above. In this case, the proposed assistance system tried to guide the user to another free collision path by providing the haptic torques which gradually increase as in Fig. 6.22 and Fig. 6.23. The wheelchair user, without knowing the presence of an obstacle, tried to follow his initial intention by applying an opposite torque to the joystick. Once the three conditions in section 6.2.2 are verified, the conflict between user and system is confirmed, the flag *conflict* switches on as in Fig. 6.22 . The system now has to switch to normal driving assistance mode, therefore the flag *solve conflict* switched on and the *conflict* and *risk* flags are turned off. The flag *solve conflict* is maintained until the *iscollis* flag is turned off to avoid switching continuously between normal driving and obstacle avoidance assistance mode.

It should be noted that when the assistance mode is switched between normal driving and obstacle avoidance assistance mode, the initial conditions of the observers will be reset to zero and therefore the estimated torques are reset to zero, too, as shown in Fig. 6.22.
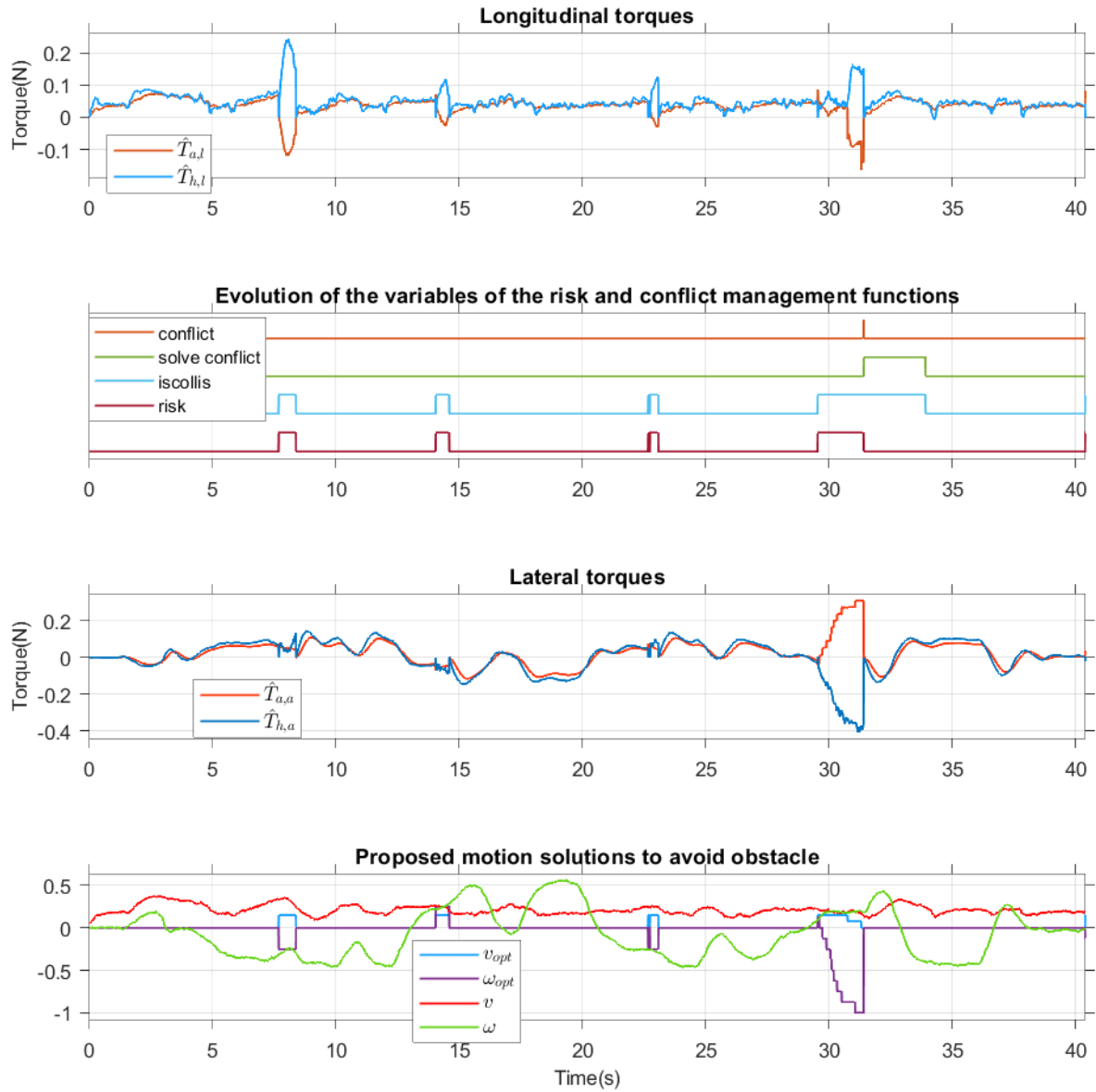
Figure 6.22: The evolution of the estimated hand torques, assistance torques and the variable of the risk-conflict management functions.
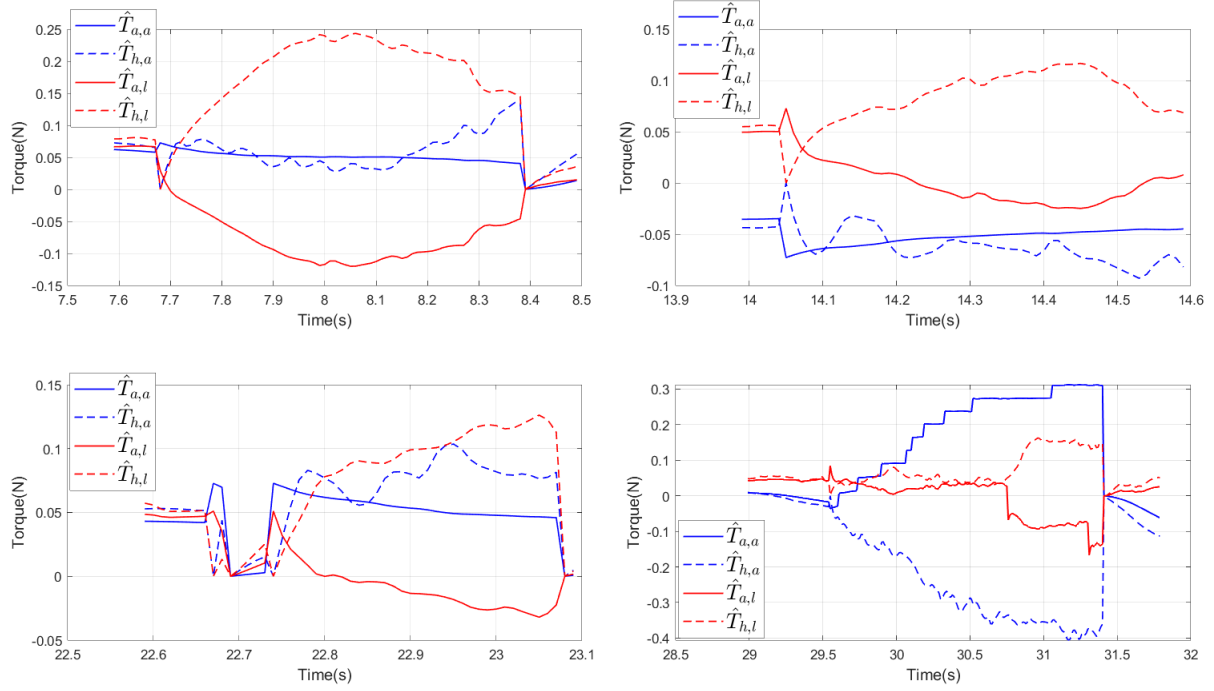
Figure 6.23: The evolution of the estimated hand torques, assistance torques when the risk of collision is detected.

6.5   Conclusion

This chapter presents the design of the proposed assistance system in obstacle avoidance assistance mode. The goals of this mode are to guide the user in avoiding potential collision through a haptic joystick and to manage the conflict, if exist, between the user and the system. The human-in-the-loop experiments were conducted with a virtual simulator platform to validate the proposed approach. The experimental results show that the proposed assistance system can predict the user's intentions, help them to realize them, and improve their comfort. If a potential collision is detected, the assistance system can communicate to the user about this as well as guide her/him to avoid this through force feedback joystick. The user can overrule the suggestions anytime if he/she want and the assistance system will follow the user's decision. The assistance level can be adjusted by reducing the user's effort in the user's path-following model.

Chapter 7

General conclusion and perspective

7.1 Conclusion

Throughout this thesis, we explore several new things in three aspects of the wheelchair assistance system design including (i) the dynamical model of wheelchair dedicated to the virtual reality simulator; (ii) the biomechanical model of hand-joystick interaction for personalizing the assistance system; (iii) model-based shared-control approach for wheelchair assistance system design.

The proposed dynamical model of wheelchair considered most of the external factors which affect the motions of a wheelchair. The tire-ground interaction model allows simulating the behaviour of the wheelchair with different pavement conditions. The influences of front free casters wheels are also considered because they affect considerably the motions of the wheelchair at near-zero speed region. The experimental results showed that the proposed model can well reflect the behavior of the wheelchair in a real-world test. This suggests that a comprehensive dynamic model is essential for a wheelchair simulator which aims to provide a realistic sense of movement for the user. Besides, the complexity of rotation resistance torques, especially in the low-speed region, suggests that there exists still room for deeper researches on the behavior of these torques.

The biomechanical model of hand-joystick interaction is a new approach to study on per-

sonalizing assistance system according to the wheelchair user's impairments. Instead of using a "pure" biomechanical model of the hand with many muscles inside, we proposed an equivalent model which consists of only four "virtual" muscles to maneuver the joystick during driving the wheelchair. These muscles operate a 5-bars robot arm mechanism that reproduces the extension/flexion and radial/ulnar motions of hand-wrist to manipulate the joystick. The Hill model containing the biomechanical parameters of muscles allows to represent the muscle weakness problems of the wheelchair users. The simulation results of joystick movements compared to the published data showed that the proposed model can reproduce the driving behavior at the operational level. At the execution level, the evolutions of muscle activation were estimated thanks to the proposed model.

The assistance system for power wheelchair users through the force feedback joystick has been developed using the model-based shared control approach. This allows integrating many functions of the assistance system into a unique systematic design procedure. These functions are used to estimate the user's intention, reduce the user's effort in manipulating the joystick, guide her/him to avoid a potential collision and, preserve her/his role as the final decision maker (allow her/him to overrule the suggestion of the system). To do that we first developed an augmented dynamical model of the wheelchair-user system. The unknown input observers were exploited to estimate user intentions. The TS-fuzzy model and the optimal fuzzy controller are used to calculate the haptic torque feedback to the user. To assist the user in obstacle avoidance assistance mode, a path following controller was designed to provide an appropriate haptic guide. We developed also the conflict management functions which are based on the haptic torques at the joystick. The experiments were conducted in a virtual simulator with a haptic joystick developed at our laboratory to validate the proposed approach. The results confirmed all the intended functions. In normal driving assistance mode, the assistance torques reduced considerably the efforts of users in manipulating the joystick. The level of assistance torques can be adjusted by changing the user model parameters. The experiments also validated the guiding effect of this system in the case there is a risk of collision. The conflict management function allows users to communicate their intention and overrule the guidance of the system effectively to maintain their activeness in driving a wheelchair.

Generally, this thesis can be considered as a preparation step for further researches on assistance solutions for the wheelchair. With a simulator platform, a biomechanical approach, and a systematic controller design procedure for the assistance system, there are many open research directions from the perspective of this work.

7.2   Perspective

This thesis treated three aspects of the assistance system for power wheelchair users. While each aspect has its potential to be researched deeper, the combination of these aspects is also necessary to improve the performance of the assistance system.

Firstly a dynamical model of the wheelchair should pay more attention into the near-zero speed region, especially the rotation stiffness of the tires, which is the most different from the vehicle model. A more detailed model may be necessary to integrate these behaviors. The effects of the castor wheels are also complicated because it depends on the external factors such as the instantaneous rotation angles of these wheels, tire-ground contact conditions. Besides, the influence of the front and the rear wheels are superposed to the rotation motions of a wheelchair and therefore it is a bigger challenge to treat them separately.

In addition, the biomechanical model of hand-joystick interaction still an open research direction. This thesis proposed a simplified model of a system of muscles. This model can be used for controller synthesis instead of the augmented model as in chapter 5. The combination of the proposed controller design procedure in chapter 5 with the biomechanical model of the user is the further goal of this research which allows us to personalize the assistance according to the motor difficulties of each user. The most important question is how to simplify the biomechanical model to satisfy both requirements: still keeping the main properties reflecting the impairment of users while being enough simple so that it can be used to synthesize the controller. Besides, in the next step, we will try to measure the activation levels of the hand-wrist muscles by using the EMG signals and then identify the parameters of the proposed model. While the EMG measurement of the superficial muscles is feasible, there is a technical obstacle to measure the EMG signals of the deep muscles.

The proposed assistance system in chapter 5 and chapter 6 has proved its effectiveness through the experimental validation. However, there are many things for further improvement.

We used the linear unknown input observers for estimating user intentions. For simplicity reason, we neglected the nonlinear term in the user-joystick-wheelchair model that leads to some estimation errors when the yaw rate is small. Therefore, future research should use a nonlinear observer for this purpose. The fuzzy observer may be a good candidate when the fuzzy controller was used for assistance system design.

In the current works, the robustness of the assistance to the uncertainties of the system was not considered in the controller design procedure. This property is important to deal with the uncertainties of the system parameters or the external disturbances which are unavoidable in real working conditions. The biomechanical model of user containing many uncertain parameters makes this feature essential. The robust control method will be certainly applied in future works.

The validation experiments were conducted with the assumption that the positions of the obstacles are known prior which is not the case in the real world. Wheelchair and obstacle positions can not be known exactly without tolerance as in simulation. Therefore, to implement the real-world test, the mapping methods should be employed for positioning purposes. Besides, the choice of appropriate proximity sensors is also a negotiation problem among the factors such as the range, the precision of sensors, and the cost of the system.

The most important device in our proposed system is the haptic force feedback joystick. Using the electric motors and the gearbox, as in this work, this device proved its capacity to assist the user. However, this joystick structure may be too heavy and requires much space for a compact joystick in a commercial wheelchair. Therefore improving the joystick design is one of the most important tasks of future researches.

The effectiveness of the proposed assistance system should be evaluated by the experiments with the participation of the wheelchair users who have different levels of difficulty in driving the power wheelchair. These experiments can be conducted firstly on the PSCHITT PMR simulator, and then on the real-world scenarios. Due to the Covid-19 epidemic, these experiments cannot be implemented within this thesis. Therefore, the next step of this research is to imple-

ment these experiments.

Bibliography

[1] L. Schur, D. Kruse, and P. Blanck, *People with Disabilities: Sidelined Or Mainstreamed?* 1st ed. New York: Cambridge University Press, 2013, p. 288, ISBN: 9781107000476.

[2] S. Mitra, *Disability, Health and Human Development*. New York: Palgrave MacMillan, 2018, p. 177, ISBN: 978-1-137-53637-2.

[3] K. Edwards and A. McCluskey, "A survey of adult power wheelchair and scooter users," *Disability and Rehabilitation: Assistive Technology*, vol. 5, no. 6, pp. 411–419, 2010.

[4] M. Gillham, M. Pepper, S. Kelly, *et al.*, "Feature determination from powered wheelchair user joystick input characteristics for adapting driving assistance," *Wellcome Open Research*, vol. 2(93), pp. 1–40, 2018.

[5] L. Fehr, W. E. Langbein, and S. B. Skaar, "Adequacy of power wheelchair control interfaces for persons with severe disabilities : A clinical survey," *Journal of Rehabilitation Research and Development*, vol. 37, no. 3, pp. 353–360, 2000.

[6] T. Carlson and J. Del R. Millan, "Brain-controlled wheelchairs: A robotic architecture," *IEEE Robotics and Automation Magazine*, vol. 20, no. 1, pp. 65–73, 2013.

[7] T. Carlson, Y. Demiris, and S. Member, "Collaborative Control for a Robotic Wheelchair: Evaluation of Performance, Attention, and Workload," *IEEE Transactions On Systems, Man, And Cybernetics*, vol. 42, no. 3, pp. 876–888, 2012.

[8] M. Letaief, N. Rezzoug, and P. Gorce, "Comparison between joystick- and gaze-controlled electric wheelchair during narrow doorway crossing: Feasibility study and movement analysis," *Assistive Technology*, 2019.

[9] P. D. Nisbet, "Who's intelligent? Wheelchair, driver or both?" In *Proceedings of the IEEE International Conference on Control Applications*, Glasgow, 2002, pp. 760–765.

[10] D. A. Abbink, M. Mulder, and E. R. Boer, "Haptic shared control : smoothly shifting control authority ?" *Cogn Tech Work*, vol. 14, pp. 19–28, 2012.

[11] L. Devigne, F. Pasteau, T. Carlson, *et al.*, "A shared control solution for safe assisted power wheelchair navigation in an environment consisting of negative obstacles: A proof of concept," in *Proceedings of the IEEE International Conference on Systems, Man and Cybernetics*, 2019, pp. 1043–1048, ISBN: 9781728145693.

[12] H. U. Yoon, N. Anil Kumar, and P. Hur, "Synergistic Effects on the Elderly People's Motor Control by Wearable Skin-Stretch Device Combined with Haptic Joystick," *Frontiers in Neurorobotics*, vol. 11, no. June, pp. 11–31, 2017.

[13] J. Leaman and H. M. La, "IChair: Intelligent Powerchair for Severely Disabled People," in *Proceedings of the ISSAT International Conference on Modeling of Complex Systems and Environments*, 2015, pp. 19–24.

[14] P. Carrington, A. Hurst, and S. K. Kane, "Wearables and chairables: Inclusive design of mobile input and output techniques for power wheelchair users," in *Proceedings of the 16th International ACM SIGACCESS Conference on Computers & Accessibility*, New York, NY, USA: Association for Computing Machinery, 2014, pp. 201–208, ISBN: 9781450324731.

[15] S. Jain and B. Argall, "Automated perception of safe docking locations with alignment information for assistive wheelchairs," in *Proceedings of the IEEE International Conference on Intelligent Robots and Systems*, Chicago, 2014, pp. 4997–5002, ISBN: 9781479969340.

[16] F. Leishman, V. Monfort, O. Horn, *et al.*, "Driving assistance by deictic control for a smart wheelchair: The assessment issue," *IEEE Transactions on Human-Machine Systems*, vol. 44, no. 1, pp. 66–77, 2014.

[17] F. Leishman, O. Horn, and G. Bourhis, "Smart wheelchair control through a deictic approach," *Robotics and Autonomous Systems*, vol. 58, no. 10, pp. 1149–1158, 2010.

[18] J. J. Park and B. Kuipers, "A smooth control law for graceful motion of differential wheeled mobile robots in 2D environment," in *Proceedings of the IEEE International Conference on Robotics and Automation*, 2011, pp. 4896–4902, ISBN: 9781612843865.

[19] V. T. Nguyen, C. Sentouh, P. Pudlo, *et al.*, "Path Following Controller for Electric Power Wheelchair Using Model Predictive Control and Transverse Feedback Linearization," in *Proceedings of the 2018 IEEE International Conference on Systems, Man, and Cybernetics (SMC)*, IEEE, 2018, pp. 4319–4325.

[20] Y. Morales, N. Kallakuri, K. Shinozawa, *et al.*, "Human-comfortable navigation for an autonomous robotic wheelchair," in *Proceedings of the IEEE International Conference on Intelligent Robots and Systems*, 2013, pp. 2737–2743, ISBN: 9781467363587.

[21] E. Demeester, A. Hüntemann, J. Philips, *et al.*, "Adaptable navigational assistance for intelligent wheelchairs by means of an implicit personalized user model," *Robotics and Autonomous Systems*, vol. 58, no. 8, pp. 963–977, 2010.

[22] P. Viswanathan, E. P. Zambalde, G. Foley, *et al.*, "Intelligent wheelchair control strategies for older adults with cognitive impairment: user attitudes, needs, and preferences," *Autonomous Robots*, vol. 41, no. 3, pp. 539–554, 2017.

[23] A. V. Nguyen, L. B. Nguyen, S. Su, *et al.*, "Shared control strategies for human - Machine interface in an intelligent wheelchair," in *Proceedings of the Annual International Conference of the IEEE Engineering in Medicine and Biology Society, EMBS*, 2013, pp. 3638–3641, ISBN: 9781457702167.

[24] N. Kuge, T. Yamamura, E. R. Boer, *et al.*, "Study on driver's car following abilities based on an active haptic support function," *SAE Technical Papers*, no. 724, 2006.

[25] D. A. Abbink, S. Member, T. Carlson, *et al.*, "A Topology of Shared Control Systems — Finding Common Ground in Diversity," *IEEE Transactions on Human-Machine Systems*, vol. 48, no. 5, pp. 509–525, 2018.

[26] A. Marouf, M. Djemai, C. Sentouh, *et al.*, "A new control strategy of an electric-power-assisted steering system," *IEEE Transactions on Vehicular Technology*, vol. 61, no. 8, pp. 3574–3589, 2012.

[27] L. Profumo, L. Pollini, and D. A. Abbink, "Direct and indirect haptic aiding for curve negotiation," in *Proceedings of the 2013 IEEE International Conference on Systems, Man, and Cybernetics (SMC)*, 2013, pp. 1846–1852, ISBN: 9780769551548.

[28] D. Katzourakis, M. Alirezaei, J. C. De Winter, *et al.*, "Shared control for road departure prevention," in *Proceedings of the IEEE International Conference on Systems, Man and Cybernetics*, 2011, pp. 1037–1043, ISBN: 9781457706523.

[29]   A. Benloucif, A. T. Nguyen, C. Sentouh, *et al.*, "Cooperative trajectory planning for haptic shared control between driver and automation in highway driving," *IEEE Transactions on Industrial Electronics*, vol. 66, no. 12, pp. 9846–9857, 2019.

[30]   C. Sentouh, A. T. Nguyen, J. Floris, *et al.*, "Multiple Controller Switching Concept for Human-Machine Shared Control of Lane Keeping Assist Systems," in *Proceedings of the 2018 IEEE International Conference on Systems, Man, and Cybernetics (SMC)*, 2018, pp. 2730–2735, ISBN: 9781538666500.

[31]   E. B. Vander Poorten, E. Demeester, E. Reekmans, *et al.*, "Powered wheelchair navigation assistance through kinematically correct environmental haptic feedback," in *Proceedings of the IEEE International Conference on Robotics and Automation*, 2012, pp. 3706–3712, ISBN: 9781467314039.

[32]   H. Soh and Y. Demiris, "Towards Early Mobility Independence: An Intelligent Paediatric Wheelchair with Case Studies," in *Proceedings of the IROS 2012 - Workshop on Progress, Challenges and Future Perspectives in Navigation and Manipulation Assistance for Robotic Wheelchairs*, 2012.

[33]   T. Carlson and Y. Demiris, "Collaborative control in human wheelchair interaction reduces the need for dexterity in precise manoeuvres," in *Proceedings of the ACM/IEEE International Conference on Human-Robot Interaction*, 2008, pp. 59–66.

[34]   L. Devigne, V. K. Narayanan, F. Pasteau, *et al.*, "Low complex sensor-based shared control for power wheelchair navigation," in *Proceedings of the IEEE International Conference on Intelligent Robots and Systems*, 2016, pp. 5434–5439, ISBN: 9781509037629.

[35] L. Devigne, F. Pasteau, M. Babel, *et al.*, "Design of a haptic guidance solution for assisted power wheelchair navigation," in *Proceedings of the 2018 IEEE International Conference on Systems, Man, and Cybernetics (SMC)*, 2018, pp. 3231–3236.

[36] Y. Morere, M. A. Hadj Abdelkader, K. Cosnuau, *et al.*, "Haptic control for powered wheelchair driving assistance," *IRBM*, vol. 36, no. 5, pp. 293–304, 2015.

[37] I. Iturrate, J. M. Antelis, A. Kübler, *et al.*, "A noninvasive brain-actuated wheelchair based on a P300 neurophysiological protocol and automated navigation," *IEEE Transactions on Robotics*, vol. 25, no. 3, pp. 614–627, 2009.

[38] A. Kucukyilmaz and Y. Demiris, "Learning Shared Control by Demonstration for Personalized Wheelchair Assistance," *IEEE Transactions on Haptics*, vol. 11, no. 3, pp. 431–442, 2018.

[39] L. Marchal-Crespo, J. Furumasu, and D. J. Reinkensmeyer, "A robotic wheelchair trainer: Design overview and a feasibility study," *Journal of NeuroEngineering and Rehabilitation*, vol. 7, no. 1, 2010.

[40] G. Vailland, F. Grzeskowiak, L. Devigne, *et al.*, "User-centered design of a multisensory power wheelchair simulator : towards training and rehabilitation applications," in *Proceedings of the International Conference on Rehabilitation Robotics*, Toronto, 2019.

[41] J. Rix, S. Haas, and J. Teixeira, *Virtual Prototyping: Virtual environments and the product design process*. Springer, 2016, p. 348.

[42] M. T. Schultheis and A. A. Rizzo, "The application of virtual reality technology in rehabilitation," *Rehabilitation Psychology*, vol. 46, no. 3, pp. 296–311, 2001.

[43] J.-L. Lessard, "Conception et validation d'un ergomètre, incluant un fauteuil configurable, pour la simulation et l'évaluation des performances de la course en fauteuil roulant," Ph.D. dissertation, 2013, p. 205, ISBN: 978-0-494-96272-5.

[44] Y. Liu, W. Tan, C. Chen, *et al.*, "A Review of the Application of Virtual Reality Technology in the Diagnosis and Treatment of Cognitive Impairment," *Frontiers in Aging Neuroscience*, vol. 11, no. October, pp. 1–5, 2019.

[45] T. Bentaleb, V. T. Nguyen, C. Sentouh, *et al.*, "A real-time multi-objective predictive control strategy for wheelchair ergometer platform," in *Proceedings of the 2019 IEEE International Conference on Systems, Man and Cybernetics (SMC)*, 2019, pp. 2397–2404, ISBN: 9781728145693.

[46] L. Devigne, M. Babel, F. Nouviale, *et al.*, "Design of an immersive simulator for assisted power wheelchair driving," in *Proceedings of the IEEE International Conference on Rehabilitation Robotics*, 2017, pp. 995–1000, ISBN: 9781538622964.

[47] C. Bigras, D. Kairy, and P. S. Archambault, "Augmented feedback for powered wheelchair training in a virtual environment," *Journal of NeuroEngineering and Rehabilitation*, vol. 16, no. 1, pp. 1–12, 2019.

[48] T. Ito, M. Shino, T. Inoue, *et al.*, "Development of a Powered Wheelchair Driving Simulator for Research and Development Use," *Journal of Mechanical Systems for Transportation and Logistics*, vol. 2, no. 2, pp. 90–101, 2009.

[49] P. S. Archambault, F. Routhier, J. N. F. Chong, *et al.*, "Comparision of power wheelchair driving performance in a real and in a simulated environment," in *Proceedings of the 2011 International Conference on Virtual Rehabilitation*, Zurich, Switzerland, 2011, pp. 1–7, ISBN: 9781612844749.

[50] H. P. Mahajan, B. E. Dicianno, R. A. Cooper, *et al.*, "Assessment of wheelchair driving performance in a virtual reality-based simulator," *Journal of Spinal Cord Medicine*, vol. 36, no. 4, pp. 322–332, 2013.

[51] M. Shino, Y. Yamakawa, T. Inoue, *et al.*, "Longitudinal stability control of electric wheelchairs for persons with severe disability," *Vehicle System Dynamics*, vol. 46, no. S1, pp. 389–402, 2008.

[52] A. Baudry, S. Guégan, and M. Babel, "Taking caster wheel behavior into account in the kinematics of powered wheelchairs," *Modelling, Measurement and Control C*, vol. 79, no. 4, pp. 168–172, 2018.

[53] L. R. Crichlow, "Development of a Comprehensive Mathematical Model and Physical Interface for Manual Wheelchair Simulation," Ph.D. dissertation, University of Toronto, 2011.

[54] C. De la Cruz, T. F. Bastos, R. Carelli, *et al.*, "Dynamic Modeling and Centralized Formation Control of Mobile Robots," *IEEE Transactions on Neural Systems and Rehabilitation Engineering*, vol. 19, no. 2, pp. 435–445, 2011.

[55] F. Chénier, P. Bigras, and R. Aissaoui, "A new dynamic model of the wheelchair propulsion on straight and curvilinear level-ground paths," *Computer Methods in Biomechanics and Biomedical Engineering*, vol. 18, no. 10, pp. 1031–1043, 2015.

[56] J. J. Kauplarich and D Ph, "Wheelchair Caster Shimmy and Turning Resistance," *Journal of rehabilitation research and development*, vol. 20, no. 2, pp. 15–29, 1984.

[57] F. Chenier, P. Bigras, and R. Aissaoui, "An orientation estimator for the wheelchair's caster wheels," *IEEE Transactions on Control Systems Technology*, vol. 19, no. 6, pp. 1317–1326, 2011.

[58] C. Sauret, J. Bascou, N. d. S. Rmy, *et al.*, "Assessment of field rolling resistance of manual wheelchairs," *The Journal of Rehabilitation Research and Development*, vol. 49, no. 1, pp. 63–74, 2012.

[59] R. N. Jazar, *Vehicle Dynamics: Theory and Application*, 2nd ed. Springer-Verlag New York, 2014, p. 1066, ISBN: 978-1-4614-8544-5.

[60] L. C. Silva, F. C. Corrêa, J. J. Eckert, *et al.*, "A lateral dynamics of a wheelchair: identification and analysis of tire parameters," *Computer Methods in Biomechanics and Biomedical Engineering*, vol. 20, no. 3, pp. 332–341, 2017.

[61] E. Demeester, A. Hüntemann, D. Vanhooydonck, *et al.*, "Bayesian estimation of wheelchair driver intents: Modeling intents as geometric paths tracked by the driver," in *Proceedings of the IEEE International Conference on Intelligent Robots and Systems*, 2006, pp. 5775–5780, ISBN: 142440259X.

[62] D. Vanhooydonck, E. Demeester, M. Nuttin, *et al.*, "Shared control for intelligent wheelchairs: an implicit estimation of the user intention," in *Proceedings of the International Workshop on Advances in Service Robotics (ASER)*, 2003, pp. 176–182, ISBN: 3816762689.

[63] J.-A. Escobedo-Cabello, "User Intention Estimation for Semi-Autonomous Navigation of a Robotic Wheelchair," Ph.D. dissertation, 2014, p. 152.

[64] S. O. Onyango, Y Hamam, K Djouani, *et al.*, "A Driving Behaviour Model of Electrical Wheelchair Users," *Computational Intelligence and Neuroscience*, vol. 2016, 2016.

[65] H. Emam, Y. Hamam, E. Monacelli, *et al.*, "Power wheelchair driver behaviour modelling," in *Proceedings of the 2010 7th International Multi-Conference on Systems, Signals and Devices*, 2010, pp. 1–7, ISBN: 9781424475346.

[66] M. Mirakhorlo, J. M. Visser, B. A. Goislard de Monsabert, *et al.*, "Anatomical parameters for musculoskeletal modeling of the hand and wrist," *International Biomechanics*, vol. 3, no. 1, pp. 40–49, 2016.

[67] D. L. Crouch and H. Huang, "Lumped-parameter electromyogram-driven musculoskeletal hand model: A potential platform for real-time prosthesis control," *Journal of Biomechanics*, vol. 49, no. 16, pp. 3901–3907, 2016.

[68] B. E. Dicianno, S. Sibenaller, C. Kimmich, *et al.*, "Joystick use for virtual power wheelchair driving in individuals with tremor: Pilot study," *Journal of Rehabilitation Research and Development*, vol. 46, no. 2, pp. 269–276, 2009.

[69] C.-w. Lung, C.-l. Chen, Y.-k. Jan, *et al.*, "Activation Sequence Patterns of Forearm Muscles for Driving a Power Wheelchair," in *Proceedings of the Advances in Human Factors in Sports, Injury Prevention and Outdoor Recreation AHFE 2017. Advances in Intelligent Systems and Computing 603*, Tareq Ahram, Ed., Springer, Cham, 2018, pp. 141–147, ISBN: 9783319608228.

[70] A. Kucukyilmaz and Y. Demiris, "One-shot Assistance Estimation from Expert Demonstrations for a Shared Control Wheelchair System," in *Proceedings of the 2015 24th IEEE International Symposium on Robot and Human Interactive Communication (RO-MAN)*, Kobe, Japan, 2015, pp. 438–443.

[71] P. E. Nikravesh, "Newtonian-based methodologies in multi-body dynamics," *Proceedings of the Institution of Mechanical Engineers, Part K: Journal of Multi-body Dynamics*, vol. 222, pp. 277–288, 2008.

[72]   M. Hajzman and P. Polach, "Application of stabilization techniques in the dynamic analysis of multibody systems," *Applied and Computational Mechanics*, vol. 1, pp. 479–488, 2007.

[73]   B. W. Infantolino and J. H. Challis, "Architectural properties of the first dorsal interosseous muscle," *Journal of Anatomy*, vol. 216, no. 4, pp. 463–469, 2010.

[74]   K. Serbest, M. Cilli, M. Z. Yildiz, *et al.*, "Development of a human hand model for estimating joint torque using MATLAB tools," in *Proceedings of the IEEE RAS and EMBS International Conference on Biomedical Robotics and Biomechatronics*, vol. 2016-July, 2016, pp. 793–797, ISBN: 9781509032877.

[75]   Z. Xu, E. Todorov, B. Dellon, *et al.*, "Design and Analysis of an Artificial Finger Joint for Anthropomorphic Robotic Hands," in *Proceedings of the 2011 IEEE International Conference on Robotics and Automation*, 2011, pp. 5096–5102.

[76]   K. W. Brown, "Electric Powered Wheelchair Control with a Variable Compliance Joystick-Improving Control of Mobility Devices for Individuals with Multiple Sclerosis," Ph.D. dissertation, University of Pittsburgh, 2007.

[77]   G. U. Sorrento, P. S. Archambault, F. Routhier, *et al.*, "Assessment of Joystick control during the performance of powered wheelchair driving tasks," *Journal of NeuroEngineering and Rehabilitation*, vol. 8, no. 1, p. 31, 2011.

[78]   R. Kirby, *Wheelchair Skills Program (WSP)-Wheelchair Skills Test (WST) Manual*, 2011.

[79]   K. Tanaka and H. O. Wang, *Fuzzy Control Systems Design and Analysis*. 2001, ISBN: 0471323241.

[80] T. Takagi and M. Sugeno, "Fuzzy Identification of Systems and Its Applications to Fault Diagnosis Systems," *IEEE Transactions On Systems, Man, And Cybernetics*, vol. SMC-15, no. 1, pp. 116–132, 1985.

[81] P. Gahinet, A. Nemirovskii, A. J. Laub, *et al.*, "The LMI Control Toolbox," in *Proceedings of the 33rd Conference on Decision and Control*, 1994, pp. 2038–2041.

[82] J. Löfberg, "YALMIP : A toolbox for modeling and optimization in MATLAB," in *Proceedings of the 2004 IEEE International Conference on Robotics and Automation*, New Orleans, LA, USA, 2004, pp. 284–289.

[83] G.-R. Duan and H.-H. Yu, *LMIs in Control Systems*. CRC Press, 2013, ISBN: 9781466583009.

[84] J. Li, H. O. Wang, L. Bushnell, *et al.*, *A Fuzzy Logic Approach to Optimal Control of Nonlinear Systems*, 2000.

[85] D. Söffker, T.-J. Yu, and P. C. Müller, "State estimation of dynamical systems with non-linearities by using proportional-integral observer," *International Journal of Systems Science*, vol. 26, no. 9, pp. 1571–1582, 1995.

[86] M. T. Houston, A. N. Cameron, and J. B. Gutierrez, "A Review of Mathematical Models for Muscular Dystrophy : A Systems Biology Approach," *PLOS Currents Muscular Dystrophy*, 2018.

[87] N. T. Nguyen, H. T. Nguyen, and S. Su, "Advanced robust tracking control of a powered wheelchair system," in *Proceedings of the Annual International Conference of the IEEE Engineering in Medicine and Biology*, Lyon, France, 2007, pp. 4767–4770, ISBN: 1424407885.

[88] C Sentouh, P Chevrel, F Mars, *et al.*, "A Sensorimotor Driver Model for Steering Control," in *Proceedings of the 2009 IEEE International Conference on Systems, Man and Cybernetics*, IEEE, 2009, pp. 2462–2467, ISBN: 9781424427949.

[89] ElectroCraft Engineered Solutions, *Product Catalog*.

[90] M. J. Grey, "Viscoelastic properties of the human wrist during the stabilization phase of a targeted movement," Master thesis, Simon Fraser University, 1997.

[91] T. E. Milner and C. Cloutier, "Damping of the wrist joint during voluntary movement," *Experimental Brain Research*, no. 122, pp. 309–317, 1998.

[92] J. How and E. Frazzoli, *Feedback Control Systems*, 2010.